CHALMERS
UNIVERSITY OF TECHNOLOGY

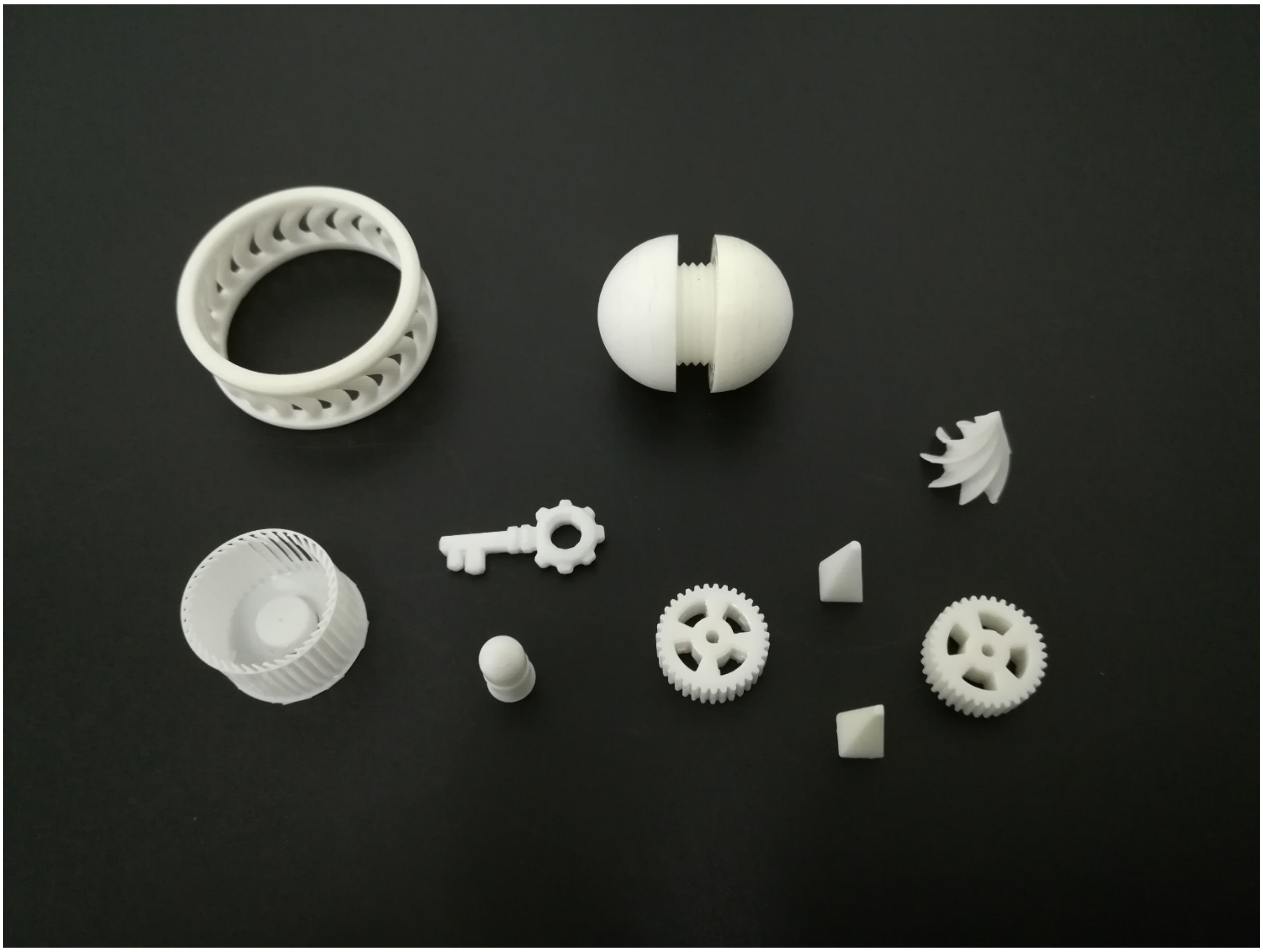

Additive Manufacturing of Zirconia

Master's thesis in Materials Engineering

Gustavo Adolfo Llanos Peñaloza

Department of Industrial and Materials Science
CHALMERS UNIVERSITY OF TECHNOLOGY
Gothenburg, Sweden 2018

MASTER THESIS IN MATERIALS ENGINEERING

Additive Manufacturing of Zirconia

GUSTAVO ADOLFO LLANOS PEÑALOZA

Department of Industrial and Materials Science
CHALMERS UNIVERSITY OF TECHNOLOGY
Gothenburg, Sweden 2018

Additive Manufacturing of Zirconia
GUSTAVO ADOLFO LLANOS PEÑALOZA

Supervisor: Erik Adolfsson, Swerea IVF
Supervisor: Emil Johansson, Swerea IVF
Examiner: Eduard Hryha, Department of Industrial and Materials Science

Thesis was performed in the frame of the Centre for Additive Manufacturing – Metal (CAM^2) in collaboration with Swerea IVF

Master's Thesis 2018
Department of Industrial and Materials Science
Division of Materials Engineering
Chalmers University of Technology
SE-412 96 Göteborg
Telephone: + 46 (0)31-772 1000

Cover: Zirconia components printed with additive manufacturing.

Chalmers Reproservice
Gothenburg, Sweden 2018

Acknowledgments

I want to thank my parents German and Rosario and my brother Cesar for their support and love during this time in Sweden.

I would like to thank my supervisors Erik Adolfsson and Emil Johansson at Swerea IVF for their collaboration and mentoring during the research, providing valuable knowledge and advice trough discussions and feedback.

I also want to thank my supervisor Eduard Hryha for his guidance and collaboration during the elaboration of the thesis.

I want to thank the Swedish Institute that supported my studies and living in Sweden during the completion of the master program.

Additive Manufacturing of Zirconia
Master's thesis in Materials Engineering
GUSTAVO ADOLFO LLANOS PEÑALOZA
Department of Industrial and Materials Science
Division of Materials Engineering
Chalmers University of Technology

Abstract

The potential of Zirconia for fabrication of components using additive manufacturing technologies extend the application range for this material. There are some limitations with the relatively simple design that can be achieved by conventional manufacturing processes for ceramics. However, there are some challenges to overcome in additive manufacturing of zirconia given the difficulty to obtain fully dense components without defects. In this research, additive manufacturing of Yttria-stabilized zirconia was investigated to increase the overall reliability of a VAT-photopolymerization technique. Powder processing was performed before suspension preparation to study the effect on further steps. An optimum resin composition was developed and printing parameters were adjusted according to the suspension characteristics. Post-processing steps were tested and investigated to analyze the effect on the component and its final properties. Powders with different stabilizing agents using the same resin were tested to evaluate the powder effect on the overall process. The results obtained show that the resin composition developed allows manufacturing of components with Yttria and Magnesia stabilized Zirconia. Powder characteristics such as grain size and surface area showed that they can limit the powders suitable for this technique. Characterization of the components shows uniform microstructure with good dimensional accuracy, allowing to obtain near fully dense components with this technology.

Key words: Additive Manufacturing, Rheology of Zirconia Suspensions, Cure depth, Photopolymerization, Powder Processing, Debinding of Polymer Matrix, Sintering, Material Characterization.

I. Table of Contents

Acknowledgments I
Abstract I
I. Table of Contents II
II. List of Figures IV
III. List of Tables V
IV. Abbreviations VI
1. Introduction 1
1.1. Background of the Project 1
1.2. Project Aim 2
1.3. Scope 2
1.4. Project Report Outline 2
2. Literature Review 2
2.1. Overview of Zirconia 2
2.2. Crystal Structures of Zirconia 4
2.2.1. Cubic Zirconia 4
2.2.2. Tetragonal Zirconia 4
2.2.3. Monoclinic Zirconia 5
2.3. Mechanical Properties 5
2.3.1. Elastic Properties 6
2.3.2. Hardness 6
2.3.3. Creep 6
2.3.4. Toughness 6
2.3.5. Toughening Mechanism of Zirconia 7
2.4. Corrosion Resistance of ZrO_2 8
2.5. Biological Properties of ZrO_2 9
2.6. Electronic Properties of ZrO_2 9
2.7. Zirconia Powders 9
2.8. Powder Processing 10
2.8.1. Ball Milling 10
2.8.2. Freeze Drying 11
2.9. Additive Manufacturing of Ceramics 11
2.10. Stereolithography of Zirconia 12
2.11. Photocurable Ceramic Suspensions 15
2.12. Removal of Organic Additives 15
2.13. Sintering 15

2.14. Characterization of Final Components 16
2.15. Summary of Literature Review 17
3. Experimental Procedure 18
3.1. Powder Characterization and Processing 18
3.2. Suspension Preparation 18
3.3. Characterization of Ceramic Suspension 21
3.4. Component Building 22
3.5. Post Processing of Components 24
3.6. Characterization of Final Component 26
3.7. Process Evaluation with Different Powders 26
4. Results and Discussion 28
4.1. Milling and Freezing 28
4.2. Effect of Dispersant on the Suspension 30
4.3. Effect of Diluent on the Suspension 31
4.4. Suspensions with Two Monomers and Diluent 32
4.5. Influence of Monomers and Diluent on Cure Depth 33
4.6. Debinding of Green Components 34
4.7. Sintering Process 38
4.8. Process viability with Different Powders 40
4.9. Characterization of Final Components 45
5. Conclusions 48
6. Future Work 49
References 50
Appendices 53
A. Raw Powder Characteristics 53
a. 3Y-TZP Tosoh Powders 53
B. Image Analysis and Grain Size Measurement – Sintered Components 54
a. 3Y-TZP – Tosoh Powders 544
b. Mg-TZP – Daiichi Powders 577

II. List of figures

Figure 1. Representation of transformation toughening in ZrO_2 7
Figure 2. Mask-projection Vat-photopolymerization. View of rotating glass plate 14
Figure 3. Schematic representation of the preparation of suspensions 19
Figure 4. Characterization of viscosity of suspensions with varying shear rate 21
Figure 5. Example of cure depth of the system with 10% Capa R=2 21
Figure 6. Components in the building plate obtained after printing 23
Figure 7. Green parts after removal and cleaning process 23
Figure 8. TGA analysis of individual monomer system components 24
Figure 9. TGA analysis of polymerized system 22 with powder and without powder 24
Figure 10. Temperature profile of one debinding process 25
Figure 11. Temperature profile of sintering process 25
Figure 12. Green part - 10%Capa R2 building direction: z 26
Figure 13. Particle size distribution 3Y-TZP - without milling 28
Figure 14. Particle size distribution 3Y-TZP - milled for 2 days 29
Figure 15. Surface area of Zirconia powder from Tosoh – after 2 days milling 29
Figure 16. Effect of dispersant in the suspension at different shear rates 30
Figure 17. Viscosity of suspensions at different shear rates 31
Figure 18. Effect of diluent in the viscosity of the suspensions 31
Figure 19. Effect of diluent in suspensions with R2 32
Figure 20. Effect of R in systems with 10% and 20% diluent 33
Figure 21. Effect of mixing ratio R and diluent on the cure depth 34
Figure 22. TGA analysis of system 22 and individual components 35
Figure 23. Heat treatment up to 150C - 10%CapaR2 36
Figure 24. Debinding process - 10% Capa R2 36
Figure 25. ZrO_2 after debinding process – x-y plane – 10% Capa R2 37
Figure 26. ZrO_2 after burn-out at 300C in direction: z - 10% Capa R2 38
Figure 27. Sintered Zirconia 3Y-TZP - building direction: z 39
Figure 28. 3Y-TZP microstructure after thermal etching at 1300ºC 40
Figure 29. Particle size analysis - 3Y-TZP Daiichi powders 42
Figure 30. Particle size analysis - Mg-TZP Daiichi powders 42
Figure 31. Particle size analysis - 12Ce-TZP Daiichi powders 42
Figure 32. Viscosity of different Zirconia powders 43
Figure 33. Cure depth of different Zirconia powders 44
Figure 34. Mg-TZP sintered component - building direction: x-y plane 44
Figure 35. Microstructure after thermal etching - Mg-TZP 45
Figure 36. Microstructure comparison between Mg-TZP (left) and 3Y-TZP (right) 46
Figure 37. EDS point and map analysis - Mg-TZP 46
Figure 38. EDS analysis results - Mg-TZP 47
Figure 39. Final components - 3Y-TZP and Mg-TZP 47

III. List of tables

Table 1. Physical properties of Zirconia [11] 3
Table 2. Crystallographic correlations in cubic Zirconia. [12] 4
Table 3. Crystallographic correlations in tetragonal Zirconia. [12] 4
Table 4. Crystallographic correlations of monoclinic Zirconia. [12] 5
Table 5. Young's and shear modulus of monoclinic Zirconia. [12] 6
Table 6. Characteristics of 3Y-TZP powder from Tosoh [37] 18
Table 7. Components of the resin 19
Table 8. Zirconia suspensions prepared, 45 Vol%. 20
Table 9. Suspension preparation - System 22 20
Table 10. Printing parameters - Lithoz CeraFab7500 22
Table 11. Characteristics of different Zirconia powders from Daiichi [38] 27
Table 12. Effect of milling and freeze drying in the particle size 28
Table 13. Particle size analysis after 2 days of milling – powders from Daiichi 41
Table 14. Surface area of different Zirconia powders 43
Table 15. Density measurements - 3Y-TZP and Mg-TZP 45

IV. Abbreviations

AM – Additive Manufacturing

SL – Stereolithography

LPBF – Laser Powder Bed Fusion

3Y-TZP – Yttria Stabilized Zirconia

Mg- TZP – Magnesia Stabilized Zirconia

12Ce-TZP – Ceria Stabilized Zirconia

PNPGDA – Neopentyl glycol propoxylate diacrylate

BIS-EDA - Bisphenol A ethoxylate diacrylate

CAPA 2054 – linear diol polyester derived from caprolactone monomer

PPG 400 – Polypropylene glycol

1. Introduction

1.1. Background of the project

Swerea IVF is a subsidiary of the Swerea Group that mainly conducts research and development for manufacturing and engineering industry. One of the company's main focuses is in the area of additive manufacturing (AM). This is a general term for fabrication methods based on layer by layer buildup of components. There are several AM technologies available for manufacturing of ceramic components such as Powder Bed Fusion, Material Jetting, Binder Jetting and VAT Photopolymerization. In this last category there is a technique known as Stereolithography (SL) [1-6].

SL is an important additive manufacturing technology for polymers which involves the curing of a liquid photosensitive polymer through the use of a light source that provides the energy for the chemical reaction (curing reaction) forming a highly cross-linked polymer [5]. This technique can be used together with powder suspensions to build ceramic components [1-6].

Conventional production processes for Zirconia materials is powder compaction followed by green machining or injection molding and densification as a final step. This process limits the complexity and freedom in design of the component that can be fabricated and additive manufacturing may thus be an interesting option that offers the possibility to make more complex components in shape, lightweight and flexible manufacturing [4]. However, there are some restrictions and limitations with AM process used for the Zirconia material. The main issue is the mechanical performance of the commercial material, which only reaches around 60% of the strength when compared to conventional prepared materials [1-6].

The high toughness that can be obtained in Zirconia ceramics is dependent on the phase transformation. Tetragonal grains can be transformed to monoclinic when exposed to an external stress inhibiting crack propagation. This makes Zirconia and Zirconia based materials to be among the strongest and toughest ceramics available, which makes them attractive in several demanding applications such as dentistry, medical implants, knives and bearings [3].

Swerea IVF currently has a SL printer machine acquired from Lithoz GmbH available for manufacturing components in Alumina, Zirconia and Hydroxyapatite. A new monomer resin that works for AM of Zirconia ceramics have been developed at Swerea IVF. Initial evaluation of the prepared materials indicated strength almost at the same level as reported from the commercial materials [1-6].

1.2. Project Aim

The aim of the project is to improve the overall process and reliability of the AM Zirconia material to reach a strength level that is comparable to materials prepared from conventional processes.

1.3. Scope

The project will be focused on improving the overall process of Zirconia 3D printed components using the printer provided by Lithoz GmbH and available at Swerea IVF. This will include powder characterization, preparation of suspensions, printing of components, debinding and sintering process.

1.4. Project Report Outline

The report contains 5 chapters; An Introduction to the topic, a Literature Review relevant to the work done. Experimental Procedure, Results and Discussion and finally Conclusions of the work. References, Acknowledgments and Appendices are presented at the end of the report.

2. Literature Review

2.1. Overview of Zirconia

Engineering ceramics such as oxides, carbides, and borides have a unique combination of mechanical, chemical and thermal properties. They can be used in highly demanding applications such as aerospace, automotive, electronics, and biomedicine. Zirconium dioxide (ZrO_2) or Zirconia provides high toughness, thermal insulation, biocompatibility and ion conductivity. Typical applications are found in body implants, dental crowns, stamping dies, oxygen sensors, and micro components.

Zirconium (Zr) element was discovered by the German chemist Martin Heinrich Klaproth in 1789. After his discovery, the oxide was used as a pigment for several years. It was not until the end of the sixties that researchers started to consider this material in biomedical applications. Zirconium oxide as a new material for hip head replacement instead of titanium was first used in 1969 [7].

Fully stabilized Zirconia also has applications as an electrolyte in solid oxide fuel cells, oxygen sensors, and electrochemical reactors due to several properties such as high ionic conductivity, thermal and chemical stability and mechanical strength [9].

Pure Zirconia is monoclinic at room temperature and atmospheric pressure, increasing the temperature transforms the material to tetragonal phase at approximately 1170 °C and to a cubic phase at 2370 °C. The melting point occurs at 2716°C. These transformations are martensitic therefore three main characteristics are distinguished. The transformation is diffusionless with no movement of atoms, only coordinated shifts in the lattice positions. This process occurs at a temperature range instead of a specific temperature and finally, a shape deformation takes place in the material [8].

The tetragonal to monoclinic phase transformation involves a volume expansion of about 7%. Zirconia is partially stabilized above 1700°C in the cubic phase that results in grain sizes around 50 to 70 microns. When the material is cooled, tetragonal precipitates can be formed in the cubic phase matrix. The combined cubic and tetragonal phase result in a stronger material. When the precipitates expand due to transformation to monoclinic phase, crack closure occurs and inhibits its propagation in the material. The main properties of Zirconia are shown in table 1 [11].

Property	Values		
Polymorphism^{a,b}	Monoclinic - Tetragonal	1273 - 1473 K	
	Tetragonal - Cubic	2643 K	
	Cubic - Liquid	2953 K	
Crystallography	Monoclinic	Tetragonal	Cubic
a	5.1454 Å	3.64 Å	5.065 Å
b	5.2075 Å	5.27 Å	
c	5.3107 Å		
β	99°14'		
Space Group	$P2_1/c$	$P4_2/nmc$	Fm3m
Density (g/cm^3)	Monoclinic	Tetragonal	Cubic
	5.68	5.86^{a}	6.29^{b}
Thermal Expansion Coefficient (10^{-6}/K)	Monoclinic	Tetragonal	
	7	12	
Heat of Formation (kJ/mol)	-1096.73		
Boiling Point (K)	4549		
Thermal Conductivity (W/m/K)	at 100°C	1.675	
	at 1300°C	2.094	
Mohs hardness	6.5		
Refractive index	2.15		

Table 1. Physical properties of Zirconia [11]

Most engineering applications involve components with tetragonal or cubic phase. The usage of pure Zirconia is rare. In recent years cubic Yttria-stabilized Zirconia has been investigated as Yttria (Y_2O_3) stabilizes high temperature phases at room temperature. The addition of yttrium oxide greatly increases the electrical and mechanical properties of Zirconia. Stabilized Zirconia can be found as thermal coatings in combustor liners, transitions sectors, nozzle guide vanes and rotor blades. This is one of the most important applications due to its low thermal conductivity, high temperature stability in oxidizing and reducing environments, thermal expansion similar to iron alloys and high toughness. The usage of Zirconia coating increases the operational temperature of engines up to 200ºC and therefore increases the efficiency [12].

Another common application of Zirconia is oxygen sensors due to the high ionic conductivity of Y_2O_3 or CaO doped Zirconia. When a sensor is exposed to a gas that requires oxygen measurements, the difference in partial pressures of oxygen between the inside and outside of the sensor drives the oxygen transport through the ceramic. This can be translated to a voltage measurement. A similar application can be found in solid oxide fuel cells. The cell converts chemical energy into electrical energy and consists of two electrodes and an electrolyte in the middle in a sandwich structure. At the interface of the electrode and the electrolyte, oxygen dissociates and travels across the electrolyte by ionic conduction. Typical solid fuel cells are made of Zirconia doped with 8 mol% of Y_2O_3 as the electrolyte [12].

A unique combination of mechanical and optical properties can be achieved by polycrystalline cubic Zirconia with 8 mol% of Y_2O_3. The cubic phase has a refractive index of 2.2 which is higher than other oxides (refractive indexes are commonly between 1.0 and 2.0). The combination of high transparency, large refractive index, and high dielectric constant make this ceramic material interesting for optical applications [11].

2.2. Crystal Structures of Zirconia

2.2.1. Cubic Zirconia

Cubic Zirconia has a fluorite structure. The cell contains one Zr ion located at (0, 0, 0) coordinated with eight equidistant oxygens. Two oxygen ions in the positions (1/4, 1/4, 1/4) and (3/4, 3/4, 3/4) are coordinated to four zirconium ions. Zr ions constitute the FCC structure. Crystallographic correlations are presented in table 2. Measurements of lattice parameters a_c at 2683, 2388 and 2503 K show 0.5269, 0.52438 and 0.5247 nm respectively [12].

Space Group	Fm3m
Reflection Conditions	hkl: h+k, k+l, l+h = 2n 0kl: k,l = 2n hhl: h+1 = 2n h00: h = 2
Coordination Number	8
Z	1
Lattice Parameter	a_c
Unit Cell Volume	$V_c = a_c^3$
Ionic Positions	Zr^{4+} : 4a O^{2-}: 8c

Table 2. Crystallographic correlations in cubic Zirconia. [12]

2.2.2. Tetragonal Zirconia

Tetragonal Zirconia is a result of movement of oxygen anions along one of the cubic axes in the fluorite cubic structure which results in a tetragonal distortion along the axis. The two zirconium ions are located at (0, 0, 0) and (1/2, 1/2, 1/2). The four oxygen ions are located at (0, 1/2, z), (1/2, 0, -z), (0, 1/2, 1/2+z) and (1/2, 0, 1/2-z) where z=0,185. This configuration gives a tetragonal BCT structure [12]. Crystallographic correlations are shown in table 3. The transformation from cubic to tetragonal structure is displacive. This means that four Zr^{+4} cations in the 4a cubic positions separate in two groups to occupy the 2b positions in the tetragonal structure. The O^{2-} anions in the 8c cubic positions also divide into two groups in order to occupy the 4d positions in the structure. The *a* and *b* axes directions in the tetragonal structure are 45° shifted compared to the cubic structure. The c axis in both structures remains unchanged [12].

Space Group	$P4_2$/nmc
Reflection Conditions	kh0: h +k = 2n hhl: l=2n 00l: l=2n h00: h=2n
Coordination Number	8
Z	2
Lattice Parameter	$a_t=b_t \approx a^*/2^{1/2}$ $c_t \approx a^*$
Unit Cell Volume	$V_t \approx V_c/2$
Ionic Positions	Zr^{4+} : 2b O^{2-}: 4d

Table 3. Crystallographic correlations in tetragonal Zirconia. [12]

2.2.3. Monoclinic Zirconia

The structure of monoclinic Zirconia consists of layers of triangular coordination polyhedra of three O_1-Zr bonds and 4 distorted tetrahedral O_2-Zr bonds. This results in seven oxygen ions around Zirconium. The crystallographic correlations are shown in table 4. The distance between Zr and O is around 0.1885 to 0.2360 nm for the O_1-Zr cell and 0.1914 to 0.2511 nm for the O_2-Zr cell [12].

The average distance between Zr-Zr subshells is 0.372 nm. Zr ions form layers parallel to the (100) planes of the unit cell with O_1 ions on one side and O_2 ions on the other side. The distance between layers of Zirconium ions is larger when they are separated by O_1 ions [12].

Space Group	$P2_1/c$
Reflection Conditions	h0l: h+l = 2n
	0k0: k=2n
	h00: h=2n
	00l: l=2n
Coordination Number	7
Z	4
Lattice Parameter	$a_m \neq b_m \approx a_c$
	$c_m > a_c$
Unit Cell Volume	$V_m \approx 2V_c$
Ionic Positions	Zr^{4+} : 4e
	O_I^{2-}: 4e
	O_{II}^{2-}: 4e

Table 4. Crystallographic correlations of monoclinic Zirconia. [12]

2.3. Mechanical Properties

Ceramic materials are brittle by nature. There are two main explanations for the lack of plasticity in these materials. In first place, the nature of the bonding is ionic and/or covalent; they have a nonsymmetrical crystal lattice and there are limited slip systems in the structure. According to Von Mises rule, five independent slip systems are required for general homogeneous plastic deformation which allows free dislocation movement from one grain orientation to another. Most ceramics have one or two slip systems at room temperature while metals tend to have five or more. The second aspect to be considered is the inherent flaws in the material during fabrication that act as stress concentration sites and contribute to brittle fracture of the material. [8-10].

In addition to brittleness, ceramic materials have high costs. There are high levels of rejection during manufacturing due to internal and surface flaws which increase the cost of the components.

Research and development are being done to increase the toughness of parts that can reduce the level of rejection in production and increase the reliability during service. The most important toughening mechanism for Zirconia is transformation toughening discovered by Garvie et al. in 1975 [8-10].

Mechanical properties of cubic and tetragonal phases are difficult to measure given the high temperatures required for those measurements. Monoclinic Zirconia is the only phase extensively studied in pure form. Properties of cubic and tetragonal phases have been determined for many stabilized Zirconia materials since these materials have more important engineering applications.

2.3.1. Elastic Properties

Measured elastic stiffness and compliance moduli for monoclinic Zirconia are shown in table 5. The Young's modulus and shear moduli are determined by Voigt, Reuss, and Hill approximations. Voigt and Reuss approximations give upper and lower limits. 10% error is common between these values but it can increase up to 20% for some transverse directions in the crystal. Monoclinic and tetragonal structures have a bulk modulus between 150-200GPa. Cubic Zirconia is between 171-288GPa. [12].

	20°C	300°C	600°C	800°C
E_{Voigt}	266	256	250	245
E_{Reuss}	215	216	220	222
E_{Hill}	241	236	235	234
G_{Voigt}	104	99.1	96.8	94.9
G_{Reuss}	83.4	83.2	84.7	85.3
G_{Hill}	93.6	91.1	90.7	90.1

Table 5. Young's and shear modulus of monoclinic Zirconia. [12]

2.3.2. Hardness

Hardness of Zirconia materials depends on the density and addition of dopants. Zirconia with a density higher than 98% has hardness around 9,2GPa while densities around 95% of the theoretical density have a hardness between 4.1 to 5.2GPa. Zirconia stabilized by 1.5% Yttria increases the hardness significantly achieving hardness around 11GPa in tetragonal form. Higher amounts of Yttria can give hardness values up to 15GPa [12].

2.3.3. Creep

The creep rate in ceramics is affected by different parameters such as temperature, stress, crystal structure, and microstructure. The instability of pure Zirconia makes creep measurements difficult to perform. Most of the experiments on creep behavior were performed on stabilized Zirconia. 6 mol% of Yttria stabilized Zirconia will transform from tetragonal phase into a distorted cubic (fluorite structure) at approximately 700°C. This means that creep tests done between 1100 to 1500°C will correspond to the cubic fluorite structure [13]. The activation energy for creep in monoclinic Zirconia has been reported to be 330-360 kJ mol^{-1} and stress component values between diffusional creep and superplastic deformation by two different authors showed that creep deformation is likely due to superplastic deformation [3, 12].

Creep resistance of single crystals is better than polycrystalline ZrO_2. This effect is strongly related to the grain boundaries. The rate controlling mechanisms at high temperatures (>1500°C) is dislocation climb. At low temperatures (<1500°C) the controlling mechanism is dislocation cross-slip. [13].

2.3.4. Toughness

Monoclinic Zirconia toughness measurements is difficult to obtain given the difficulties to sinter this type of material. When the material is heated above the tetragonal-monoclinic transformation temperature (1471K) to achieve full density, the material is prone to cracking upon cooling. Studies with nanocrystalline monoclinic Zirconia showed that it can be sintered at a lower temperature (1273K).

Cracking can be avoided but this type of material has not been tested for toughness [12].

Porous specimens of monoclinic Zirconia have been evaluated for fracture toughness. Experiments with 92.2±0.4% density gave a value of 2.06 $MPam^{1/2}$ and extrapolating these results to a full density material gives a value of 2.6 $MPam^{1/2}$. The fracture toughness of this phase is low as well as the toughness of cubic Zirconia which is has been reported as 1.8 and 2.8 $MPam^{1/2}$ by different authors. [12]. The addition of alloying elements such as Y^{3+}, Ce^{3+} and Mg^{2+} stabilizes tetragonal phase which increases the fracture toughness. This process is called transformation toughening.

2.3.5. Toughening Mechanism of Zirconia

As mentioned before, transformation toughening mechanism is the most important process to increase the toughness of Zirconia materials. Crack shielding is known as a stress-induced microstructural change that reduces the stress at the crack tip. This also affects a zone around the crack. There are several types of crack shielding such as microcracking, ductile zone and transformation zone. Among these, the introduction of transformation zone or toughening is a relatively new approach to obtain high toughness and strength in ceramics.

Zirconia is used for this purpose, given that martensitic transformation from tetragonal to monoclinic phase during cooling takes place in a temperature range from 1150°C to 1000°C. By controlling the composition, particle size and heat treatment cycle, Zirconia can be sintered at high temperatures and cooled so that the tetragonal phase is maintained as individual grains or as precipitates to room temperature [3].

Tetragonal phase is not stable at room temperature and therefore it will spontaneously transform to monoclinic phase. This process will involve a volume increase and if the grain size is small enough (≤0.5μm), the strength of the grains will prevent the volume expansion and thus the transformation. When a stress is applied to the material and a crack tries to propagate, the metastable tetragonal grains near the crack tip will expand and transform to stable monoclinic phase. This martensitic transformation around the crack tip will put the crack under compression preventing propagation. Additional tensile stress will be required to extend the crack resulting in a very tough and strong ceramic that has been referred to as “ceramic steel” by some authors [3]. In figure 1 we can observe the transformed zone around the crack and crack tip creating compressive stresses that close the propagating crack.

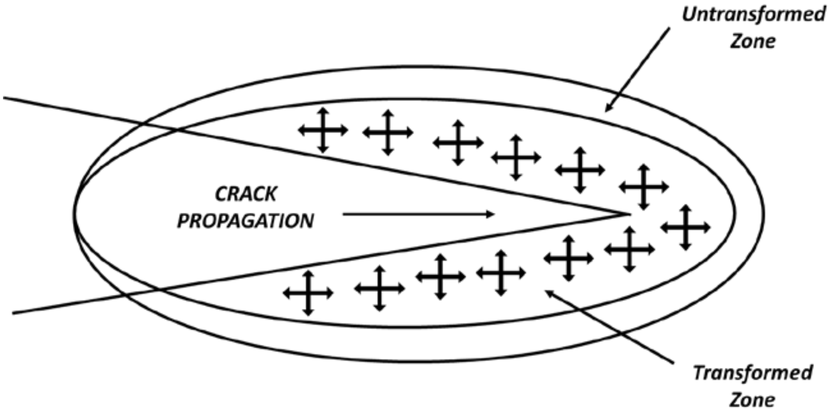

Figure 1. Representation of transformation toughening in ZrO_2

Pure ZrO_2 does not have transformation toughening behavior and additives are necessary for this purpose. CaO, MgO, Y_2O_3, CeO_2 and other rare earth oxides are commonly used. An excess in the use of additives will stabilize cubic Zirconia phase which does not have transformation toughening either. The toughening mechanism requires tetragonal metastable phase.

This transformation toughening is not limited to stabilized ZrO_2 entirely. Small grains of Zirconia can be added to other ceramics and retained as tetragonal phase during cooling. These small grains can transform near the crack tip and prevent propagation in the same way.

To obtain a component with a tetragonal phase using CaO or MgO as additives, the material is generally shaped in the first place. After the material has the desired form, it is sintered to obtain a uniform polycrystalline structure. The next step is to quench the component to retain the tetragonal phase and aged in the last stage to allow grain growth to an optimum size.

Tetragonal precipitates have also been obtained in single crystals of Zirconia using CaO, MgO, and Y_2O_3. Single crystals are grown at high temperatures and then heat treated to precipitate tetragonal particles in the cubic phase.

Another approach is also used to obtain tetragonal phase in the material. Very fine ZrO_2 powder (<0.3μm) with 2 to 3 mol% Y_2O_3 can be densified to obtain fine tetragonal microstructure inside the grains. Each grain in this material can transform near the crack tip to prevent crack propagation. Similar grains can be obtained with CeO_2 [3].

Materials containing tetragonal and cubic phase are usually referred to partially stabilized Zirconia PSZ. The prefix is usually the element used as additive such as Ca-PSZ, Mg-PSZ or Y-PSZ. If enough additive is added and the powder only contains cubic phase it is referred as fully stabilized Zirconia. Y_2O_3-ZrO_2 and CeO_2-ZrO_2 materials that contain only tetragonal phase are called tetragonal Zirconia polycrystal Y-TZP or Ce-TZP.

For toughening through phase transformation, tetragonal phase must be able to transform to monoclinic. Above 1150°C, tetragonal phase is in equilibrium and no toughening takes place. Transformation toughened ceramics will exhibit a reduction in strength as temperature increases. Therefore, Zirconia materials are sensitive to thermal aging. Mg-PSZ and Ca-PSZ show changes in grain size and size of precipitates around 1000°C that result in an increase of monoclinic phase and reduction of tetragonal phase. This will cause a reduction in strength and toughness [3].

2.4. Corrosion Resistance of ZrO_2

Zirconia behaves like an acid in presence of strong bases and like a base with strong acids. Metals of the 5th, 6th, and 7th group of the periodic table do not react with Zirconia. It shows stability and low solubility with basic and acid glasses. Molten neutral salts do not corrode ZrO_2. However, molten alkali silicates strongly attack the material.

Si and Ti do not react with ZrO_2 at low temperatures. However, at high temperatures (1800°C) and in vacuum, Si reduces ZrO_2 and Ti becomes partially oxidized with ZrO_2.

At elevated temperatures and presence of Carbon, Zirconia can form ZrC according to the reaction shown below [10].

$$ZrO_2 + 3C \rightarrow ZrC + 2CO$$

2.5. Biological Properties of ZrO_2

A high isoelectric point, chemical inertness, lack of toxicity, pH stability and availability of oxygen groups in ZrO_2 are important properties for immobilization of biomolecules. In vitro and in vivo studies confirmed the high biocompatibility of Zirconia and even higher when the material is purified from radioactive elements, this material is called bioceramic ZrO_2. When inserted in the body no local reaction is observed in the tissue. Prostheses that are highly polished can contact very easily with gum tissue and chemical inertness provides good cell adhesion with no systemic reactions [7, 14].

Toxicity of ZrO_2 is lower than titanium oxide and similar to alumina. However, radioactive elements like Thorium (Th) and Uranium (U) can be present in the material. These elements can emit two types of radiation, alpha and gamma. Alpha emission was observed in ZrO_2 used for implants due to high ionization of the oxide. This type of emission can damage cells of hard and soft tissues. Gamma radiation associated with Zirconia it is not significant. Despite all the advantages of bioceramic ZrO_2, purification is very expensive and can be difficult to achieve [7, 14].

2.6. Electronic Properties of ZrO_2

Doped cubic Zirconia is commonly used for high temperature applications due to its high ionic conductivity at medium and high temperatures. In tetragonal Zirconia the conductivity depends on oxygen pressure and the material can have both, electronic and ionic conductivity. The contribution of ionic conductivity is large in most cases except at high temperatures or low oxygen partial pressure. The electronic conductivity at 1400°C and low oxygen pressure come from double charged oxygen vacancies. The movement of oxygen is preferential along two directions in the tetragonal structure, the x-y plane along the [100] direction and the perpendicular direction to the x-y plane in the [001] direction [12].

Monoclinic Zirconia can have electronic and ionic conductivity that also depends on temperature and oxygen pressure. At low pressure, the charge carriers are double charged oxygen vacancies commonly known as n-type behavior. At high pressure, the material has a p-type behavior where the charge is carried by single ionized oxygen interstitials [12].

When the pressure is constant and the temperature is increased the conductivity can also increase. At lower temperatures (<600°C) the conductivity is ionic while at higher temperatures (>700°C) the conductivity is electronic. Between 600 and 700°C the conductivity is both electronic and ionic [12].

2.7. Zirconia Powders

Zirconium dioxide or Zirconia (ZrO_2) is usually obtained from zircon ($ZrSiO_4$). Several processes are available for production of Zirconia such as chlorination-thermal decomposition, lime fusion, and alkali oxide decomposition [10].

The main production process is electric arc melting of Zircon at temperatures around 2100 to 2300°C. Dissociation can be achieved at these temperatures and solid Zirconia is produced along with liquid silica, achieving a purity of 99% [15].

Zircon can also decompose by injecting zircon sand in plasma with temperatures above 6000°C. Zirconia is solidified and along with silica as a glassy coating. The coating can be removed afterward by leaching in hot sodium hydroxide solution and Zirconia is recovered by centrifugation [15].

In the chlorination-decomposition process zircon is chlorinated in an electric furnace with carbon after milling and pelletizing according to the following reaction:

$$ZrO_2.SiO_2 + 4C + 4Cl_2 \rightarrow ZrCl_4 + SiCl_4 + 4CO$$

After heating to 800-1200°C, Zirconium chloride $ZrCl_4$ is distilled and condensed at 150°C. Silicon Chloride is condensed at -10°C. Hydrolysis is then conducted with water to produce a solution of zirconium oxychloride and crystals are obtained by cooling and separation of the solution at 85°C. Zirconium oxide is recovered by calcination of the crystals [10].

Zirconia can also be found in nature as baddeleyite mineral which is impure monoclinic Zirconia often containing small contents of hafnium oxide (1,5-3%wt) and a double oxide compound of Zirconia and silica ($ZrO_2.SiO_2$) [10]. The mineral also contains other contaminants such as silica, iron oxide and rutile. The high similarity between Hf and Zr makes the separation expensive. Usually, technical grade Zirconia is sold with a content of Hf up to 3% [15].

2.8. Powder Processing

Ceramic powders must be selected according to the properties required in the final component. Purity, particle size, reactivity, and morphology can affect the properties and must be carefully considered before selecting the powder for manufacturing [3].

Purity affects high temperature behavior, strength, and oxidation resistance. The effect of impurities depends on the chemistry of the impurity and the matrix. Inclusions may not affect properties like creep or oxidation resistance, but these impurities can act as stress concentrator sites and reduce the tensile strength. The effect of inclusions depends on the particle size of these inclusions compared to the grain size of the ceramic material [3].

Particle size is a major factor to be considered in order to achieve full packing and uniformity in the component, also to obtain low porosity and minimum shrinkage.

A single particle size powder will not achieve full density in the component due to the voids created in between the particles and therefore a particle size distribution is desired [3].

Reactivity of ceramic powders is also very important to achieve full density. The driving force for densification is the change of surface free energy. Small particles with high surface area have high surface free energy and thus high thermodynamic drive to decrease the surface area by bonding with adjacent particles at high temperature [3].

2.8.1. Ball Milling

In most cases, screening, classifying or elutriation of powders is not enough to achieve the desired particle size. Thus, a reduction process is needed. Ball milling is a common process where particles are placed in a cylindrical container along with cylindrical or spherical grinding media made of hard material. The container rotates around its axis creating a cascade effect of the grinding media along with the particles and the powder is fractured by shear forces and impact. Milling process can be done in a wet or dry environment [3] [10].

Ball milling produces a broad range of particle size distribution with smaller grains opposite to screening which produces a narrow distribution. Particle sizes of 5μm or less can be only obtained by milling. In addition, the milling process can produce an active powder that is easier to densify in later processes creating an active surface and increased strain energy in the particle [3].

2.8.2. Freeze Drying

Manufacturing of ceramics usually requires a granulation operation to obtain free flowing granules with high homogeneity. Commonly used methods involve drying in air with liquid transport in the granules. These methods are sensitive to segregation of binder and small particles to the periphery. Therefore, granules will not disintegrate properly resulting in poor properties in the material [16].

Freeze granulation or lyophilization sprays the powder into liquid nitrogen and the granules are instantly frozen. The granules are then dried by sublimation and water is separated from the solid phases without segregation effects. Freeze drying offers control over the particle shape obtaining softer particles compared to other methods. This allows to obtain a homogeneous green body in the shaping stage of the manufacturing process [16, 17].

After freeze drying the particles show spherical shape, free flowing of granules and are easily crushable. This is beneficial for obtaining dense components minimizing the risk of defects caused by granule defects. This procedure has shown to effectively eliminate the capillary forces which are the origin of agglomeration of particles [16, 17].

2.9. Additive Manufacturing of Ceramics

Conventional shaping methods for ceramics like dry pressing, isostatic pressing, slip-casting, tape-casting and injection molding are widely used to manufacture Zirconia parts. However, these methods present various limitations and cannot be used to manufacture complex shapes and parts with high dimensional accuracy. These processes are also time consuming and expensive due to the need of a mold and post-machining processes like cutting and grinding [18].

An alternative to conventional methods that allows manufacturing of complex parts is additive manufacturing. AM is defined by ASTM F2792-12a (Standard Terminology for AM) as “a process of joining materials to make objects from 3D model data usually layer upon layer as opposed to subtractive manufacturing” [18-21].

The component is build based on a CAD 3D model that is later converted into an STL file. The file is manipulated and transferred to the printing machine to be sliced into thin layers. The component is then printed layer by layer. After the printing is complete, post-processing steps are needed to obtain the final part.

This technology offers a good alternative to manufacture ceramic parts quicker, without molds and without the need of change the manufacturing process or parameters if the geometry of the part changes [18-21].

The materials used in 3D-printing of ceramics are usually fed as a powder/granulate or as a paste or suspension that allows easy deposition of layers. The material is built in the desired shape with sufficient mechanical strength to be transferred to the next processing steps which are generally heat treatment processes [19]. At first, the AM technologies were developed to allow flexibility in the design. Today the physical and mechanical properties are most important and AM of polymeric and metallic materials have been successful in fulfilling these requirements. However, there are some challenges associated with AM of ceramics depending on which type of material is required.

Additive manufacturing technologies can produce either porous components or fully dense monolithic components. A major part of the research in AM of ceramics is focused on porous structures given that this type of structure is desired for biomedical, lightweight, and other applications, and AM technologies are suitable for these types of materials [19]. The main reason of success is that residual and random porosity is often tolerated and even desired in such components. AM technologies that can produce fully dense ceramic bodies and at the same time maintain and/or achieve the required physical and chemical properties is, still a challenge [19, 21].

Additive manufacturing of ceramics can be divided into direct processing and indirect processing. Selective Laser Sintering (SLS) is a direct process where components are fabricated directly from loose powder by selective fusion of the material. Stereolithography (SL) is an indirect process based on photopolymerization of a liquid monomer system filled with ceramic particles [18].

Selective Laser Sintering can also be categorized in direct or indirect manufacturing. Indirect SLS is based on a slurry containing a sacrificial organic binder to produce green parts and then sintered to produce the final component. Direct powder bed fusion (PBF) does not involve a binder phase [22].

PBF uses a laser beam as a power source to selectively melt the powder. In principle, any material available as a powder can be used. Local melting of the material is particularly difficult when powders of high melting point are used. This is the case of ceramics. Densification of these materials is a solid-state diffusion process that requires high temperature and time to obtain full density that is difficult to achieve with the laser source. Another issue with this technology is the internal stresses caused by local melting and cooling and low thermal shock resistance of ceramics that can lead to cracks in the consolidated components [20, 21].

Hence, the SL process is one of the most important AM technologies for fabrication of ceramics. The main aspects of this technique are explained in the following sections.

2.10. Stereolithography of Zirconia

The beginning of stereolithography technology was in the middle of 1980’s when Charles Hull experimented with UV curable materials. He discovered that specific patterns using a scanning laser could be used to create solid layers and even more curing one layer over another could be done to create a solid 3D part [1].

Manufacturing of ceramic components using Stereolithography requires a resin system containing a photosensitive monomer and a ceramic powder. The layer by layer build-up of the part is similar to other AM technologies. Thus, the resin system or suspension containing the monomer and the powder is spread in a plane surface and specific areas in the surface are irradiated with UV light to cure the monomer and produce a single polymerized layer. These layers are stacked and cured together to form the 3D part [21-23].

For photosensitive liquids, the profile of cure is defined by the line width L_w and the cure depth C_d. Jacobs’s equation derived from Beer-Lambert law of absorption can be used to determine the cure depth:

$$C_d = D_p \ln\left(\frac{E_{max}}{E_c}\right)$$

In this equation D_p is the penetration depth of the light, E_{max} is the peak value if the light exposure and E_c is the minimum exposure to light needed to initiate the polymerization of the monomer. The line width can be calculated by the following equation where W_o is the Gaussian half-width of the light beam [20, 23].

$$L_w = \sqrt{2} W_o \sqrt{\ln\left(\frac{E_{max}}{E_c}\right)}$$

These relations provide a good approximation for curing pure monomers. However, when ceramic suspensions are used the behavior is different. The particles are chemically inert and interfere with the polymerization by scattering and absorption. Kubella-Munk model can be used to calculate the energy released at a certain cure depth z in ceramic suspension using the following equation [20]:

$$E = E_{max} e^{[-(\sqrt{K(K+2S})Z]}$$

Where S is the specific scattering coefficient and K is the specific absorption coefficient. These parameters mainly depend on the total reflectance, optical thickness and physical density of a layer. Applying this model, the cure depth is proportional to the difference between reflective indices of the monomer n_o and the ceramic particles n_p $\Delta n = (n_o - n_p)$, the average size of the ceramic particles d_{50} , the volume fraction of the ceramic particles in the suspension ϕ and the scattering efficiency Q [20, 23]:

$$D_p = \frac{2}{3}\left(\frac{d_{50}}{\phi Q}\right)\left(\frac{n_o}{\Delta n}\right)^2$$

Monomers used in the suspension do not produce initiating species upon radiation, therefore, organic molecules with low molecular weight or initiators must be added to the system. The curing reaction creates a highly cross-linked polymer [23].

The typical concentration of the suspension is between 40 to 60% powder in volume. Due to these high concentrations in the suspension and very fine particle size, high green densities are obtained and it is possible to obtain almost fully dense components. Different light sources can be used to cure the monomer such as UV lasers, Helium-cadmium gas lasers, argon lasers or solid-state lasers. The laser scans the contour and surface of the CAD model in the resin to create a single layer. An alternative method developed in the early 1990’s to cure layers was the UV light focused by a digital micromirror device (DMD) that generates single layer images. This technology is known as mask-projection photopolymerization. The array of mirrors of 30μm in size can project a single layer with a spatial resolution of 1.1μm [20]. The main advantage of this method is the speed compared to laser scan as one entire cross-section of the component can be irradiated at once. [1, 20, 24].

Lithoz machine CeraFab 7500 principle is based on this UV mask projection method combined with an upside building platform. The part is not fully immersed in the suspension instead, it is spread in a rotating glass plate. This allows smaller amounts of suspension required to build the part compared to other methods where the parts are immersed [19, 24]. Figure 2 shows a view of the vat where the suspension is poured and then spread by the blade when the vat rotates to create a uniform layer.

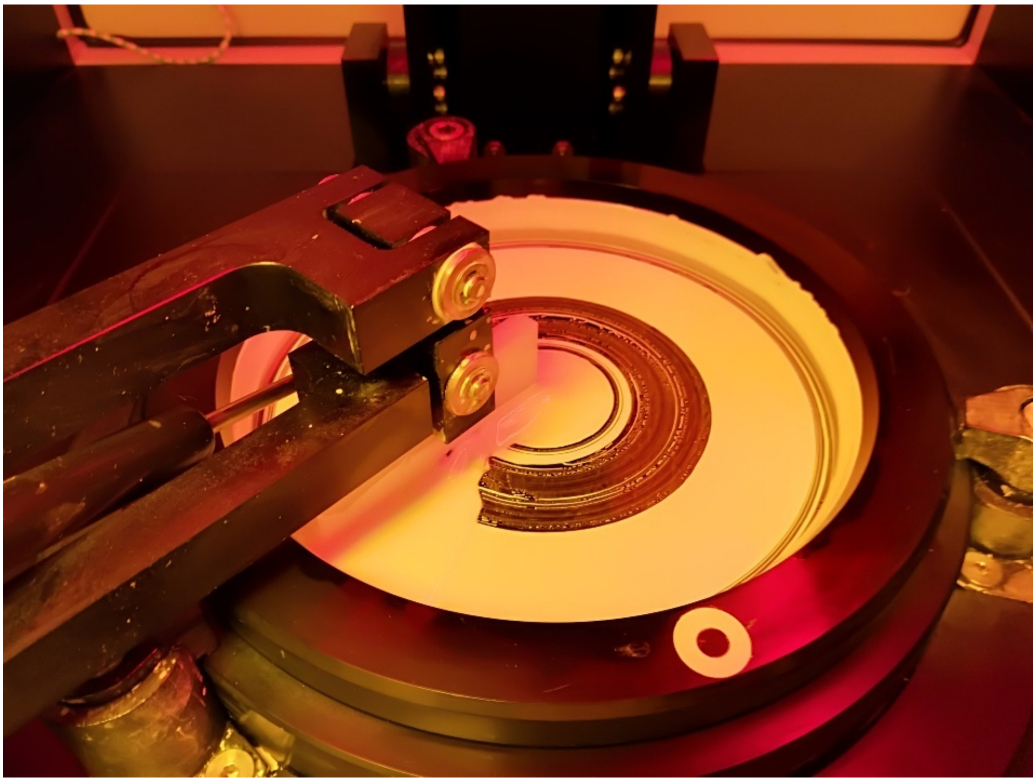

Figure 2. Mask-projection Vat-photopolymerization. View of rotating glass plate

Other companies such as CeraMaker provide printers with the same photopolymerization principle but larger building envelope. Digital Wax systems and K20 are also companies that use a laser Stereolithography principle to print ceramic composites [25].

Stereolithography of ceramics using the mask projection technique requires support structures if the component cannot support itself to the building platform given the liquid suspension cannot provide any support. Once the polymerization is complete, the photopolymer forms a stiff matrix around the ceramic particles and the green component has enough strength to maintain the original shape to be able to manipulate the piece for cleaning and removing it from the building platform. The organic phase is removed at this stage by heat treatment or debinding. The final stage is the sintering process where the component achieves its final properties.

SL process with ceramic suspensions presents two main challenges. The first one is to obtain a uniform layer and layer recoating during the entire build. The combination of ceramic powders and liquid resins increase the viscosity of the system which may cause problems during printing. Additives like diluents can be used to reduce the viscosity. However, the diluent can cause other problems such as excessive shrinkage and fragility of the components. Increasing the temperature of the suspension can also reduce the viscosity. Yet, adding a heating system for the suspension can cure the resin before the build also increasing the viscosity. The second issue is the reduced cure depth in ceramic suspensions. Ceramic particles scatter and block the light reducing the cure depth. As a consequence, the bonding between layers may be weak causing defects and cracks. The layer thickness must be reduced to ensure a sufficient cure between layers and coating or spreading such thin layers can become difficult [26].

2.11. Photocurable Ceramic Suspensions

The behavior and selection of ceramic suspensions for Stereolithography is greatly defined by two properties, the light absorption and rheology. The light absorption depends on the intensity and the exposure time. These two parameters must be properly defined to ensure a sufficient cure depth that will result in a homogenous and continuous build without defects.

Mitteramskloger et al. [24] showed that cure depth close to 150 μm are needed to increase the bonding between layers and more important to increase the structural properties of the green part during building. They concluded that higher cure depths are also helpful in the thermal post-processing of the 3D printed components improving the interlaminar bonding between layers.

The viscosity of the ceramic suspensions usually shows a non-Newtonian behavior that is shear dependent. It is very important to obtain a shear thinning suspension which will not cause problems during printing such as jamming of the coating mechanism in the printer or inhomogeneous spread of the layers.

Adding monomers with high viscosity can lead to shear thickening behavior in the suspensions. Increasing the number of ceramic particles will also increase the inter-particle adhesion resulting in a highly viscous fluid. Decreasing the particle size of the ceramic powder has the same effect on the viscosity due to high contact forces between particles [27, 28].

2.12. Removal of Organic Additives

After the green part is built the polymer matrix must be removed by heat treatment. The burn out process must be conducted carefully to avoid cracks and it is considered the most critical post-processing step in additive manufacturing of ceramics. The debinding behavior depends on several factors such as the composition of the resin, solids loading, and geometry of the component.

Pfaffinger et al. [29] found that heating the green body results in internal gas pressure due to pyrolysis of the polymer and this can lead to cracks in the piece if a certain degradation rate is exceeded. During the first stages, the diluent is evaporated and pressure inside the component increases. As a consequence, an open porosity is created in the component. As the temperature increases, the remaining diluent is evaporated and pyrolysis of the polymer is achieved. They also showed that the increase of “surface to volume ratio” contributes to a successful debinding. Thin and porous components are easier to debind than bulky samples.

Chang-Jun Bae and Halloran [30] studied the effect of residual monomer in the formation of cracks. They found that the cracks in the components might be a result of mechanical strains that are not related to pyrolysis reaction. Instead, the heat treatment can decompose the photoinitiator and release free radicals that polymerize the residual uncured monomer. Because of the polymerization shrinkage, mechanical strain could be causing cracks in the component.

2.13. Sintering

After debinding is complete, the last stage in the process is sintering or densification where pores between particles are eliminated as the component shrinks. To achieve the desired properties with Zirconia, such as high strength and fracture toughness, fully dense or nearly fully dense components are required as well as a controlled microstructure. The driving force for the sintering stage is minimization of surface energy. Y-PSZ containing 3 to 6 mol% of Y_2O_3 is sintered in the cubic phase between 1700°C to 2100°C. Tetragonal precipitates are nucleated in Y-PSZ during cooling.

These precipitates in the sintered component present equiaxed orientation and they are approximately 20nm in size [31, 32]. The densification and strength of sintered Zirconia depend on sintering temperature and can be limited by processing defects that must be minimized in previous stages of the manufacturing process.

Stawarczyk et al. [33] studied the effect of sintering temperature in Zirconia components. Measurements of optical contrast ratio, three-point flexural strength, and grain size were performed. Their results showed that increasing sintering temperatures can have a significant impact on the flexural strength of the material. The highest values of flexural strength are achieved with sintering temperatures between 1400°C to 1550°C. Temperatures above 1550°C should not be exceeded as the grain size is increased. Higher sintering temperatures can also cause migration of Yttrium to the grain boundaries which result in cubic phase in the microstructure.

2.14. Characterization of Final Components

Components fabricated using SL must have properties comparable to conventionally manufactured Zirconia when fully dense materials are required. These properties are minimum porosity, few defects, and homogeneous microstructure. The high volume fraction of monomer system used for curing and building the 3D component could lead to large defects such as porosity and cracks. Additionally, if the bonding between printed layers is weak, defects and delamination cracks could appear in post-processing steps.

A study presented by Harrer [34] examined the architecture of layers in stereolithography process and the influence on the mechanical properties. Different building directions were tested using a CeraFab 7500 printer machine. Uniaxial and biaxial strength tests were performed as well as hardness tests. Fracture surfaces were also analyzed to determine the fracture origin and defects. The study showed that five types of fracture origins can be found in the components. These are agglomerates, pores, cleaning defects, edge damage and machining damage. Among these, pores and agglomerates are the most important to control. Another type of defect that can be seen is delamination during debinding of the component. This type of defect is visible as cracks between the layers perpendicular to the building direction and they can significantly reduce the strength of the component.

Porosity in the piece can appear due to air entrapment in the suspension. High viscosity suspensions lead to pores that act as stress concentration sites. Porosity may be reduced by lowering the viscosity of the suspension and degassing the suspension by vacuum before printing [34].

Agglomerates are originated in the powder processing. This defect can be reduced by achieving a highly dispersed and homogeneous suspension. Edge damage and delamination are originated when the parts are removed from the building platform. These types of defects can be minimized by carefully handling the components after printing. If the parts are plastically deformed when they are removed or cleaned, the defect will not be eliminated after sintering. [34].

2.15. Summary of literature review

Zirconia is a technical ceramic that has outstanding mechanical properties. Transformation toughening is the most important property of Zirconia. In addition to high toughness and hardness, thermal shock and corrosion resistance, ionic conductivity and biological compatibility give this material a wide range of applications. Additive manufacturing of Zirconia extends, even more, across the spectrum of possible applications allowing fabrication of complex designs that are not possible with conventional methods.

The review of the literature on stereolithography of Zirconia materials led to the following conclusions:

- Powder characteristics and powder processing are essential to ensure a good dispersion of the powder in the photocurable suspension and avoid defects in the final component.
- Among the different additive manufacturing technologies available for ceramics, stereolithography using mask projection technique provides advantages compared to the others. The printing speed and resolution are the most important ones.
- SL of ceramics combines photocurable resins with finely dispersed powders. The rheological properties of such suspensions and light absorption define the printability. These properties depend both on the powder and the monomer system.
- After printing, debinding is the most critical stage in the post-processing. Avoiding cracks during burn out process depends on several factors and must be performed carefully to obtain fully dense components with good mechanical properties.
- Sintering is the final stage of the manufacturing process. Sintering temperature must be sufficient to obtain a fully dense material and at the same time not cause grain growth or changes in the microstructure of the material.
- Characterization of the final components can help to improve the additive manufacturing process by defining fracture origins and defects in the components.
- There is a limited amount of information regarding material properties, sintered density and strength of printed zirconia. One of the reasons for the lack of information is the difficulty to make the process reliable even though there is a commercial equipment available.

3. Experimental Procedure

3.1. Powder Characterization and processing

For this research, Yttria stabilized Zirconia TZ-3YS-E (Tosoh, Japan) powder was used as base material for the resin system development. This powder is commonly used for tape casting or injection molding followed by mechanical pressing or CIP. The main characteristics of the powder are presented in table 6.

POWDER CHARACTERISTICS	TZ-3YS-E
Y_2O_3 (mol %)	---
Actual Particle Size (µm)	0.09 (90nm)
Y_2O_3 (wt. %)	5.2 ± 0.5
HfO_2 (wt. %)	< 5.
Al_2O_3 (wt. %)	≦ 0.1 ~ 0.4
SiO_2 (wt. %)	≦ 0.02
Fe_2O_3 (wt. %)	≦ 0.01
Na_2O (wt. %)	≦ 0.06
Pigment (wt. %)	-
Specific Surface Area (m^2/g)	7 ± 2
TYPICAL PROPERTIES OF SINTERED BODY	
Density (g/cm^3)	6.05
Bending Strength R.T. (MPa)[*1]	1,200
Hardness (Hv 10)[*2]	1,250
*1: JIS R1601 (3-point bending test)	
*2: JIS R1610 (loads: 98.07N)	
*Above is typical data and not guaranteed	

Table 6. Characteristics of 3Y-TZP powder from Tosoh [37]

For particle size measurements, suspensions containing 10% volume of Zirconia in water were prepared using 4% water soluble diluent. Particle size distribution was measured using a laser diffraction technique. Four different measurements were performed: as received from the manufacturer, 24 hours milled, 48 hours milled and 48 hours milled and freeze dried. The powder was milled in a ball mill using ceramic pellets as grinding media. After milling, the powders were freeze dried using liquid nitrogen to obtain the dried powder by sublimation.

For surface area measurement, 5 grams of the powder was dried at 200ºC for 12 hours. The surface area was measured using a Nitrogen adsorption technique at different partial pressures. Two measurements were done to compare surface area, as received from the manufacturer and after milling and freeze drying.

3.2. Suspension preparation

Once the powder was completely dried, it was mixed with the monomer system by stirring in a beaker using a metallic propeller. To prepare the suspensions, a volume of 25 ml containing 45% volume of powder was mixed. The system contained the following photocurable monomers:

- Neopentyl glycol propoxylate diacrylate (PNPGDA) – Sigma Aldrich, Germany
- Bisphenol A ethoxylate diacrylate (Bis-EDA) – Sigma Aldrich, Germany

PNPGDA is a low viscosity difunctional monomer. Bis-EDA is a high density monomer with high refractive index and high viscosity. Non-reactive diluents tested were a linear diol polyester derived from caprolactone monomer (CAPA^{TM} 2054) and Polypropylene glycol (PPG-400). The photoinitiator used in all the suspensions was a phenyl-bis (2,4,6-trimethylbenzoyl)-phosphine oxide (BAPO, Irgacure 819DW). The dispersant used was a polymeric cationic dispersant for inorganic particles Hymermer^{TM} KD1-SO-(AP). Characteristics of the compounds used in the investigation can be seen in table 7.

Components	Molar M [g/mol]	Density [gr/cm^3]	Ref Index [n20/D]	Viscosity [mPa.s]
PNPGDA	328	1.007	1.446	10 --20
Bis-EDA	468	1.146	1.545	1450--1950
PPG-400	400	1.01	1.447	100
Capa 2054	550	1.05		60

Table 7. Components of the resin

The ceramic suspensions were prepared by dissolving the dispersant and the photoinitiator in the monomers and diluent applying slow heating and agitation. Once the dispersant was completely dissolved, the powder was added until and a homogenous system was obtained (see figure 3). The suspensions were de-aired in vacuum before characterization of the suspension and subsequent printing.

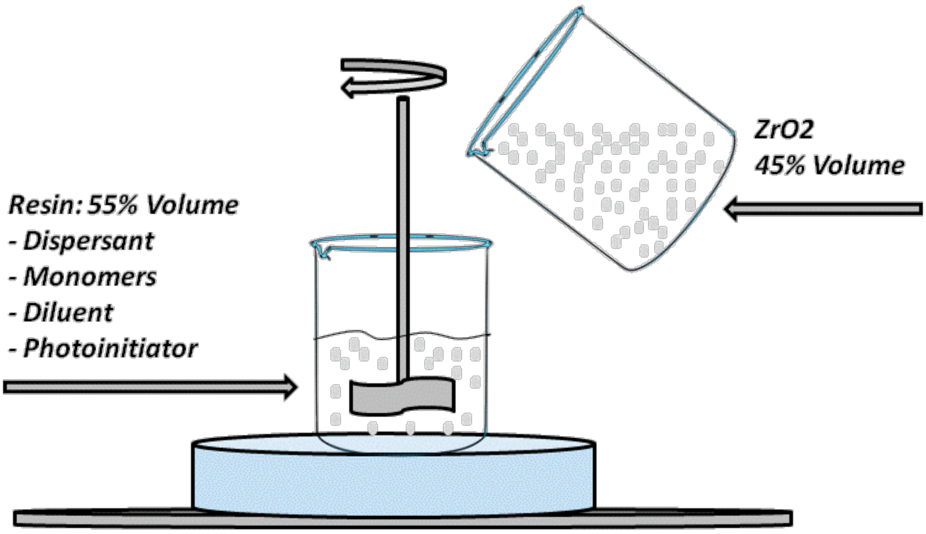

Figure 3. Schematic representation of the preparation of suspensions

Several compositions were investigated until the optimal suspension was selected based on the viscosity of the suspension, printability, and response to thermal debinding and sintering. Table 8 shows the systems prepared. The parameter R was used to express the mixing proportion between Monomer 1 (PNPGDA) and Monomer 2 (Bis-EDA). The effect of fraction of dispersant was studied with systems 1 to 7. The fraction of diluent and type of diluent were tested with systems 8 to 11. Proportions of the two monomers in the suspension was investigated with systems 12 to 18. The systems 19 to 24 were prepared to test the diluent and mixing ratio R adding 2% of dispersant. In this study, the influence of photoinitiator and solids loading was not addressed. Both were kept constant at 1% and 45 volume %, respectively.

System	% Dispersant	% PNPGDA (M1)	% Bis-EDA (M2)	% Diluent CAPA	% Diluent PPG	R M1/M2
1	0.5	100.0	0.0	0.0	0.0	-
2	0.8	100.0	0.0	0.0	0.0	-
3	1.0	100.0	0.0	0.0	0.0	-
4	1.2	100.0	0.0	0.0	0.0	-
5	1.5	100.0	0.0	0.0	0.0	-
6	2.0	100.0	0.0	0.0	0.0	-
7	3.0	100.0	0.0	0.0	0.0	-
8	1.0	90.0	0.0	0.0	10.0	-
9	1.0	80.0	0.0	0.0	20.0	-
10	1.0	90.0	0.0	10.0	0.0	-
11	1.0	80.0	0.0	20.0	0.0	-
12	1.0	55.0	25.0	20.0	0.0	2
13	1.0	48.0	22.0	30.0	0.0	2
14	1.0	48.0	22.0	20.0	10.0	2
15	1.0	55.0	15.0	30.0	0.0	4
16	1.0	65.0	15.0	20.0	0.0	4
17	1.0	75.0	5.0	20.0	0.0	15
18	1.0	62.0	28.0	10.0	0.0	2
19	2.0	45.0	45.0	10.0	0.0	1
20	2.0	75.0	15.0	10.0	0.0	5
21	2.0	55.0	25.0	20.0	0.0	2
22	2.0	62.0	28.0	10.0	0.0	2
23	2.0	73.0	17.0	10.0	0.0	4
24	2.0	45.0	45.0	10.0	0.0	1

Table 8. Zirconia suspensions prepared, 45 Vol%.

The fraction of dispersant is calculated based on the volume fraction of powder. The fraction of diluent and fraction of monomers are based on the resin composition system that is composed of the monomers and the diluent. The fraction of photoinitiator is calculated based on the monomer system without the diluent. In table 9 the system 22 is presented as an example for suspension preparation.

Suspension Data				
Material	33Y-TZP	Resin [ml]		
Density [gr/ml]	6.080	13.75		
Suspension Volume [ml]	25.0	Zirconia [ml]		
ZrO_2 [Vol%]	45%	11.25		
Initiator [wt.%]	1%	Total Vol [ml]		
Dispersant [wt.%]	2%	25.00		
Components	**Name**	**Fraction Resin**	**Density [gr/ml]**	**Weight [gr]**
Powder	33Y-TZP	-	6.080	68.400
Dispersant	Hypermer KD-1	-	1.050	1.396
Monomers	Bis-EDA	0,28	1.146	3,587
	PNPGDA	0,62	1.007	6.979
Diluent	Capa 2054	0,10	1.050	1.174
Initiator	BAPO	-		0.106

Table 9. Suspension preparation - System 22

3.3. Characterization of ceramic suspension

In order to select an appropriate monomer system, the viscosity of each suspension was measured at 7 different shear rates as seen in figure 4, at two different temperatures, 20 and 25ºC.

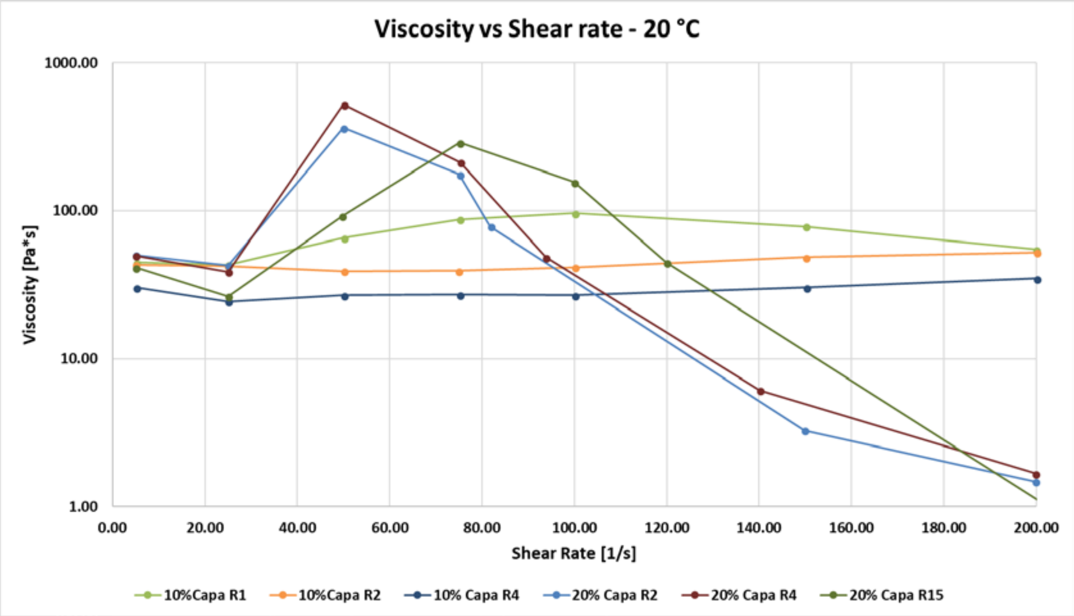

Figure 4. Characterization of viscosity of suspensions with varying shear rate

The cure depth of the ceramic suspensions was also measured to define the exposure time to be used in the printing process. The thickness of the cured monomer layer was performed in the printer machine curing layers at 2, 4, 6, 10 and 16 seconds. The thickness of the layers was measured with a micrometer screw gauge. A logarithmic curve was constructed and used to calculate the exposure time for a certain cure depth based on Jacob’s equation as seen in figure 5. This parameter was used as input in the printer machine before building the components.

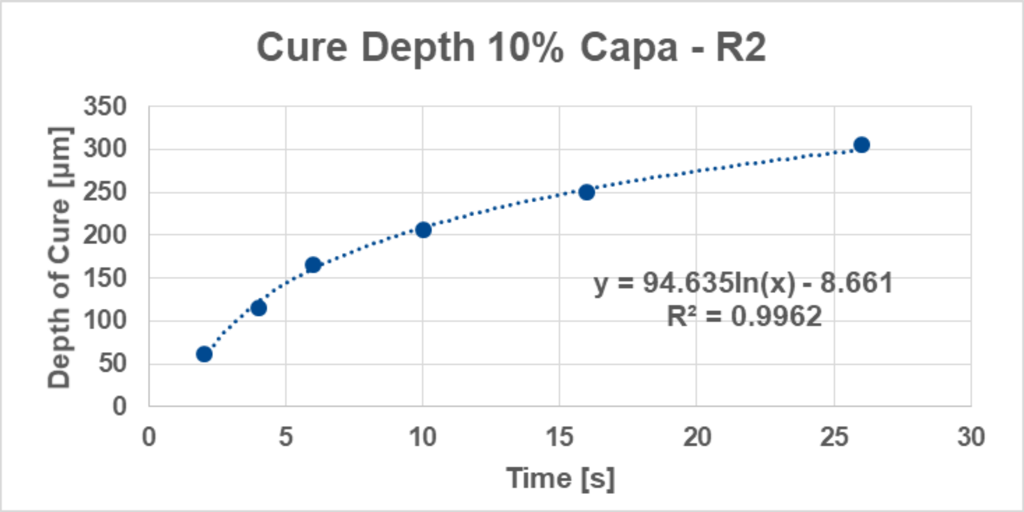

Figure 5. Example of cure depth of the system with 10% Capa R=2

3.4. Component Building

The components were printed using a Lithoz GmbH machine Model Cerafab 7500. The Stereolithography machine has a building platform of 78 mm x 43 mm and a DMD resolution of 1920x1080 pixels with a lateral resolution of 40 x 40 um build plane. The blue light source of the LED has a wavelength of 460 nm.

The ceramic suspension is poured into the rotating glass vat and spread uniformly using a fixed wiper blade. The building platform lowers into the vat until the desired layer thickness is reached and the DMD projects the cross section of the component that is being printed. The platform moves up and the glass vat rotates again to spread a new layer of suspension. The building platform moves down again to create a new layer. This process is repeated layer by layer until the part is completed.

Parameters used in the printer machine are shown in table 10. These parameters were constant during the entire study except for the light exposure time (Exposure time general). This parameter as mentioned before is a measurement of the cure depth.

General Settings	
Layer Thickness	25 µm
Wall thickness support structures	300 µm
Backlight exposure	1.8 s
Exposure time start	3,5 s
Exposure time general	**3,5 s**
Exposure intensity start	100%
Exposure intensity general	80%
Number of starting layers	5
Shrinkage compensation x	1,354
Shrinkage compensation y	1,354
Shrinkage compensation z	1,365
Full projector intensity	1600
Waiting Times	
Waiting time backlight exposure	120 s
Waiting time exposure start	30 s
Waiting time exposure general	4 s
Velocities	
Tilting down start	10 steps/s
Tilting down general	20 steps/s
Tilting up start	10 steps/s
Tilting up general	20 steps/s
Rotation speed general	200 steps/s
Moving distances	
Rotation angle start	360°
Rotation angle general	360°

Table 10. Printing parameters - Lithoz CeraFab7500

Once the parts are finished, the building platform can be taken off and the components are removed for post-processing (see figure 6). The components were removed carefully using a metallic blade and the excess of uncured monomer was cleaned with a solution provided by Lithoz and compressed air. Figure 7 shows components after the cleaning process and before the debinding process.

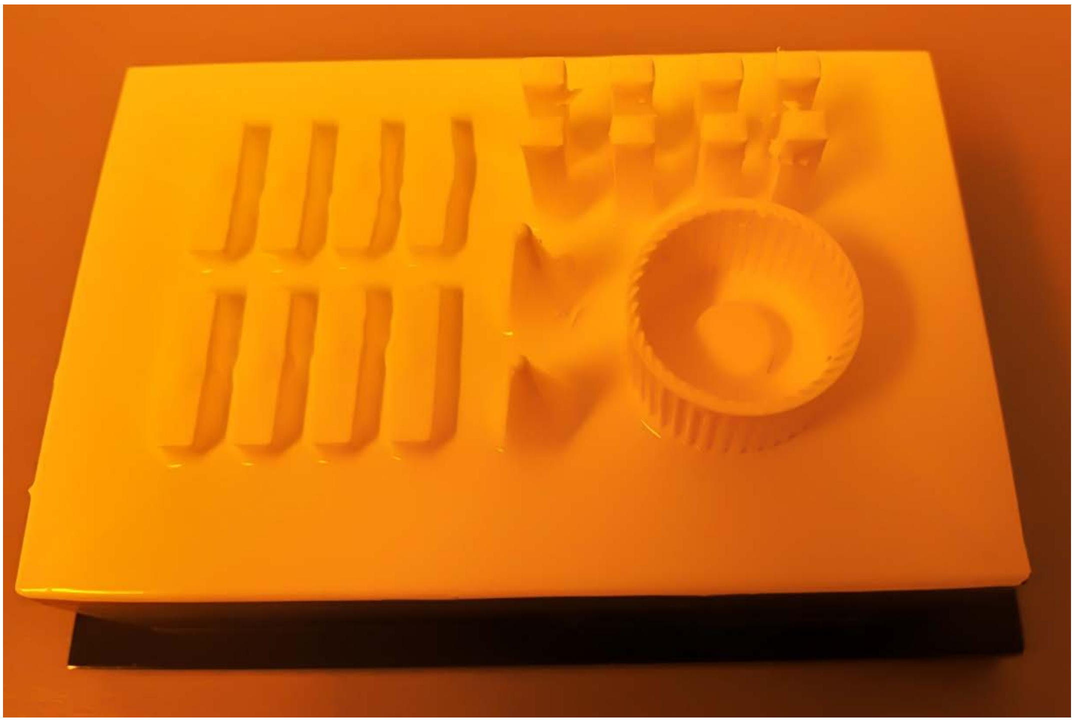

Figure 6. Components in the building plate obtained after printing

Figure 7. Green parts after removal and cleaning process

3.5. Post Processing of Components

Once the printed green parts are cleaned and dried, they were subjected to a post curing process. A UV box is used to irradiate the components for 30 min using a UV light source. Thermal debinding of the green parts was done using slow heating rates and holding times. A thermogravimetry analysis (TGA) of the individual components of the system (Figure 8) and the polymerized systems with and without a powder (Figure 9 as an example) were done. The temperature range was from 25°C to 600°C at a rate of 2 °C/min in air.

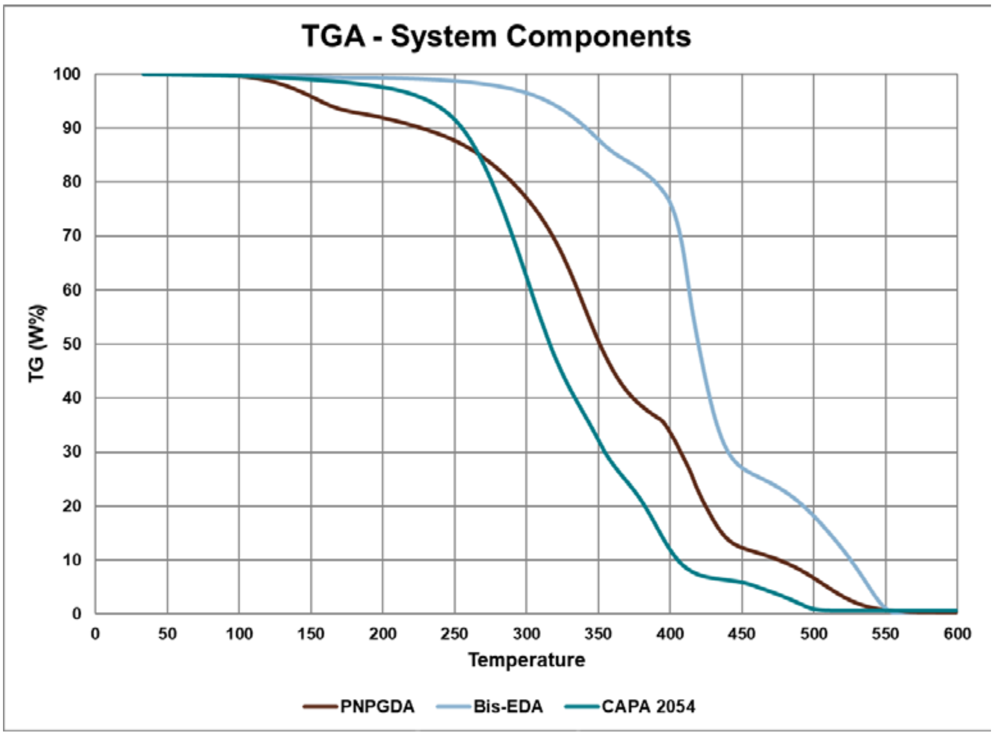

Figure 8. TGA analysis of individual monomer system components

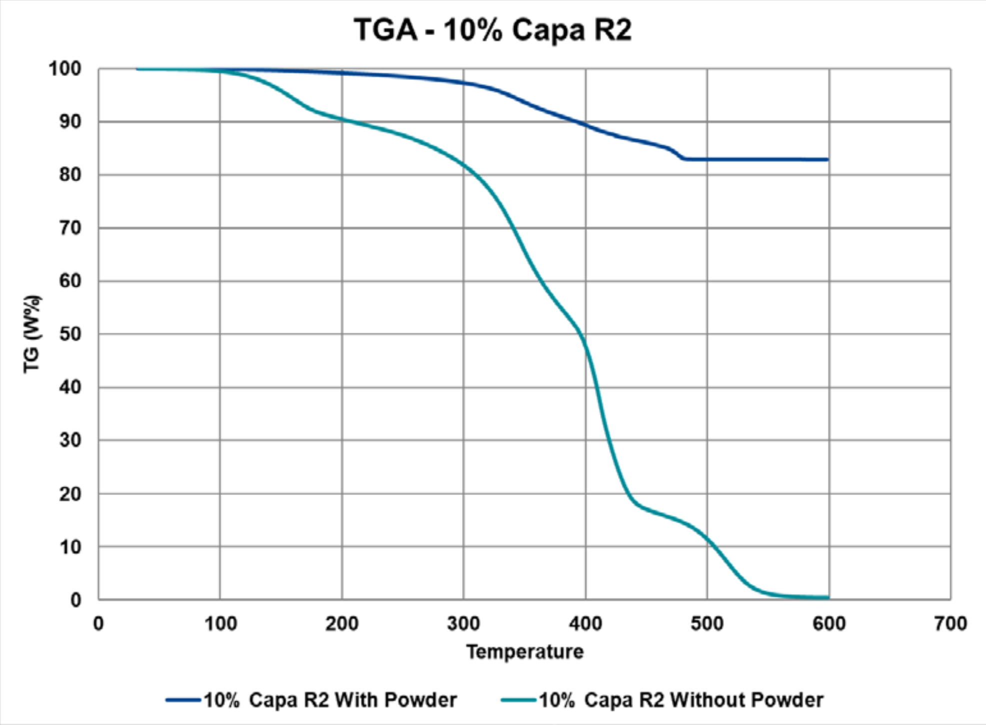

Figure 9. TGA analysis of polymerized system 22 with powder and without powder

Different heating profiles were tested where heating rates and holding times were varied. The debinding process was performed in air using slow heating rates and applying holding times to remove the organic binder without causing defects in the components. Several debinding profiles were tested to optimize the process time and achieve good quality parts. The figure 10 shows one of the debinding curves studied.

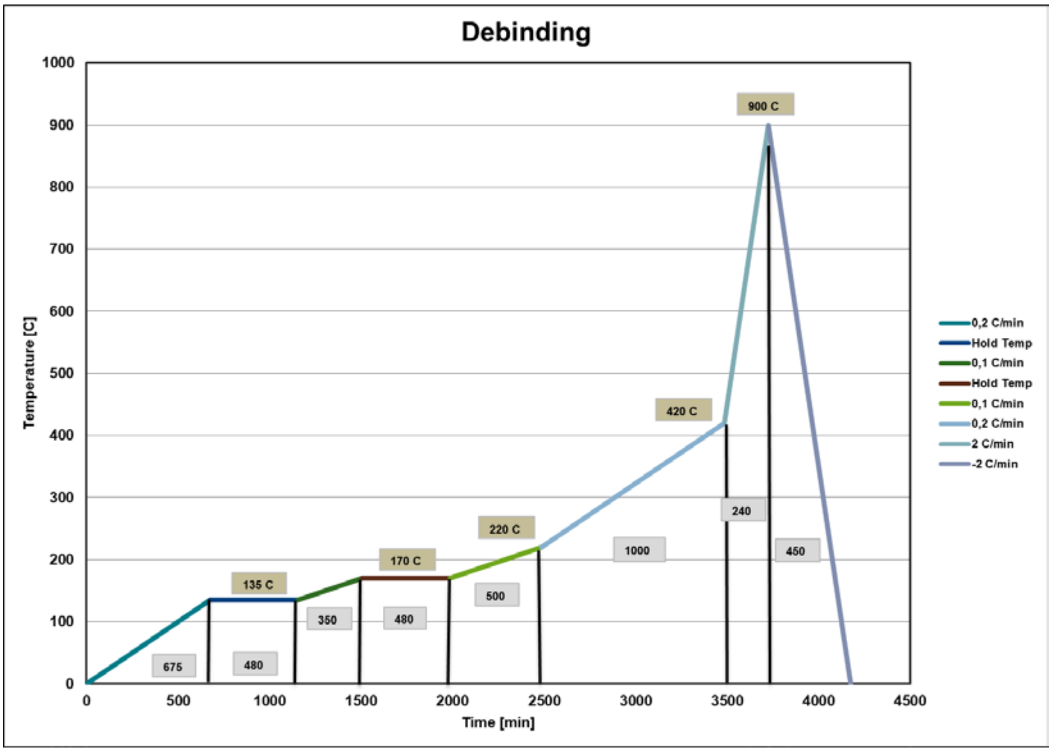

Figure 10. Temperature profile of one debinding process

The sintering process (figure 11) was carried out at 1450°C with a holding time of 2 hours, the heating rates for both heating and cooling was 5 °C/min.

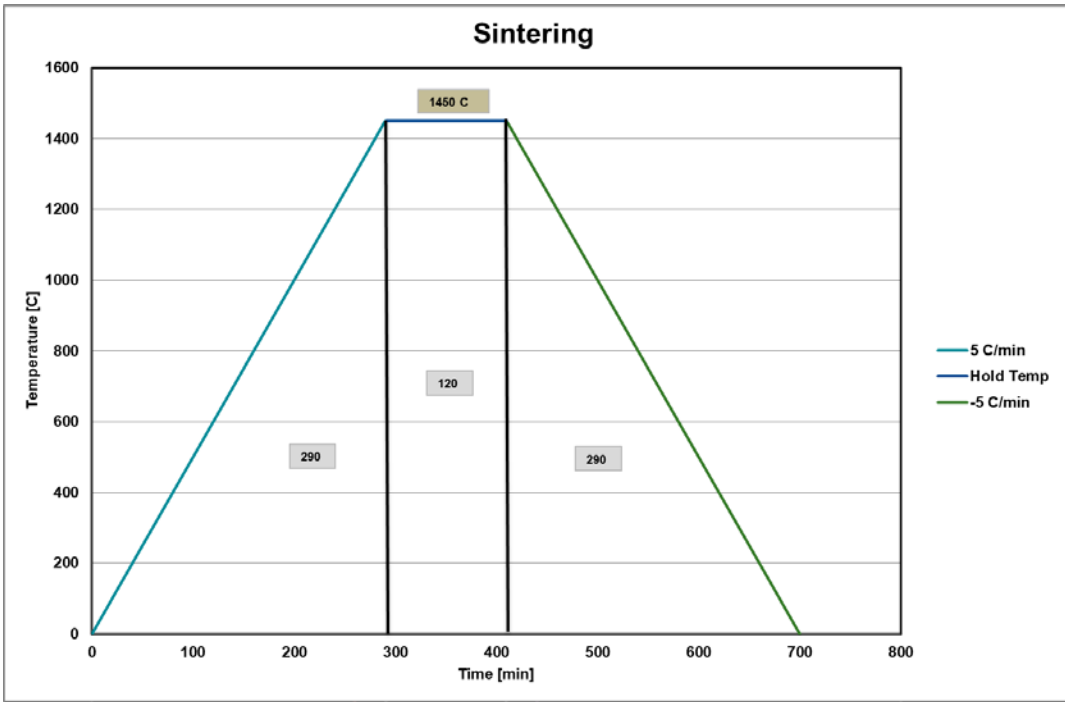

Figure 11. Temperature profile of sintering process

3.6. Characterization of Final Component

The characterization of the components was first made by visual inspection and light microscopy in order to detect delamination cracks and macro defects. The macroscopic and microscopic inspection was done on the green body (after printing), the brown body (after debinding), and the sintered components. SEM microscope was used in the same stages of the process to analyze in detail the origin of defects as shown in figure 12 where the layering in z direction after printing can be observed.

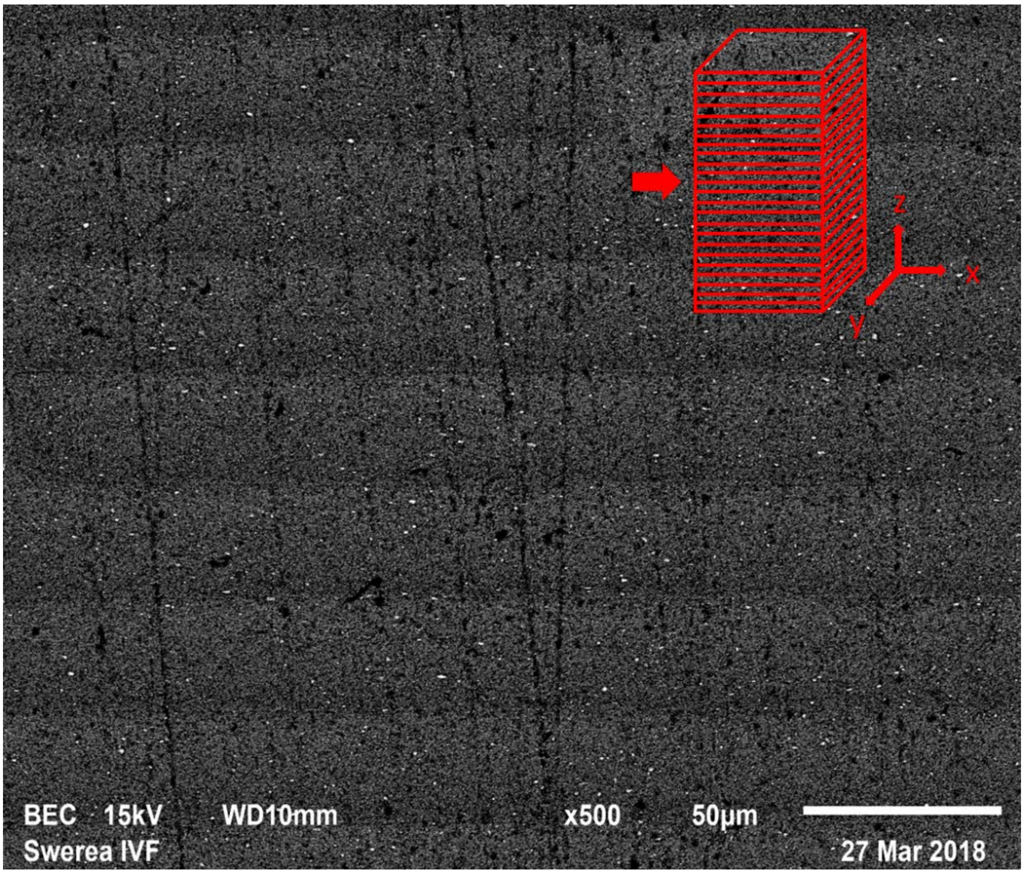

Figure 12. Green part - 10%Capa R2 building direction: z

Density measurements were performed in accordance with ISO standard EN-623-2 and compared with theoretical densities of each powder. Dimensional accuracy and surface finishing were evaluated after sintering, the final components were compared with the CAD models to observe and determine the shrinkage compensation necessary to obtain the final piece with the correct dimensions.

The determination of the grain size after sintering was performed based on SEM images utilizing a digital image analyzer and compared to the particle size distribution measured before suspension preparation.

3.7. Process Evaluation with Different Powders

To test the resin system developed and process parameters with other ceramic powders and compare the response to the process, 3 different powders were tested. Magnesia and Ceria stabilized zirconia powders were used as well as Yttria stabilized from Daiichi powders (Daiichi Co Ltd, Japan). Characteristics of the powders can be seen in table 11. Particle size measurements were conducted to compare different powders after 48 hours of milling. Also, the specific surface area was measured before the milling process.

Magnesia Stabilized Zirconia - MSZ-8

Chemical Formula :	(MgO)x (ZrO2)1-x
Form & Appearance :	White powder
Application :	Advanced ceramics
Typical Packing :	---

Analytical value (Max %) Typical Specifications

ZrO2+HfO2	MgO	Al2O3	SiO2	Fe2O3	TiO2	Na2O	CaO	H2O	Ig.loss
97.2±0.4	2.4 - 3.2	-	0.15	0.08	0.25	0.08	0.08	0.5	0.5

Average particle size(µm)	BET(m^2/g)
0.6 - 2.0	0.6- 2.0

Yttria Stabilized Zirconia - HSY-3F-J

Chemical Formula :	(Y2O3)x (ZrO2)1-x
Form & Appearance :	White powder
Application :	Advanced ceramics
Typical Packing :	Fiber drum

Analytical value (Max %) Typical Specifications

ZrO2+HfO2	Y2O3	Al2O3	SiO2	Fe2O3	TiO2	Na2O	CaO	H2O	Ig.loss
94.35±0.30	5.65±0.30	0.25±0.15	0.02	0.02	0.02	0.02	0.02	0.5	1

Average particle size(µm)	BET(m^2/g)
0.55±0.12	6.5- 9.5

Ceria Stabilized Zirconia - CEZ-12

Chemical Formula :	(CeO2)x (ZrO2)1-x
Form & Appearance :	Light yellow powder
Application :	Advanced ceramics
Typical Packing :	Fiber drum

Analytical value (Max %) Typical Specifications

ZrO2+HfO2	CeO2	Al2O3	SiO2	Fe2O3	TiO2	Na2O	CaO	H2O	Ig.loss
83.4±0.4	15.6-16.4	0.25±0.15	0.02	0.02	0.02	0.02	0.02	0.5	0.5

Average particle size(µm)	BET(m^2/g)
0.5 - 1.0	10.0-15.0

Table 11. Characteristics of different Zirconia powders from Daiichi [38]

4. Results and Discussion

4.1. Milling and Freezing

The results for particle size measurements after different milling times are presented in Table 12. The milling process had a clear effect on the particle size compared to the powder as-received from the manufacturer. When the powder is not milled, the average particle size was 211 µm, which shows that granules of considerable size are present in the powder and they are not destroyed when the solution is prepared, or the dispersant is added. Figure 13 shows two particles size distributions in the suspension. Particles that are in the range of 0.3 to 0.5 µm and particles in the range of 100 to 400 µm that correspond to the granules formed.

3Y-TZP	**Dx (10) (µm)**	**Dx (50) (µm)**	**Dx (90) (µm)**	**3Y-TZP**	**Dx (10) (µm)**	**Dx (50) (µm)**	**Dx (90) (µm)**
No Milling	0.383	198.000	325.000	**1 day Milling**	0.229	0.357	0.574
No Milling	0.388	198.000	323.000	**1 day Milling**	0.229	0.357	0.574
No Milling	0.390	199.000	317.000	**1 day Milling**	0.229	0.357	0.574
No Milling	0.398	203.000	325.000	**1 day Milling**	0.229	0.357	0.574
No Milling	0.405	208.000	334.000	**1 day Milling**	0.229	0.357	0.574
No Milling	0.450	219.000	323.000	**1 day Milling**	0.228	0.355	0.570
No Milling	0.463	219.000	321.000	**1 day Milling**	0.228	0.354	0.568
No Milling	0.476	220.000	322.000	**1 day Milling**	0.228	0.353	0.565
No Milling	0.489	220.000	323.000	**1 day Milling**	0.227	0.353	0.563
No Milling	0.505	221.000	323.000	**1 day Milling**	0.227	0.352	0.560
Mean	0.435	211.000	324.000	**Mean**	0.228	0.355	0.569
1xStd Dev	0.047	10.200	4.310	**1xStd Dev**	0.001	0.002	0.005
1RSD (%)	10.800	4.850	1.330	**1RSD (%)**	0.344	0.552	0.925
3Y-TZP	**Dx (10) (µm)**	**Dx (50) (µm)**	**Dx (90) (µm)**	**3Y-TZP**	**Dx (10) (µm)**	**Dx (50) (µm)**	**Dx (90) (µm)**
2 days Milling	0.203	0.301	0.445	**2 days Milling & Freeze Drying**	0.230	0.350	0.543
2 days Milling	0.203	0.301	0.445	**2 days Milling & Freeze Drying**	0.230	0.350	0.543
2 days Milling	0.202	0.301	0.445	**2 days Milling & Freeze Drying**	0.230	0.350	0.544
2 days Milling	0.203	0.301	0.445	**2 days Milling & Freeze Drying**	0.230	0.350	0.544
2 days Milling	0.203	0.302	0.446	**2 days Milling & Freeze Drying**	0.230	0.350	0.544
2 days Milling	0.202	0.301	0.445	**2 days Milling & Freeze Drying**	0.229	0.349	0.541
2 days Milling	0.202	0.301	0.444	**2 days Milling & Freeze Drying**	0.228	0.348	0.538
2 days Milling	0.202	0.301	0.444	**2 days Milling & Freeze Drying**	0.228	0.347	0.536
2 days Milling	0.202	0.300	0.443	**2 days Milling & Freeze Drying**	0.228	0.346	0.532
2 days Milling	0.202	0.300	0.443	**2 days Milling & Freeze Drying**	0.227	0.344	0.522
Mean	0.202	0.301	0.444	**Mean**	0.229	0.349	0.539
1xStd Dev	0.000	0.001	0.001	**1xStd Dev**	0.001	0.002	0.007
1RSD (%)	0.155	0.180	0.205	**1RSD (%)**	0.450	0.636	1.310

Table 12. Effect of milling and freeze drying in the particle size

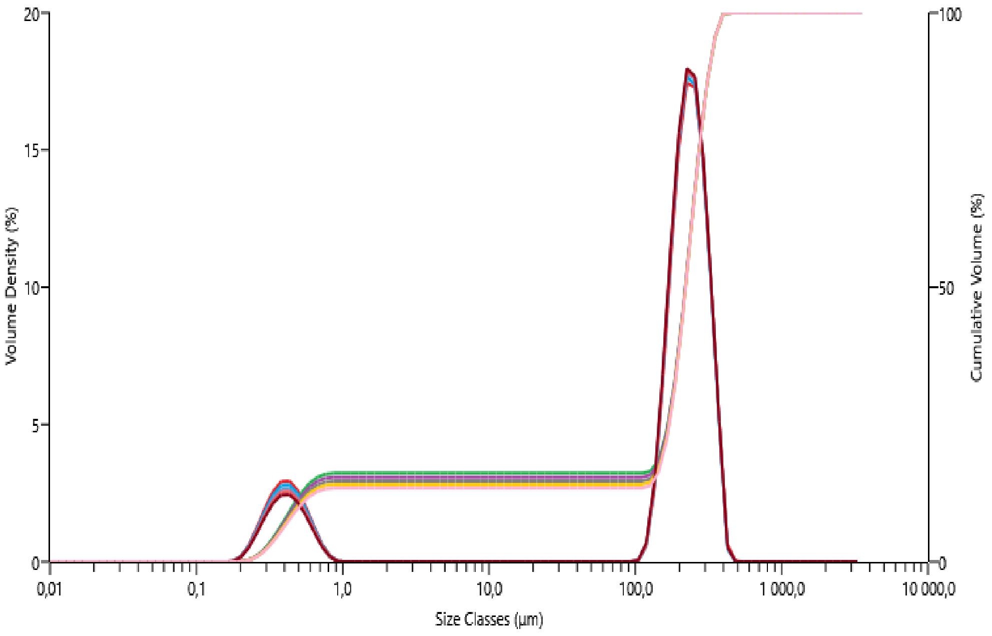

Figure 13. Particle size distribution 3Y-TZP - without milling

On the other hand, when the powder is milled for 24 hours the D50 is 0.355 µm. After 48 hours milling the D50 is 0.301 µm. The combination of milling and freeze drying increased the particle size to 0.349 µm in average. Figure 14 shows a narrow particle size distribution after two days milling in the range of 0.2 to 0.5 µm

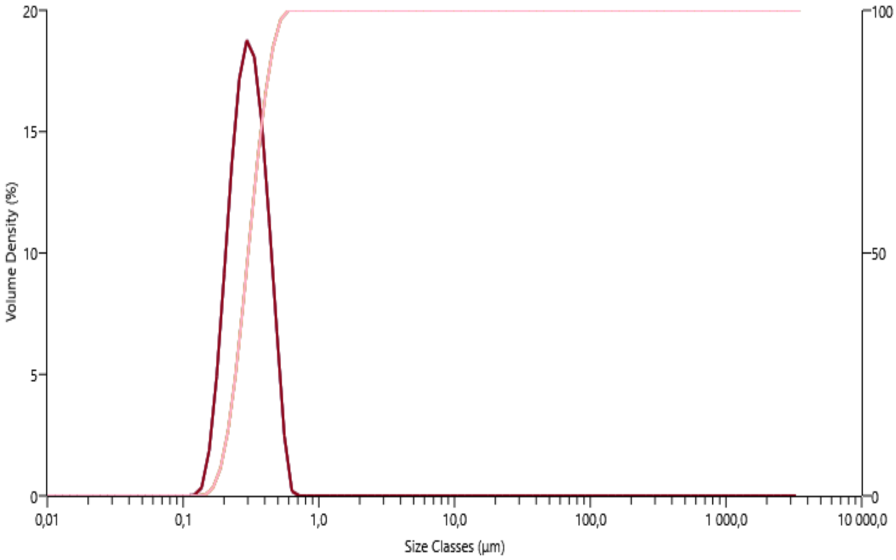

Figure 14. Particle size distribution 3Y-TZP - milled for 2 days

The freeze drying process does not reduce the particle size, instead, particles are susceptible to a small grade of agglomeration during this process. However, it was observed that these agglomerates are weak and can be easily destroyed during the preparation of the suspension by mixing. This is one of the main characteristics of the freeze drying process as explained by Lyckfeldt, Sjöstedt, and Orlenius [16]. Moreover, the powder after freeze drying contains very low humidity which is helpful in the next steps of the process to avoid defects during debinding and sintering. The powder used for printing tests in the research was milled for 48 hours and then freeze dried.

Surface area measurements also showed that milling and freeze drying increased the specific surface area from 6.64 m^2/gr to 8.19 m^2/gr. Hence, as expected, the milling process reduced the grain size and increased the surface area of the powder.

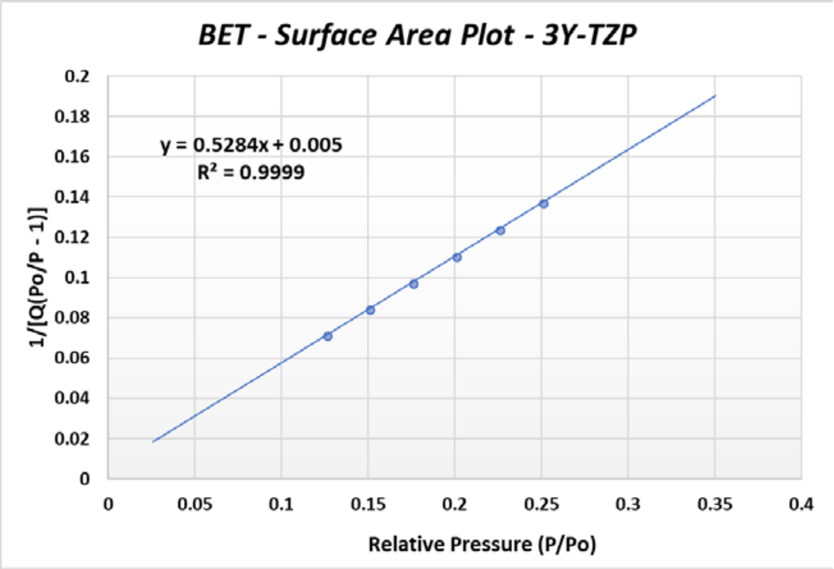

Figure 15. Surface area of Zirconia powder from Tosoh – after 2 days milling

4.2. Effect of Dispersant on the Suspension

The effect of dispersant in the rheological behavior was studied by increasing the amount of dispersant from 1% to 3% in a monomer system containing 100% PNPGDA. The viscosity of the suspension was measured at 20 and 25ºC. Figure 16 shows the viscosities at different shear rates with increasing amounts of dispersant. Increasing the dispersant in the suspension can effectively lower the viscosity with the lowest value obtained when 1% dispersant is added. Above 2% the viscosity increases significantly. The same effect was observed with additions below 1%.

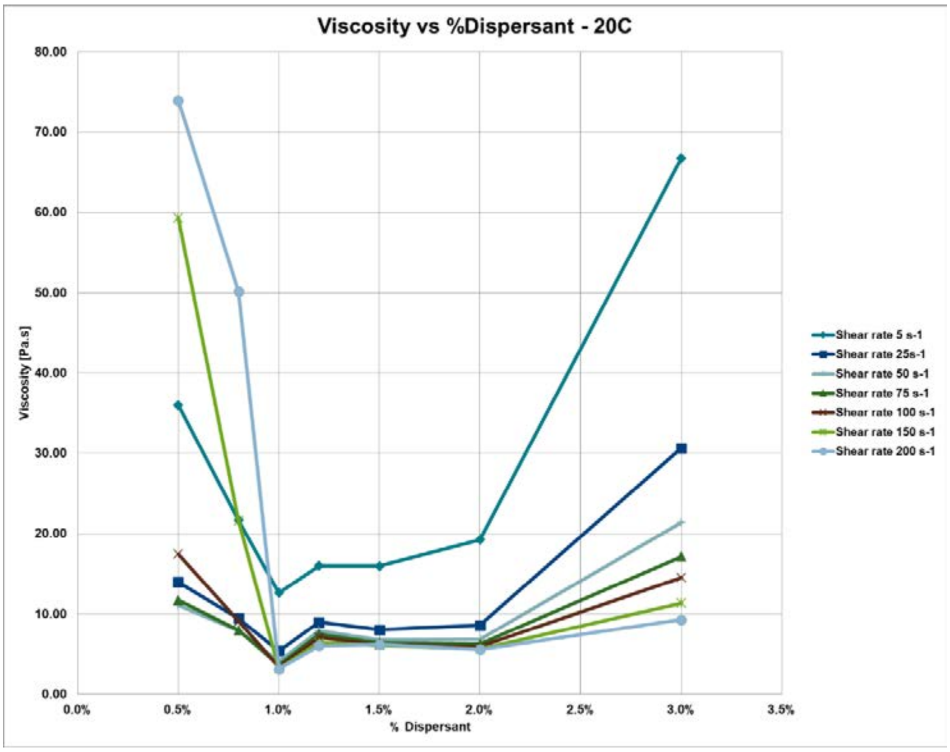

Figure 16. Effect of dispersant in the suspension at different shear rates

At 25ºC the behavior is similar for all shear rates, but the viscosities were lower compared to the measurements obtained at 20ºC. Temperature increase will lower the viscosity of the ceramic suspension. However, the viscosity increases after 2 % dispersant at every shear rate measured. In figure 17 the effect of shear rate on the viscosity of the suspension can be observed. In general, all the suspensions have non-Newtonian behavior meaning that the viscosity is shear dependent. The addition of dispersant below 1% will result in a shear thickening fluid that is not suitable for printing. Above 1% of dispersant the fluid shows a shear thinning behavior. A plateau is observed between 1 to 2 % dispersant where the viscosity is almost constant. Higher additions of dispersant increase the viscosity of the suspensions at low shear rates. With 3 % addition, the viscosity was above 50 [Pa*s] at shear rates below 20 s^{-1}.

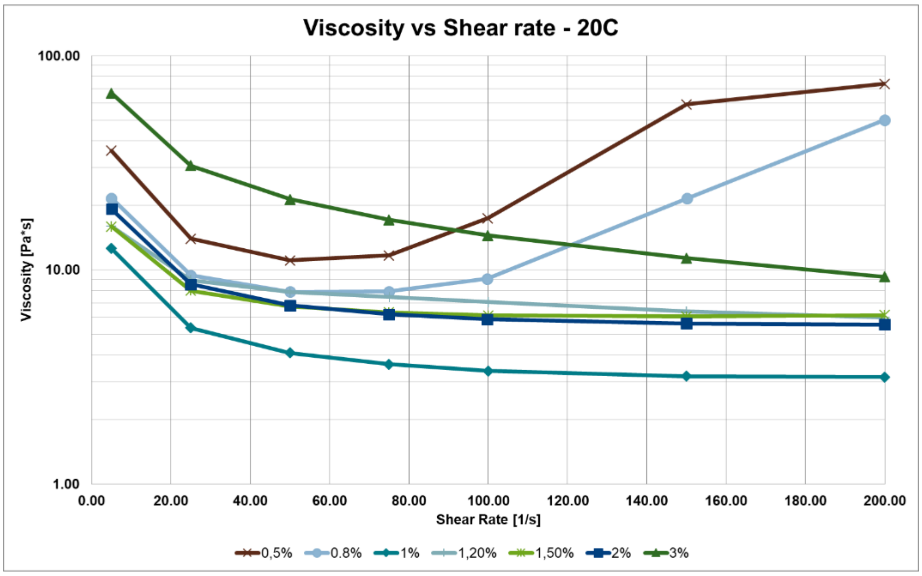

Figure 17. Viscosity of suspensions at different shear rates

The high viscosity with a low fraction of dispersant may be caused by the high disorder of the particles that tend to aggregate and increase the viscosity. The addition of dispersant between 1 to 2 % reduces the possibility of agglomeration of particles by electrostatic and steric repulsion. Gürgen, Li, and Kushan [27] suggested that at lower shear rates, shear thickening fluids can form hydro clusters that increase the viscosity of the suspension. At high shear rates, the contact forces generate force networks which cause high viscosity in the suspensions. This may be the case when the dispersant is more than 2 % in the ceramic suspension, the dispersant could be increasing the contact forces in the fluid causing high viscosity at low shear rates and decreasing its effectiveness.

4.3. Effect of Diluent on the Suspension

The addition of diluent increased the viscosity of the suspensions at high shear rates. Two diluents were tested (CAPA 2054 and PPG-400) and both showed the same behavior. Suspensions containing 20% Capa have a shear thickening behavior above 100s^{-1} and suspensions with 20%PPG have a shear thickening behavior above 50s^{-1} as can be seen in figure 18.

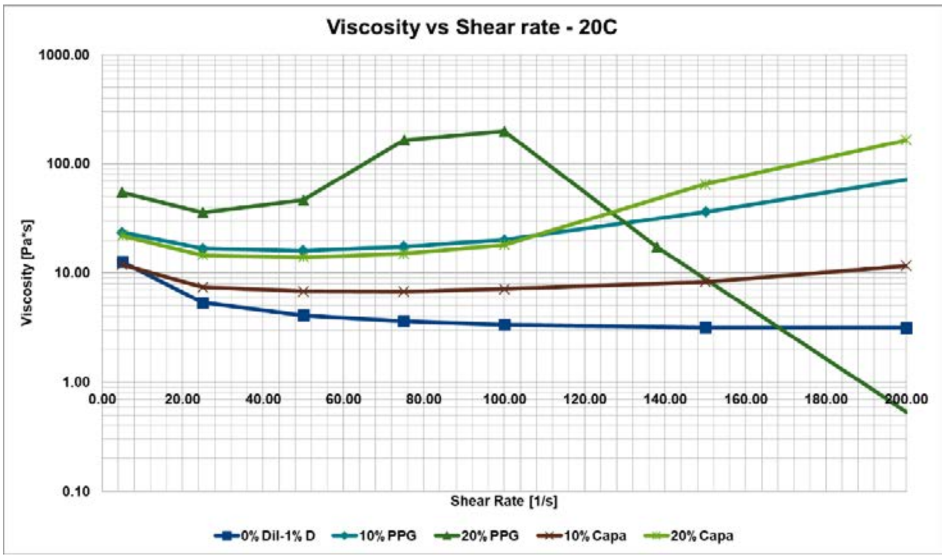

Figure 18. Effect of diluent in the viscosity of the suspensions

The addition of diluent did not decrease the viscosity. Instead, the viscosity of the suspension increases and there is a tendency to behave like a Bingham fluid. Hinczewski, Corbel, and Chartier [35] found that viscosity can be decreased significantly with the addition of diluent in alumina suspensions, but this addition also decreases the shear thinning behavior. This tendency from shear thinning fluids to shear thickening was observed in the suspensions studied.

To select the best diluent, printing tests were done using systems 8 to 11, see table 8. Capa 2054 was selected as the diluent for the subsequent tests as it showed better behavior and printability than suspensions with PPG-400 in addition to the less tendency towards shear thickening behavior.

4.4. Suspensions with two monomers and diluent

To study the effect of different proportions of monomers used in the suspension the parameter R was defined as the ratio between monomer 1 (Neopentyl glycol propoxylate diacrylate PNPGDA) and monomer 2 (Bisphenol A ethoxylate diacrylate Bis-EDA).

$$R = \frac{M1}{M2} = \frac{\%\, PNPGDA}{\%\, Bis - EDA}$$

$$Resin = \%PNPGDA + \%Bis - EDA + \%Capa2054$$

Suspensions using a constant proportion R=2 (62%M1/28%M2) and increasing the amount of CAPA 2054 diluent was tested (10%, 20% and 30%). The shear thickening behavior is significantly increased when the % of diluent is above 10% as can be seen in figure 19. The suspensions have high viscosity at low shear rates which causes the suspensions to jam while mixing.

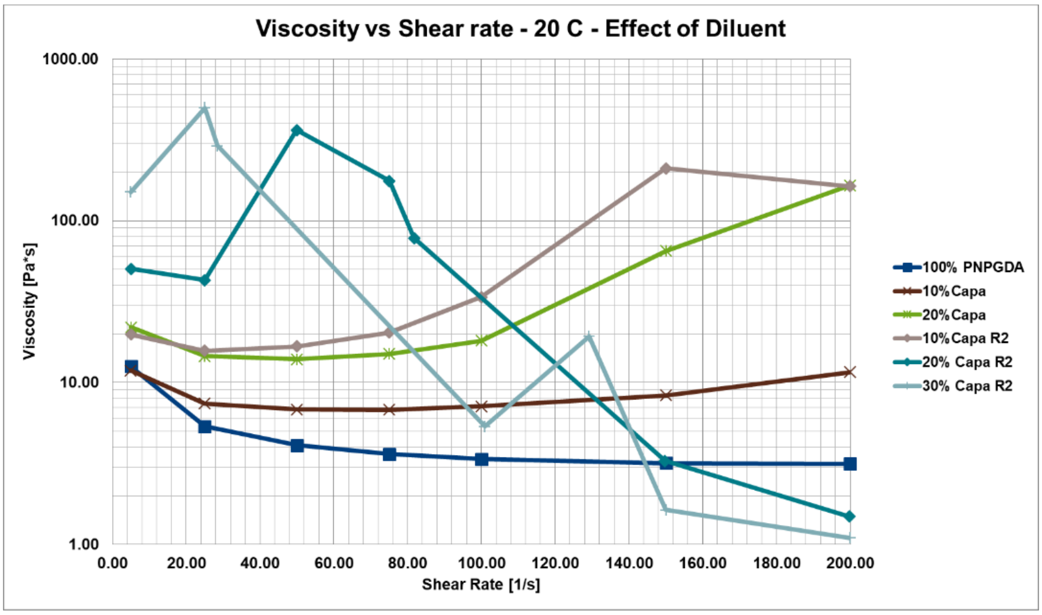

Figure 19. Effect of diluent in suspensions with R2

Resins with 30% diluent were not studied further as the shear thickening behavior and high viscosity did not allow printing tests. Resins with 20% diluent and 1% dispersant with different R were not suitable for printing as they caused problems in the printing machine due to the high viscosity and shear thickening behavior. Recoating of the glass plate in the printing machine was not possible and the printing tests were canceled. The R parameter was varied in systems with 10 and 20% diluent as seen in Figure 20.

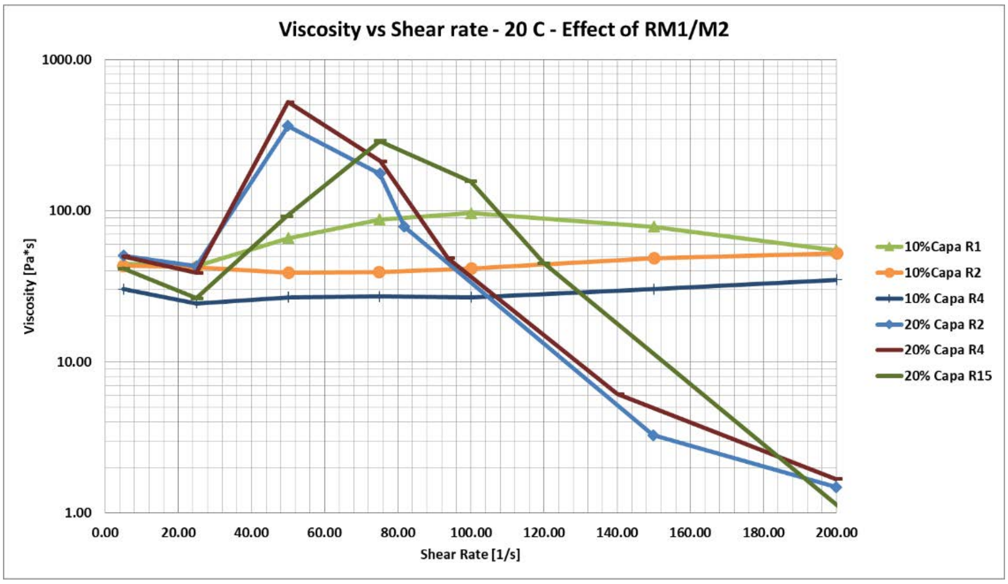

Figure 20. Effect of R in systems with 10% and 20% diluent

The shear thickening behavior of systems with 20% Capa was eliminated by increasing the fraction of dispersant to 2%. The increase in the dispersant changed the behavior to shear thinning fluids. This was also tried with systems with 30% diluent but the addition of more dispersant did not change the rheological behavior. This could be caused by chemical and physical interactions between the dispersant and the diluent which lowers the effectiveness of the dispersant.

Increasing the amount of the second monomer (Bis-EDA) also influences the viscosity but in less proportion. A system with 10% Capa and 50% of each polymer (R=1) was possible to prepare and perform printing tests.

Print tests with both 10% and 20% diluent were conducted. It was observed that the increase of diluent caused problems during the print as the parts were poorly attached to the building platform and tended to fall from the plate. The components that were finished also showed defects and fragility for cleaning and post-processing. The low crosslink density between layers and weak polymer matrix after curing may be the cause of these defects.

After several printing tests, the resin systems 22, 23 and 24 with 10% diluent and different monomer proportions were selected as suspensions for debinding optimization. The selection was based on the printability of the suspensions, rheological behavior and lower defects compared to other suspensions after debinding and sintering.

4.5. Influence of Monomers and Diluent on Cure Depth

The systems tested did not show a significant difference in cure depth. The increase in the diluent fraction or the change in proportions of monomers in the resin did not affect the cure depth of the suspensions which may suggest that this parameter is mainly influenced by the powder characteristics and solids loading in the suspension. The cure depth converges to a maximum value between 250 to 300 µm after 25 seconds with every suspension.

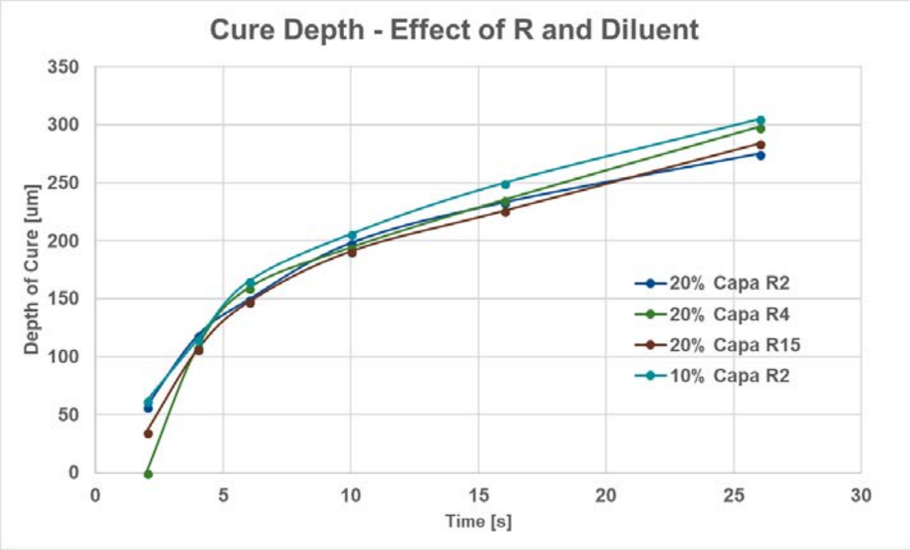

Figure 21. Effect of mixing ratio R and diluent on the cure depth

Print tests showed that a cure depth between 100 and 150 µm allowed enough strength to the component for post-processing steps as well as good control of dimensions during the build. Increasing the exposure time and thus the cure depth caused overgrowth of the component and poor dimensional accuracy due to scattering effect [24] in the x-y plane. A cure depth below 100 µm may increase the risk to low cross-linking between layers and failure during printing due to detachment between these layers, as observed when printing tests were done with cure depths of 50 and 75 µm. After these results, the exposure time was set to 3.5 sec. to reach a cure depth of 100 µm. As a final step, the components were subjected to a post curing treatment in a UV box for 30 min to cure all the residual monomer and reduce internal stresses due to photopolymerization of uncured monomer by thermal activation in the debinding stage [24].

4.6. Debinding of Green Components

The debinding of the polymer matrix was the most critical post-processing step in the manufacturing process. Different temperature profiles were tested based on previous experience in Swerea IVF with other ceramic powders. TGA analysis was also performed for systems 22, 23 and 24 using green parts and resins without powder to compare the thermal debinding behavior. TGA analysis of the green parts does not allow to observe the thermal behavior of the resin, this is better observed with the resins without the powders. Results of the analysis in figure 22, show that the theoretical weight loss is around 17%. Similar results in weight loss were observed with other resin systems compositions given that a solids loading of 45% in volume was kept constant for all the tests. On the other hand, the resin systems decompose differently compared to polymerized individual constituents. The combination of two monomers and a diluent modify the slope of the weight loss curve in different regions. It is observed that different weight loss rates are created between 100ºC and 500ºC. In addition, 80% of the total weight loss is between 200°C and 500ºC.

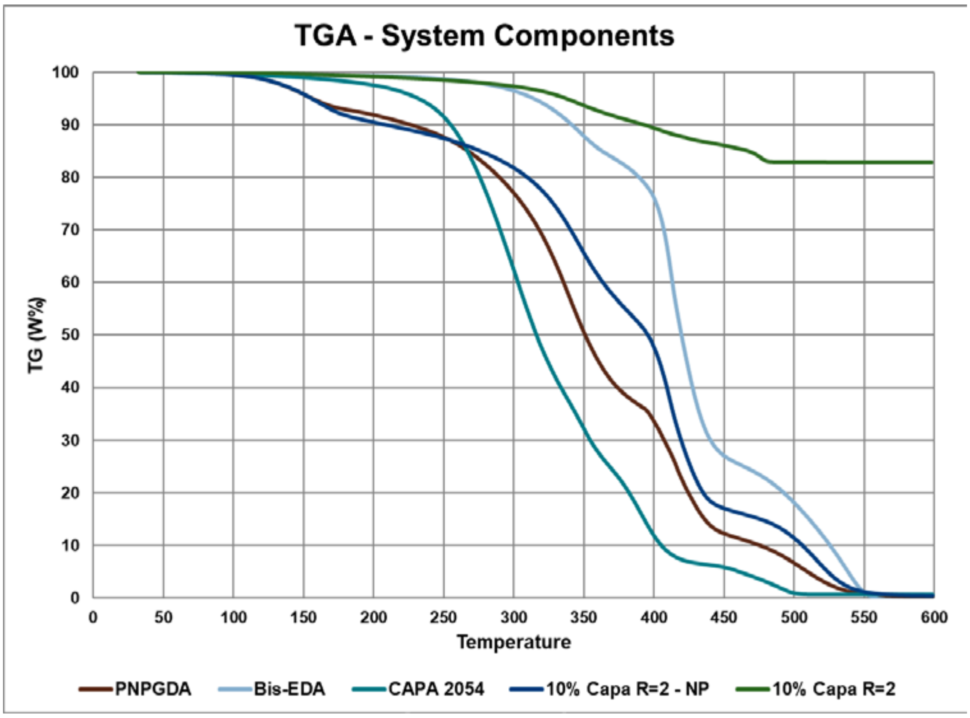

Figure 22. TGA analysis of system 22 and individual components

To avoid delamination cracks during debinding a critical degradation rate was not exceeded as suggested by Pfaffinger et al [29]. For this purpose, slow heating rates and holding times at 100ºC, 170ºC, 300ºC, and 380ºC were applied. At 100ºC and 170ºC the holding time was 4 hours for evaporation of the diluent. 8 hours was used at 300ºC and 380ºC for pyrolysis and outgassing of the polymer matrix. A final heating rate and holding time of 2 hours at 500 ºC was used to allow diffusion of carbon residues outside the component.

Figure 23 shows the layering in the z direction after debinding up to 150ºC. The difference in dark and grey areas show different composition in the component that may be caused by different polymer density between the layer boundaries and the center of the layer. After 600ºC this layered pattern is no longer observed suggesting that the polymer is completely burned.

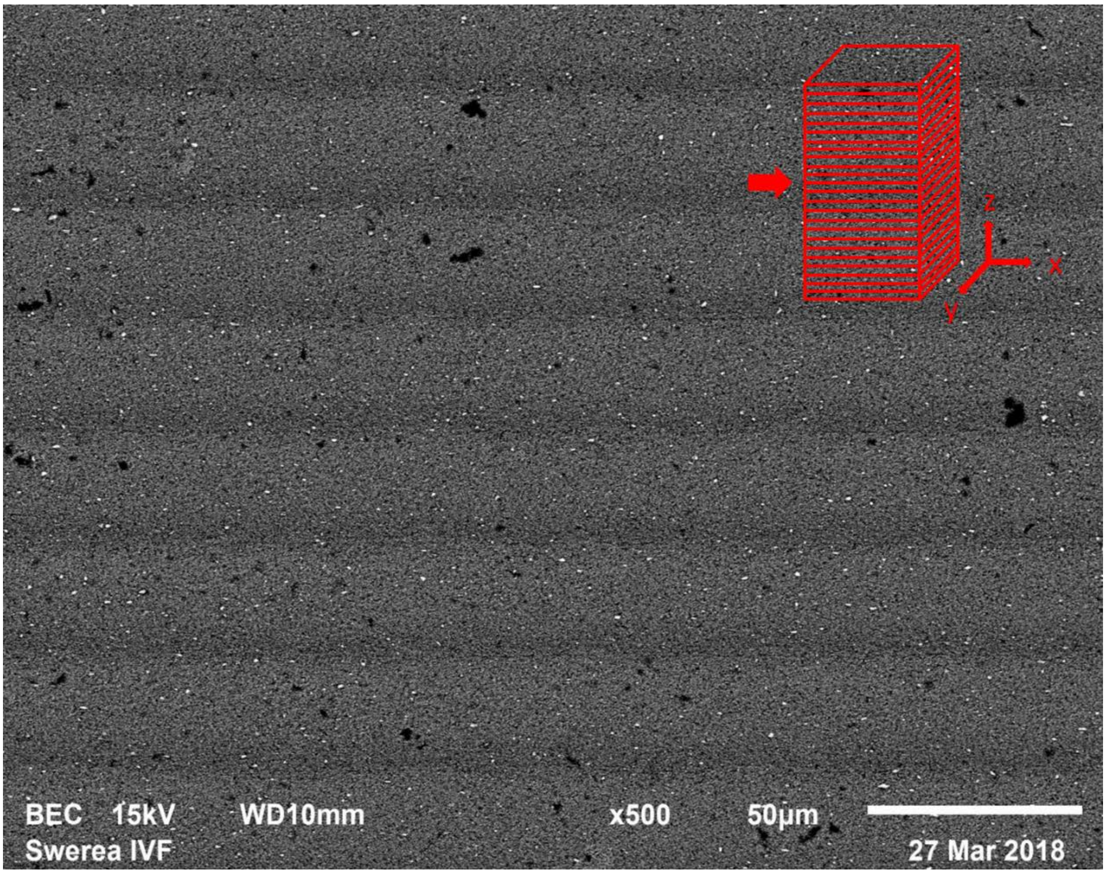

Figure 23. Heat treatment up to 150C - 10%CapaR2

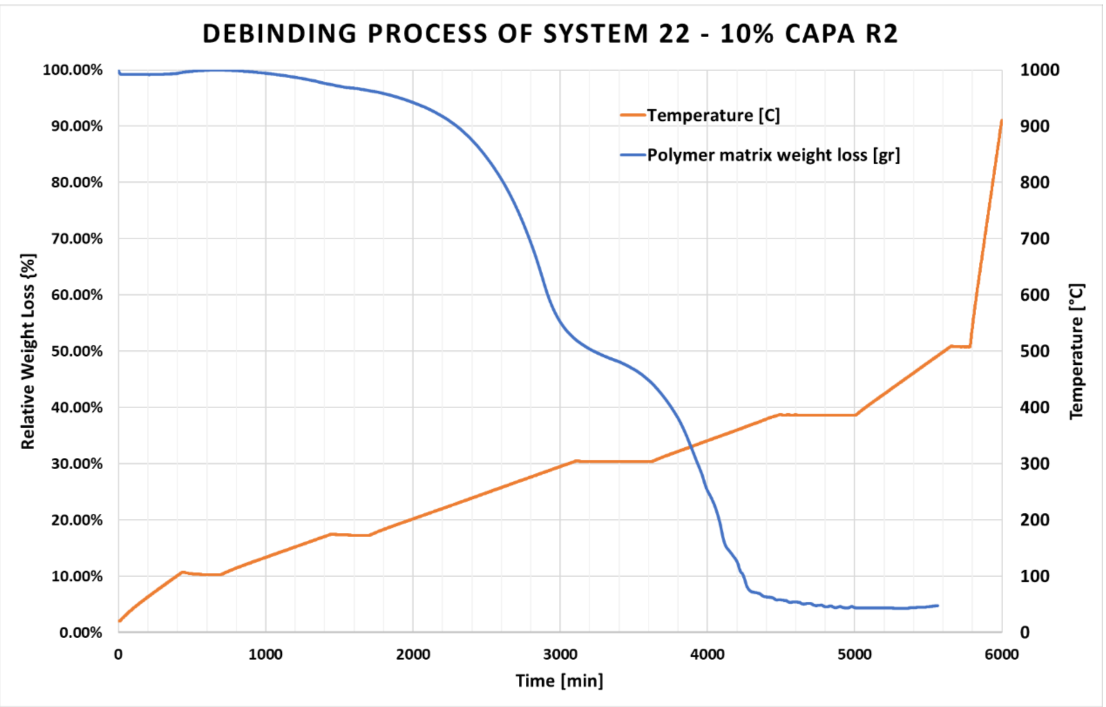

Figure 24. Debinding process - 10% Capa R2

The total thermal cycle for debinding is approximately 96 hours. The process was found to be limited in terms of variability. Increasing the heating rates or modifying holding times and temperatures can easily lead to cracks in the components. A heating rate of 0.2 ºC/min up to 170 ºC was used and 0.1 ºC/min up to 380 ºC. Higher heating rates led to delamination cracks and transversal cracks to the building plane. Figure 24 shows the resulting relative weight loss of the polymerized matrix of system 22 after a debinding process was performed using this heating profile. A major weight loss is observed between 150ºC and 380ºC showing that at this temperature range almost 100% of the polymer matrix is eliminated of the component. After this temperature, mainly carbon residues are eliminated from the material and only the ceramic material composes the piece.

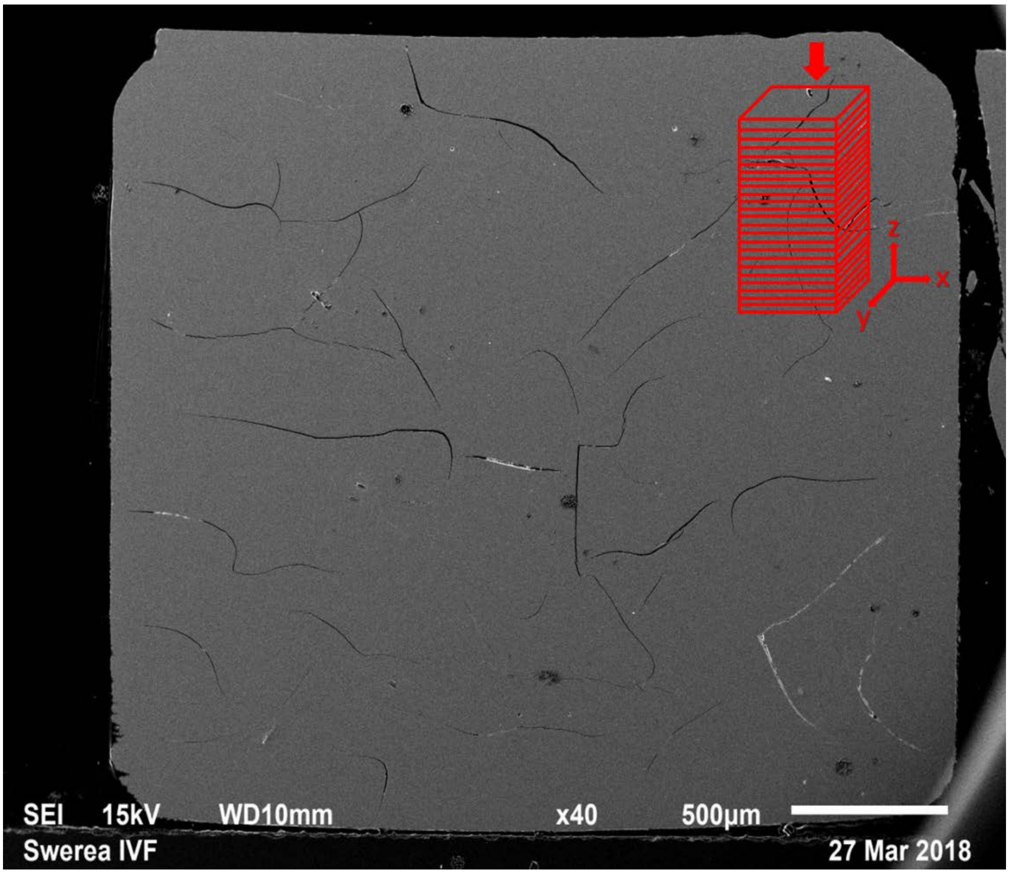

Figure 25. ZrO_2 after debinding process – x-y plane – 10% Capa R2

Figure 25 shows a SEM imaging of a component after an unsuccessful debinding process up to 600ºC. The component presents cracks up to 0.7 mm in every direction. These types of cracks can be avoided by slow heating rates and holding times that allow a slow degradation and degassing of the polymer matrix.

In figure 26 delamination cracks are showed parallel to the x-y building plane when the process is unsuccessful. This type of defect was particularly hard to eliminate and control. Powder characteristics such as particle size and distribution may be the cause of cracks. The different polymer density between the layers could also be causing this type of defect.

Bae and Halloran [30] found that the residual monomer on a laser based SL technique can be cured in the debinding process due to thermal activation of the photoinitiator. This polymerization is followed by shrinkage of the component which might be the origin of mechanical strains that cause cracking. They observed delamination cracks in the components at 200ºC before significant mass loss during pyrolysis. The same behavior was observed in this research when a heating rate up to 150ºC was performed with no holding times.

The best systems that responded well enough to the heat treatment were the ones using 10% of Capa with R=2 (62%M1/28%M2) and R=4 (73%M1/17%M2), respectively. Higher proportions than 30% of Bis-EDA monomer may cause a crosslinking density of the polymer too high to avoid cracks in the debinding process. Crack-free components were possible to manufacture using these systems and with the specified debinding profile shown in figure 23. However, these results were not easily reproduced and differed significantly with each suspension prepared, storage time of the suspension and powder batches. The reason for this variability may be the hygroscopic behavior of ceramic suspensions that can cause retention of water during printing and storage, causing changes in the behavior of components during debinding and ultimately affecting the results [29].

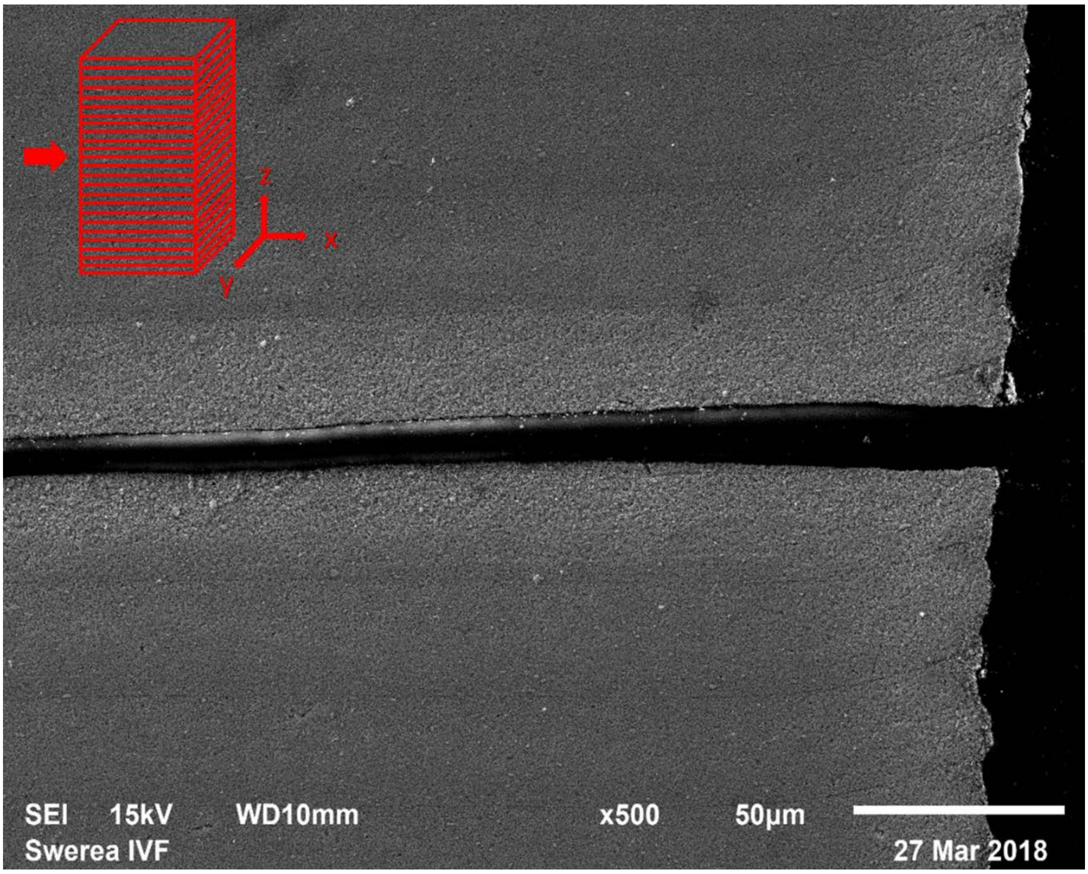

Figure 26. ZrO_2 after burn-out at 300C in direction: z - 10% Capa R2

4.7. Sintering Process

The sintering process was found to be less critical than the debinding process and did not cause large defects to the components. However, delamination cracks and defects originated during the burn out process cannot be eliminated during sintering. Instead, these type of defects were aggravated after this stage. The total cycle time is 12 hours including heating stage and holding time and thus this manufacturing stage is much less time consuming than debinding process.

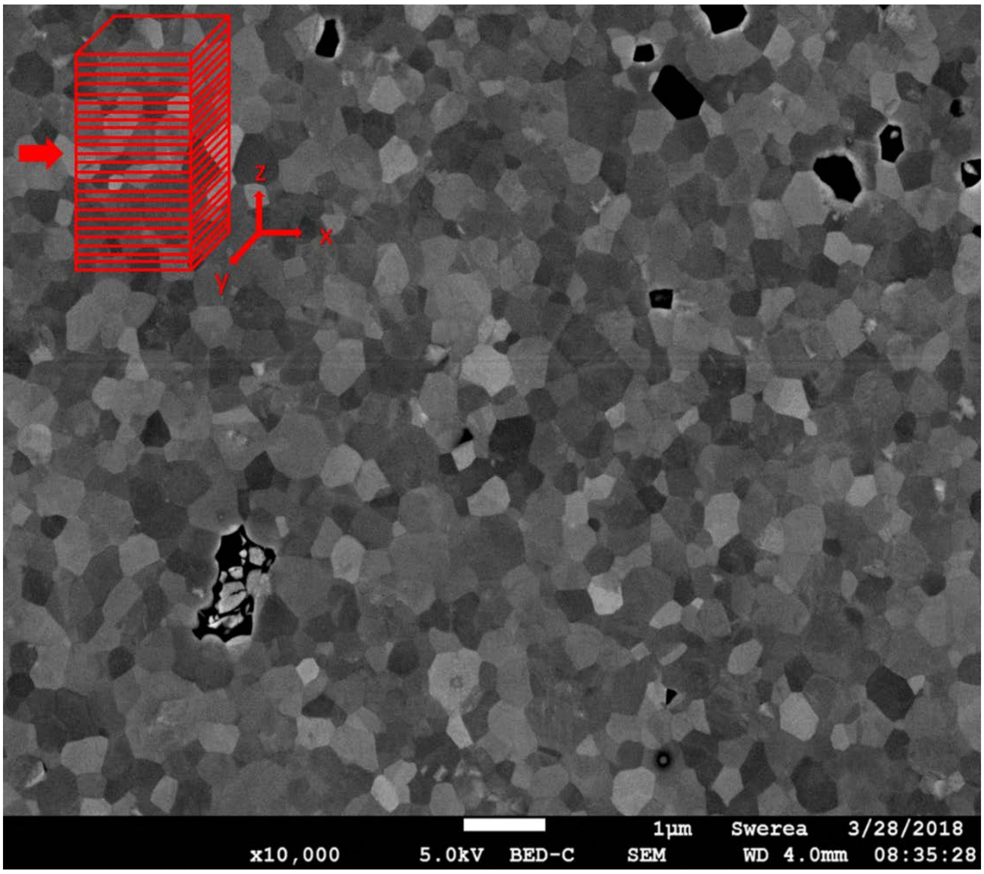

Figure 27. Sintered Zirconia 3Y-TZP - building direction: z

The sintered components show homogeneous grain size in the microstructure in both building direction x-y plane and z. Figure 27 shows the microstructure of a sintered component in the *z* direction. Similar results were observed in the x-y plane and with different components suggesting components manufactured with this technology are isotropic in every direction. The sintering holding time (2 hours) was set constant as well as the sintering temperature (1450ºC) to avoid grain growth or precipitation of stabilizers. Stawarczyk et al [33] studied the effect of the sintering temperature and sintering time in zirconia specimens. Their results showed that temperatures above 1300ºC lead to grain growth. Higher temperatures than 1600ºC can also cause Yttrium to migrate to grain boundaries. Moreover, the increase in grain size is directly related to decrease in flexural strength of the components. The highest flexural strength was reported when the sintering temperature is between 1400 to 1550ºC [33].

Thermal etching of the samples at 1300ºC for 30 minutes allowed to examine the morphology of the grains in the samples. Figure 28 shows the microstructure in the x-y plane building direction showing grains with different sizes. It can be observed that grains as small as 0.1µm are present in the material. These observations combined with an image analysis technique of the SEM images show a homogeneous shape and no excessive grain growth in the components as can be seen in Appendix B. The grain size measured in three different areas of the component show a grain size of 0.355µm in average with a standard deviation of ±0.12µm.

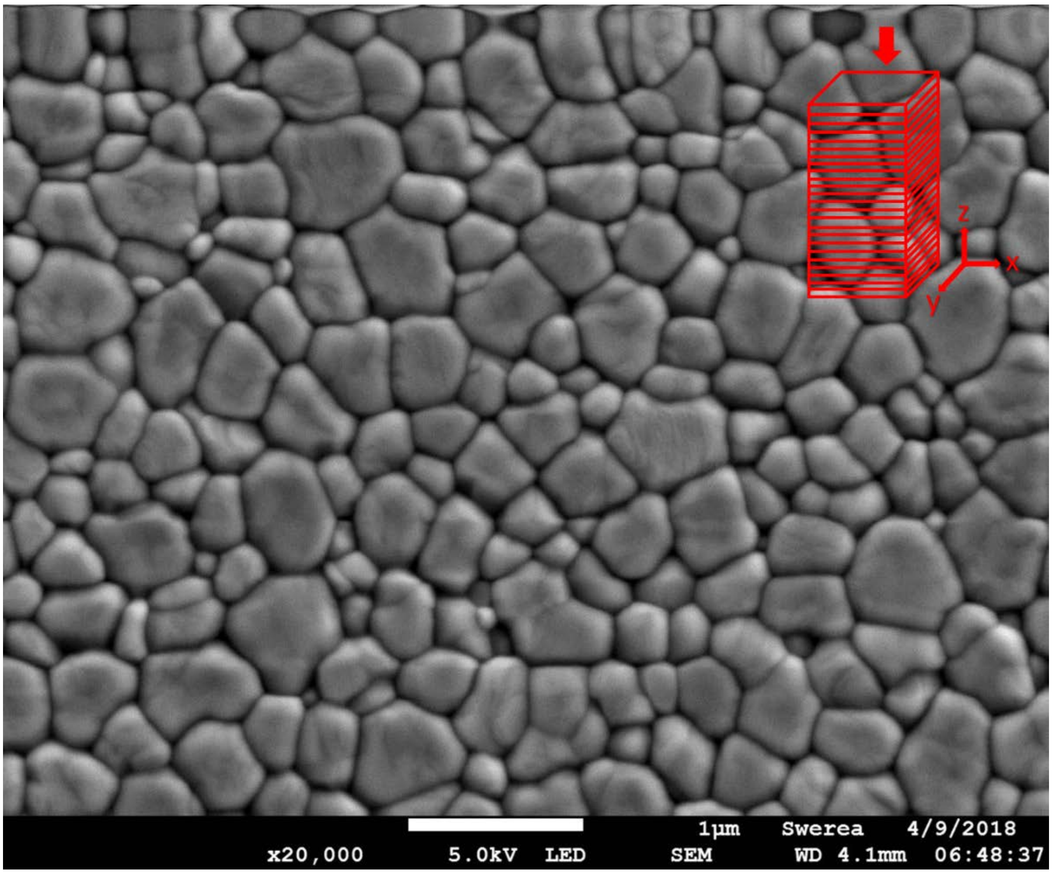

Figure 28. 3Y-TZP microstructure after thermal etching at 1300ºC

4.8. Process viability with different powders

The results show that both Yttria powders from Tosoh and Daiichi have almost the same grain size, the D50 of Daiichi 3Y-TZP is 0.306 µm and while the same value for Tosoh powder is 0.301 µm in average. The Magnesia and Ceria powders are coarser than the Yttria. The Mg-TZP shows the highest particle size with a D50 of 0.382 µm on average while 12Ce-TZP has a D50 of 0.337 µm. Moreover, the D90 shows 0.657 µm and 0.576 µm respectively. Table 13 and Figures 29 to 31 show the particle size measurements and size distribution of the powders analyzed.

Number of Measurements: 10	Dx (10) (µm)	Dx (50) (µm)	Dx (90) (µm)	D [4;3] (µm)
3Y-TZP milled 48 hours	0.199	0.309	0.475	0.324
3Y-TZP milled 48 hours	0.199	0.308	0.474	0.324
3Y-TZP milled 48 hours	0.199	0.308	0.472	0.323
3Y-TZP milled 48 hours	0.199	0.307	0.470	0.322
3Y-TZP milled 48 hours	0.198	0.307	0.469	0.322
3Y-TZP milled 48 hours	0.198	0.306	0.467	0.321
3Y-TZP milled 48 hours	0.198	0.305	0.465	0.320
3Y-TZP milled 48 hours	0.197	0.304	0.458	0.317
3Y-TZP milled 48 hours	0.197	0.303	0.458	0.317
3Y-TZP milled 48 hours	0.197	0.303	0.457	0.316
Mean	0.198	0.306	0.466	0.321
1xStd Dev	0.001	0.002	0.007	0.003
1RSD (%)	0.414	0.691	1.440	0.933
Number of Measurements: 10	Dx (10) (µm)	Dx (50) (µm)	Dx (90) (µm)	D [4;3] (µm)
Mg-TZP milled 48 hours	0.247	0.389	0.692	0.462
Mg-TZP milled 48 hours	0.246	0.387	0.682	0.460
Mg-TZP milled 48 hours	0.246	0.386	0.675	0.459
Mg-TZP milled 48 hours	0.246	0.385	0.669	0.456
Mg-TZP milled 48 hours	0.245	0.384	0.663	0.453
Mg-TZP milled 48 hours	0.244	0.380	0.644	0.442
Mg-TZP milled 48 hours	0.244	0.379	0.640	0.440
Mg-TZP milled 48 hours	0.244	0.379	0.637	0.440
Mg-TZP milled 48 hours	0.244	0.378	0.635	0.440
Mg-TZP milled 48 hours	0.244	0.378	0.632	0.438
Mean	0.245	0.382	0.657	0.449
1xStd Dev	0.001	0.004	0.022	0.010
1RSD (%)	0.448	1.070	3.360	2.220
Number of Measurements: 10	Dx (10) (µm)	Dx (50) (µm)	Dx (90) (µm)	D [4;3] (µm)
12Ce-TZP milled 48 hours	0.205	0.339	0.581	0.370
12Ce-TZP milled 48 hours	0.205	0.338	0.579	0.369
12Ce-TZP milled 48 hours	0.205	0.338	0.578	0.369
12Ce-TZP milled 48 hours	0.204	0.337	0.577	0.368
12Ce-TZP milled 48 hours	0.204	0.337	0.576	0.368
12Ce-TZP milled 48 hours	0.204	0.337	0.575	0.367
12Ce-TZP milled 48 hours	0.203	0.336	0.574	0.367
12Ce-TZP milled 48 hours	0.203	0.336	0.573	0.366
12Ce-TZP milled 48 hours	0.203	0.336	0.573	0.366
12Ce-TZP milled 48 hours	0.203	0.336	0.572	0.366
Mean	0.204	0.337	0.576	0.368
1xStd Dev	0.001	0.001	0.003	0.002
1RSD (%)	0.355	0.309	0.491	0.415

Table 13. Particle size analysis after 2 days of milling – powders from Daiichi

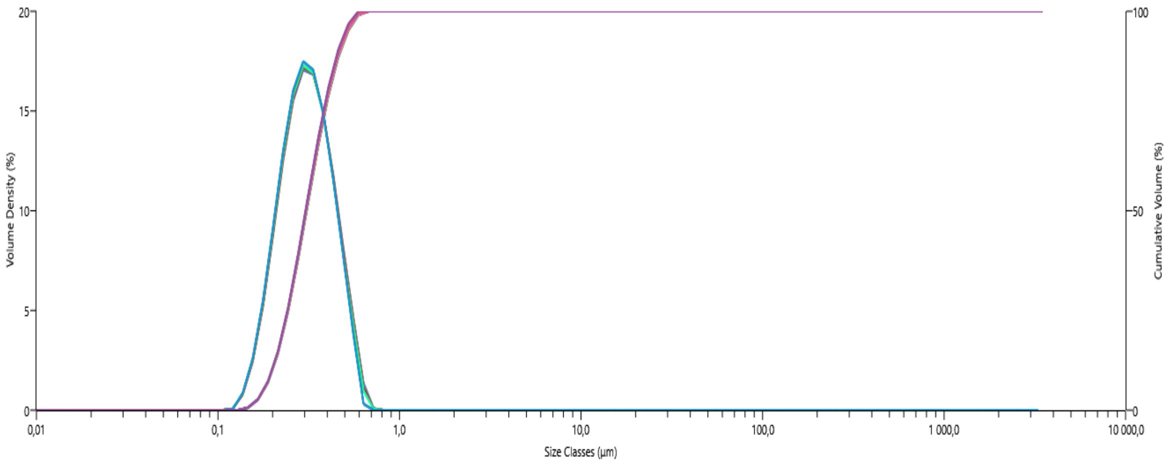

Figure 29. Particle size analysis - 3Y-TZP Daiichi powders

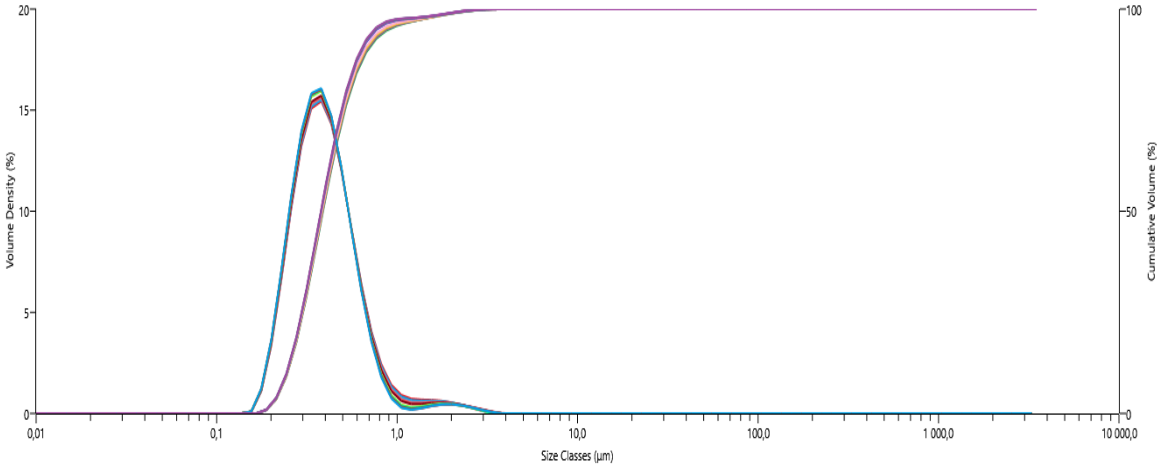

Figure 30. Particle size analysis - Mg-TZP Daiichi powders

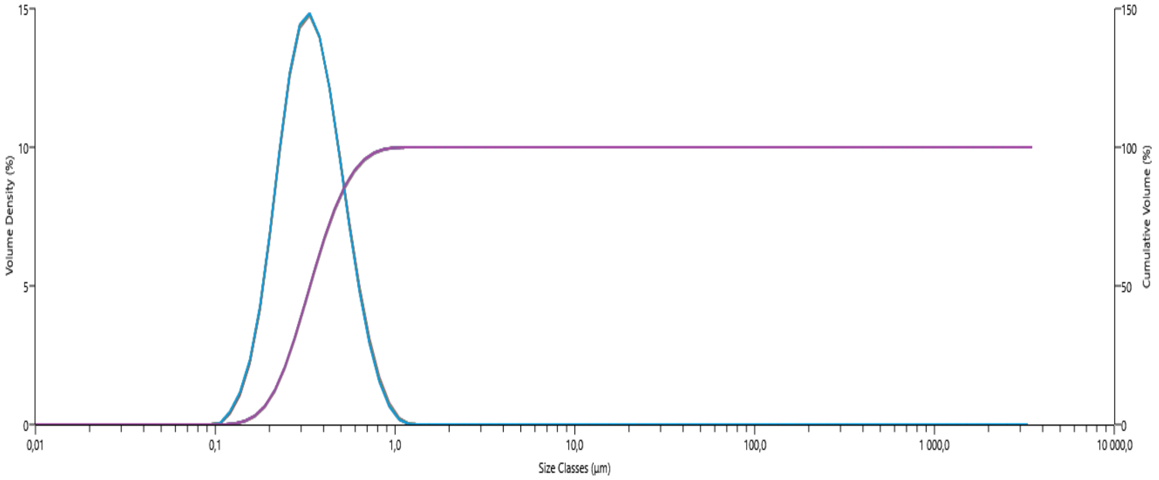

Figure 31. Particle size analysis - 12Ce-TZP Daiichi powders

Surface area measurements of Daiichi powders and compared with 3Y-TZP from Tosoh in table 14, show that the highest surface area is observed in 12Ce-TZP powder with 14.66 m^2/gr and the lowest in Mg-TZP with 3.27 m^2/gr. Differences in surface area between these powders even when the particle size distribution is similar suggest that the surface morphology and surface structure varies considerably.

Zirconia Powders	Surface Area [m^2/gr]
Tosoh Powder 3Y-TZP	6.6396
Tosoh Powder 3Y-TZP - Milled 2 days	8.1593
Daiichi Powder 3Y-TZP	8.2702
Daiichi Powder Mg-TZP	3.2673
Daiichi Powder 12Ce-TZP	14.6567

Table 14. Surface area of different Zirconia powders

The viscosity of the suspension varied significantly between powders when using the same parameters for the preparation of the system (solids loading 45%, 2% dispersant, 10% diluent and a proportion of monomers R=2). Figure 32 shows the viscosity at different shear rates compared with the 3Y-TZP from Tosoh. 12Ce-TZP showed shear thickening behavior before reaching 45% volume in solids. The high surface area and thus stronger particle interaction may be the cause for an unsuccessful preparation and shear thickening behavior. Trunec and Hrazdera [36] observed that with increasing surface area, activation energy of the viscous flow decreased when studying zirconia nanopowders with similar particle size. In addition, the maximum volume fraction of powder in the suspension also decreases with increased surface area of the powder. The high interaction of particles and agglomeration of primary particles cause the increase in viscosity. They also observed that adsorption of organic molecules on the surface of the powder increased the effective volume fraction of the ceramic suspension forming an immobilized organic layer around the particles. The investigation with 12Ce-TZP was not carried further given that similar volume fraction in the suspension was not possible to achieve and obtain comparable results with 3Y-TZP.

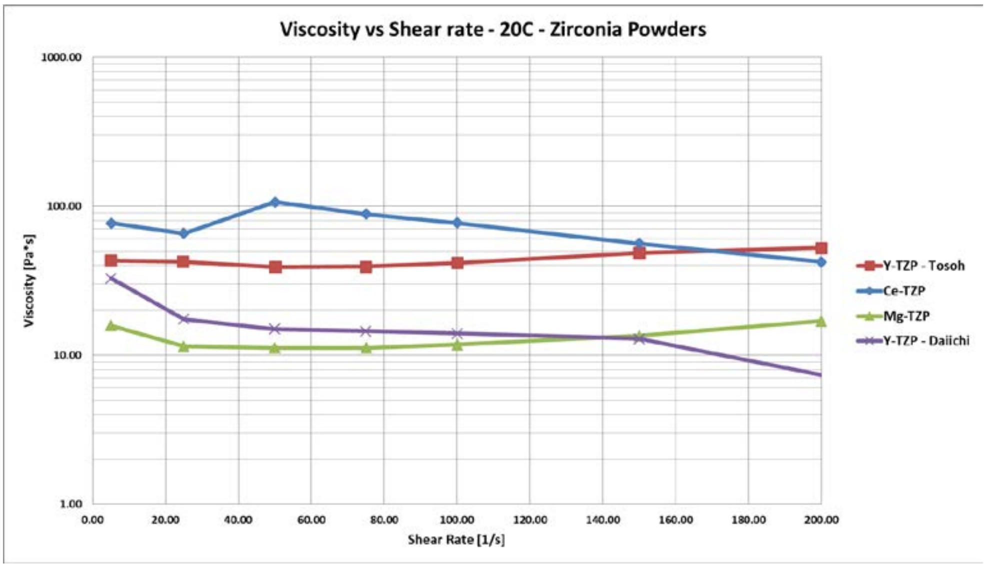

Figure 32. Viscosity of different Zirconia powders

When the cure depth was studied, the different powders showed a slight difference between them. Coarser Mg-TZP powder seems to reach less cure depth but this difference is not significant, especially with exposure times below 10 seconds as seen in Figure 33. Therefore 3.5 seconds exposure time was used for all the following tests. This also allowed the results to be comparable with 3Y-TZP from Tosoh powders.

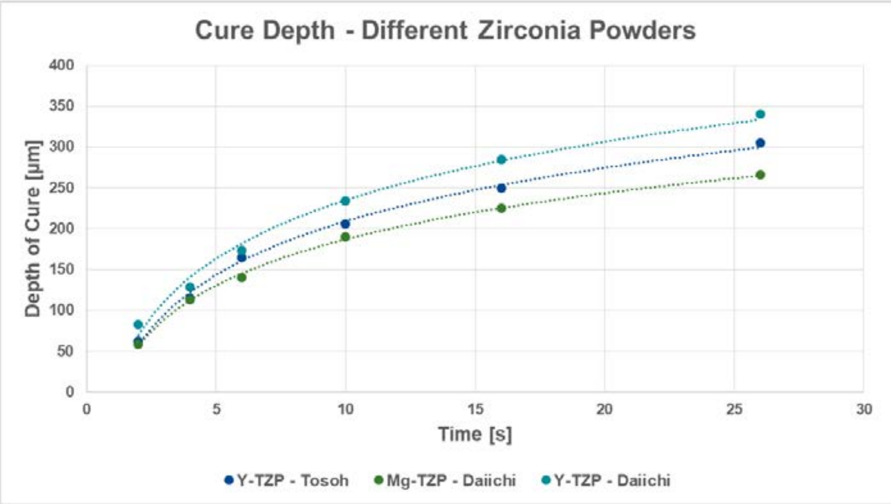

Figure 33. Cure depth of different Zirconia powders

Mg-TZP suspension showed easy flowability and printability. Moreover, the components showed good results after debinding and sintering, few cracks and defects were observed in the pieces compared to 3Y-TZP from both suppliers. Figure 33 shows the microstructure of a sintered component using this powder. Since all the other parameters were kept constant and same as 3Y-TZP powder, the response to debinding and sintering could be influenced by the particle size. Fine powders may be more difficult to debind. Pfaffinger et al [29] suggested that delamination cracks are greatly influenced by the powder size distribution. Powders with particle size lower than 1 µm can increase the risk of delamination cracks due to limited diffusion of gases in the burn-out process. The micrometer sized pores create a sieve-like network that can trap the escaping gasses inside the component [29].

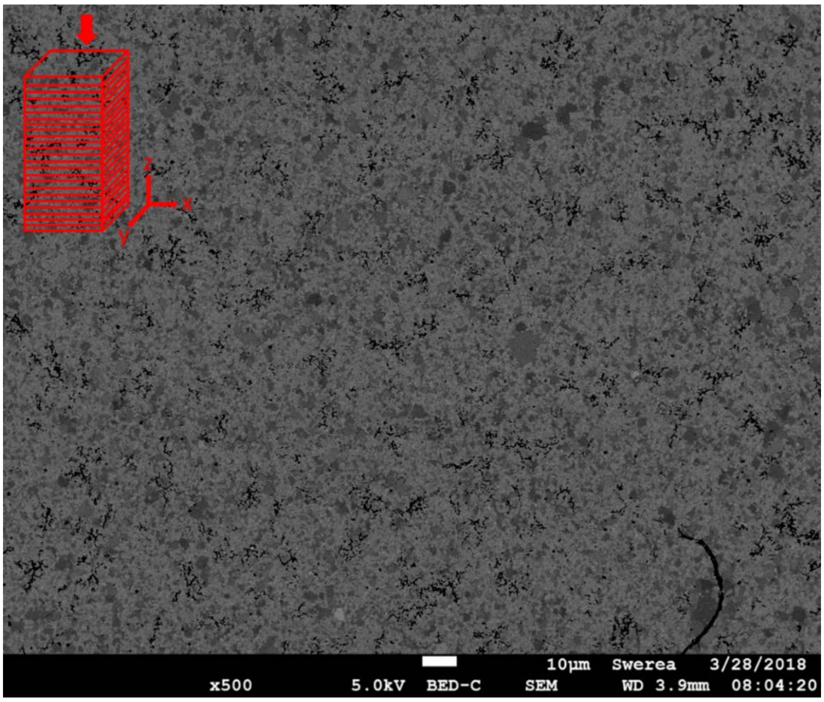

Figure 34. Mg-TZP sintered component - building direction: x-y plane

The image using the BED detector shows two different phases in the microstructure (dark and grey). Thermal etching was also used to examine the grains in more detail. Dark grains are observed in the microstructure (Figure 35) that are not present in 3Y-TZP. The material also shows more elongated and uneven grain shape compared to 3Y-TZP.

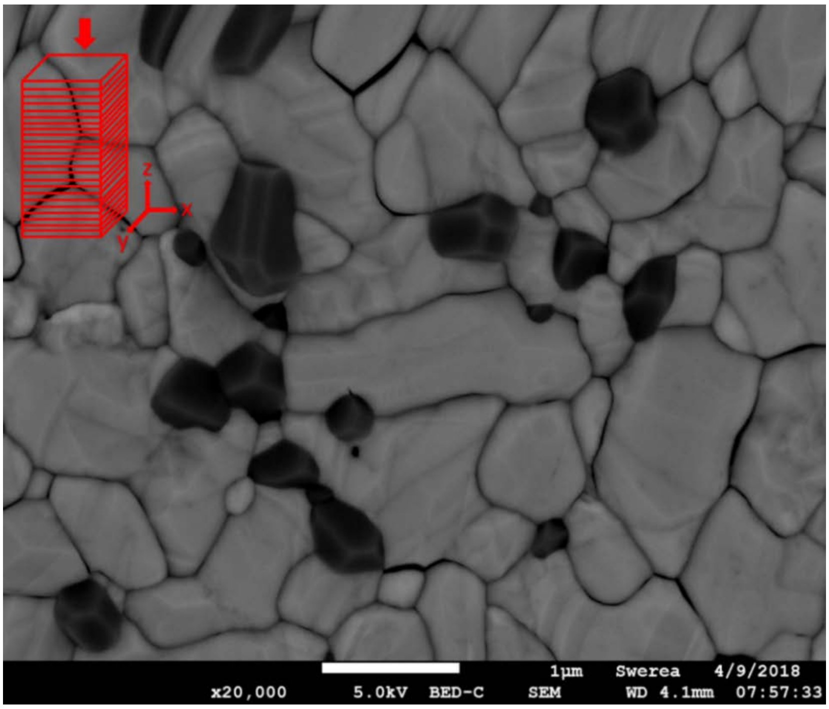

Figure 35. Microstructure after thermal etching - Mg-TZP

The 3Y-TZP powder from Daiichi showed the same behavior and results as the 3Y-TZP powder from Tosoh and no significant difference was observed during the post-processing steps and in the sintered pieces. This is mainly because of the similarities in grain size and surface area. The subsequent analysis was done with only 3Y-TZP from Tosoh and Mg-TZP from Daiichi to compare the results and behavior of the powders.

4.9. Characterization of final components

Table 15 shows the density measurements of the Yttria and Magnesia Powders. Measurements showed the highest density achieved with Mg-TZP powder. In average, 99.5% of theoretical density was obtained compared with only 98.9% with Tosoh 3Y-TZP.

Material	Dimensions (mm)	M air	M water	M moist	Open (%)	Closed (%)	Total Porosity	Density (g/cm3)	Density (%)
3Y-TZP Tosoh	20x10x1	1.47	1.23	1.47	0.98	0.12	1.10	6.01	98.90
	20x10x1	1.44	1.21	1.45	0.98	0.00	0.98	6.02	99.02
	20x10x3	3.67	3.07	3.68	1.15	0.03	1.18	6.01	98.82
Mg-TZP Daiichi	20x10x1	1.35	1.11	1.35	0.09	0.13	0.21	5.74	99.79
	20x10x2	2.02	1.67	2.03	0.23	0.04	0.27	5.73	99.73
	20x10x3	3.89	2.71	3.39	0.00	0.74	0.74	5.71	99.26

Table 15. Density measurements - 3Y-TZP and Mg-TZP

Comparing the Magnesia and Yttria powders as observed in figure 36, 3Y-TZP shows a uniform single phase microstructure and no inclusions are observed. Unevenly closed pores of approximately 1 µm in size are present in both the materials but Mg-TZP shows slightly bigger pores in some images. Nonetheless, Mg-TZP has much less closed pores compared to 3Y-TZP which can also be confirmed by the density measurements in table 15. The grains in Mg-TZP are more heterogeneous in shape and size compared to 3Y-TZP. The greatest difference observed between these two materials is the dark grains in the microstructure of Mg-TZP that were not present in the 3Y-TZP.

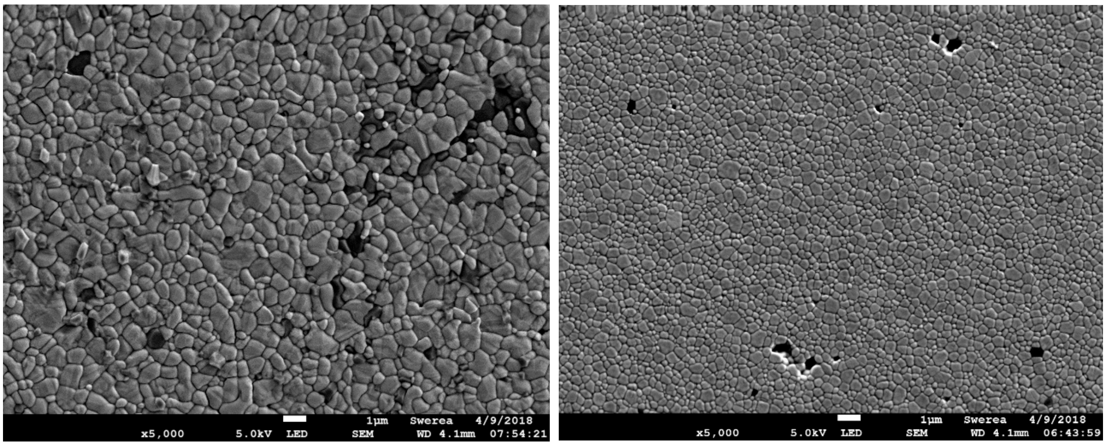

Figure 36. Microstructure comparison between Mg-TZP (left) and 3Y-TZP (right)

An EDS point analysis and a mapping in two areas were made to identify these dark grains in Mg-TZP. The results show that both areas correspond to tetragonal phase. However, the dark grains observed in the microstructure contain Si. This impurity in the material may come from the manufacturing and refining process of the powder as Silica. A high amount of Magnesia is also observed in the dark grains. This may suggest that magnesia and silica precipitate during the sintering process.

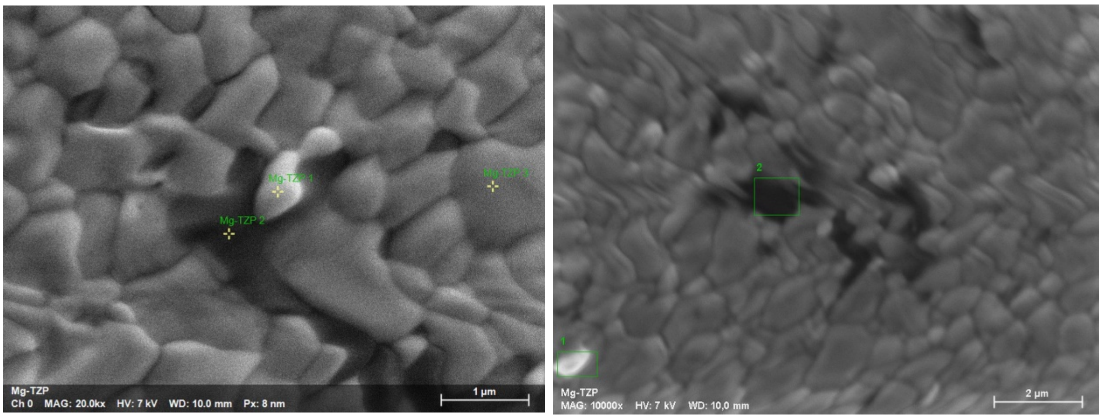

Figure 37. EDS point and map analysis - Mg-TZP

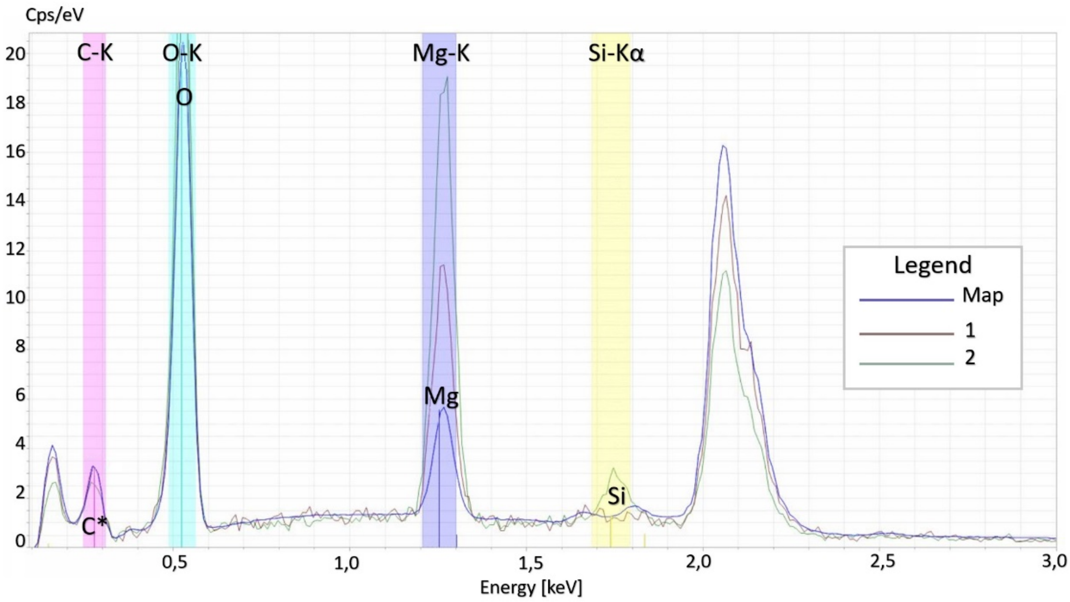

Figure 38. EDS analysis results - Mg-TZP

Image analysis was also performed for this material. The result shows a broad particle size distribution with an average size of 0.669µm and standard deviation of ±0.283µm. This broad range in particle size distribution shows the material is more heterogeneous than 3Y-TZP when is sintered. In addition, slight grain growth is observed in the sintered component compared to the original grain size of the powder.

Printed components with both materials show good dimensional accuracy and surface finish as seen in figure 39. The shrinkage compensation in every direction that is set in the printer before the process in combination with the high solids loading suspension was effective to minimize the possibility of warping or change in dimensions during post-processing.

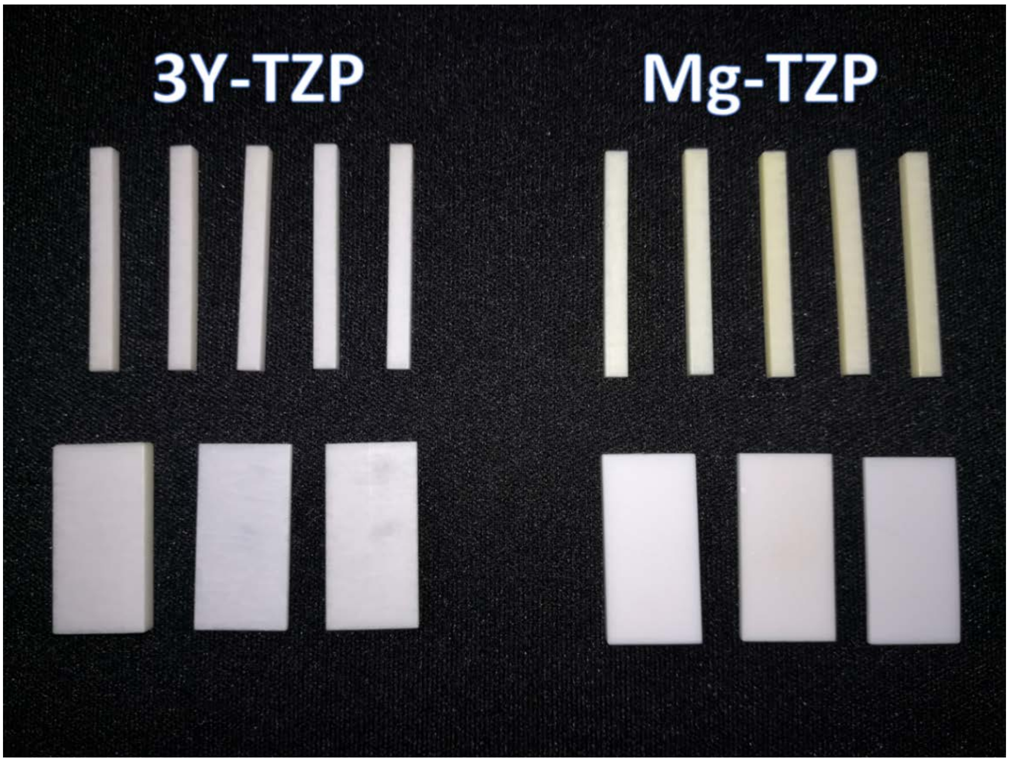

Figure 39. Final components - 3Y-TZP and Mg-TZP

5. Conclusions

Additive manufacturing of Zirconia powders with a special focus on Yttria stabilized zirconia was investigated in this research in order to increase the overall reliability of the process using a VAT-photopolymerization technique. Resin compositions, printing parameters, and post-processing steps were investigated. Powder characteristics, rheology of suspensions, photoreactivity, and characterization of the components were made to compare powders with different stabilizers and their response to the entire process.

Powder processing steps such as milling and freeze drying before suspension preparation improves the behavior and flowability. Hard granules between 100 to 400 µm were present in the powder as received from the manufacturer and they were not destroyed easily by mixing. These steps are necessary to avoid hard agglomerates in the suspension and obtain a homogeneous dispersion with a narrow particle size distribution in the range of 0.4 to 0.5µm. Increased specific surface area after milling was also beneficial in the sintering process as this is the driving force that allows particles to fuse together. Surface area increased from 6.64 m^2/gr to 8.19 m^2/gr after 48 hours of milling.

It was observed that the addition of dispersant between 1 and 2% change the rheological behavior from shear thickening to shear thinning behavior and it was possible to achieve a homogeneous dispersion in the resin with 45% solid loading. Addition of dispersant lower than 1% does not change the behavior effectively. Amounts of dispersant higher than 2% increase contact forces that lead to an increase in the viscosity, affecting the printability. The addition of diluent increases the viscosity of the suspensions and tendency to shear thickening behavior after 10%. However, the debinding process and sintering are improved with the addition of diluent as the components show fewer cracks and defects. 20% diluent in the suspensions produce weak parts that were not possible to handle and post process. 30% diluent highly increases the viscosity and it is not possible to perform print tests. The addition of a more viscous second monomer does no influence the rheological behavior of the suspensions in the same proportion as the diluent. The use of the second monomer between 20 and 30% provides a stronger and more flexible polymer matrix that also improves the post-processing steps. Higher amounts of Bis-EDA create too dense cross-linking that complicates the burning process creating defects and inefficiently extending the burning-off time.

The cure depth was tested in different suspensions showing that this parameter is mainly dependent on the solid loadings and powder characteristics. Increasing the exposure time to achieve cure depths higher than 150 µm can lead to overgrowth of the components in the x-y plane and compromise the dimensional accuracy of the components. Exposure times to reach a cure depth lower than 100 µm increase the risk of weak cross-linking between layers and failure of the components during printing and post-processing.

The debinding process is a critical stage that can easily lead to cracks and defects even if the suspension is optimum regarding its rheological properties and printability. Heating rates at 0.2 ºC/min up to 100 ºC and 0.1 ºC/min up to 380 ºC was used for diluent evaporation and pyrolysis of the polymer, respectively. Holding times of 4 and 8 hours at 4 different temperatures must be applied to allow an easy pyrolysis and outgassing of the polymer matrix. A final heating rate of 0.2 ºC/min up to 500 ºC is used for the final diffusion of carbon residues. The sintering process was performed at 1450 ºC for two hours with heating and cooling rates of 5 ºC/min. These parameters for the heat treatment allowed manufacturing of defect-free components using the resin compositions with 10% Diluent and mixing ratios R=2 (62%M1/28%M2) and R=4 (73%M1/17%M2).

The reliability of the process was tested with other Zirconia powders that contain different stabilizer elements. Mg-TZP showed good behavior and response to the entire process. The coarser particle size distribution and lower surface area are the main factors that allowed easy printability and post-processing steps. 12Ce-TZP was not investigated further as the conditions of solids loading and rheological behavior of the suspensions were not achieved caused by the high surface area of the powder. Differences in photoreactivity using different powders were not significant as the cure depth reached similar values for exposure times below 10 seconds. Cure depth is a parameter that is mainly determined by a combination of solid loading, the monomer system, and the powder characteristics such as refractive index.

Characterization of the components showed delamination cracks as the main and most common defect when the process is not successful. Closed pores are observed when examining the cross section of the materials even in crack free components. However, the highest density obtained with Mg-TZP and fewer defects are the consequence of an optimum suspension and a good thermal response reaching 99.5% on average. 3Y-TZP shows uniform grain size and morphology while Mg-TZP shows more heterogeneous shapes of the grains. Moreover, the microstructure contains a second phase that is not observed in 3Y-TZP. This is caused by Silica and Magnesia segregations present in the material. Image analysis for grain size measurements shows slightly higher grain growth in Mg-TZP components than 3Y-TZP after sintering compared to powder particle size in the suspension.

6. Future Work

A study of the mechanical, optical and electronic properties of zirconia printed components could be interesting topics for further investigation. This could help to better understand the potentialities of additive manufacturing with this material.

Further investigation and research in adding Zirconia powders to other materials to elaborate composites could also be of interest. The toughening mechanism and the possibility to use this property in other materials may lead to interesting developments in this field. In this regard, powder characteristics and powder processing steps before the printing process could also be studied with more depth. That may also help to fully understand the interactions between the resin system and the powder.

References

[1] I. Gibson, D. Rosen and B. Stucker, *“Additive Manufacturing Technologies, 3D Printing, Rapid Prototyping and Direct Energy Manufacturing”*, Second Edition. Ed. Springer US, 2010, pp 30-40.

[2] S. Corbel, O. Dufaud and T. Roques-Carmes, *"Materials for Stereolithography", in Stereolithography: Materials, Processes and Applications,* P. J. Bártolo, Ed., Springer US, 2011, pp. 141-159.

[3] D.W. Richerson, *“Modern Ceramic Engineering”*, Third Edition, Ed. Taylor and Francis Group LLC, Boca Raton FL, US, 2006, pp 371-402, 640-675.

[4] T. Chartier and A. Badev, *"Chapter 6.5 - Rapid Prototyping of Ceramics," in Handbook of Advanced Ceramics: Materials, Applications, Processing, and Properties,* Second Edition, S. Sōmiya, Ed., Oxford, Academic Press, 2013, pp. 489-524.

[5] U. Scheithauer et al., *“Thermoplastic 3D Printing - An Additive Manufacturing Method for Producing Dense Ceramics”,* International Journal of Applied Ceramic Technology, 12: 26–31, 2015.

[6] C. Montanari, *“Additive Manufacturing of Silicon Nitride”* (Master Thesis), Luleå University of Technology, Department of Engineering and Mathematics, 2017, pp 44-55.

[7] O.S. El-Ghany, A. H. Sherief, *“Zirconia Based Ceramics, some clinical and biological aspects: Review”, Future* Dental Journal, Volume 2, Issue 2, December 2016, pp 55-64.

[8] J.R Kelly, I. Denry, *“Stabilized Zirconia as a structural ceramic: An overview”* Science Direct, Dental Materials 24, 2008, pp 289-298.

[9] A. Ghazanfari et al., *“Additive manufacturing and mechanical characterization of high density fully stabilized Zirconia”,* Ceramics International 43, 2017, pp 6082-6088.

[10] M. Bengisu *“Engineering Ceramics”* First Edition, Ed. Springer-Verlag Berlin Heidelberg New York, 2001, pp 28-29, 85-102.

[11] L.B. Kong et al., *“Topics in Mining, Metallurgy and Materials Engineering: Transparent Ceramics”,* Ed. Springer International Publishing, Switzerland, 2015, pp 35-38.

[12] J. F. Shackelford, R.H. Doremus, *“Ceramic and Glass Materials: Structure, Properties and Processing”,* Ed. Springer Science + Business Media, 2008, pp 169-199.

[13] J. Pelleg, *“Solid Mechanics and its Applications: Creep in Ceramics”,* Volume 241 Ed. Springer International Publishing, 2017, pp 311-354.

[14] Z.H. Khan, *“Advanced Structured Material: Recent Trends in Nanomaterials”,* Volume 83, Ed. Springer Nature Singapore, 2017, pp 285- 305.

[15] C.B. Carter, M.G. Norton, *“Ceramic Materials: Science and Engineering”*, Second Edition, Ed. Springer Science + Business Media, 2013, p 362.

[16] O. Lyckfeldt, M. Sjöstedt, and J. Orlenius, “Freeze Granulation,” Swerea IVF Product Sheet, vol. 46, pp. 1–2, 2013.

[17] C.F. Gutierrez-Gonzalez et al, *“Ceramic/metal nanocomposites by lyophilization: Spark plasma sintering and hardness”*, Ceramics International, Volume 40, Issue 3, pp 4135-4140, 2014.

[18] H. Wu et al, *“Fabrication of dense zirconia-toughened alumina ceramics through a stereolithography-based additive manufacturing”*, Ceramics International, Volume: 43 Issue: 1, pp: 968-972, 2017.

[19] Zocca, A., Colombo, P., Gomes, C. M. and Günster, J. (2015), *“Additive Manufacturing of Ceramics: Issues, Potentialities, and Opportunities”*, J. Am. Ceram. Soc., 98: 1983–2001.

[20] Travitzky, N., Bonet, A., Dermeik, B., Fey, T., Filbert-Demut, I., Schlier, L., Schlordt, T. and Greil, P. (2014), *“Additive Manufacturing of Ceramic-Based Materials”*, Advanced Engineering Materials, 16: 729–754.

[21] Mühler, T., Gomes, C. M., Heinrich, J. and Günster, J. (2015), *“Slurry-Based Additive Manufacturing of Ceramics”*. Int. J. Appl. Ceram. Technol., 12: 18–25.

[22] Shahzad K at, *“Additive Manufacturing of Zirconia parts by indirect selective laser sintering”*, Journal of the European Ceramic Society, Volume: 34 Issue: 1, pp 81-89, 2014.

[23] Bartolo P.J, *“Stereolithography: Materials, Processes and Applications”, Ed* Springer, Science+Business Media, pp 1-36, 141-160, 2011.

[24] G. Mitteramskogler, R. Gmeiner, R. Felzmann, S. Gruber, C. Hofstetter, J. Stampfl, J. Ebert, W. Wachter, and J. Laubersheimer, *“Light curing strategies for lithography-based additive manufacturing of customized ceramics,”* Additive Manufacturing, Volume 1-4, pp 110-118, 2014.

[25] E. Castro, J. Pinto, P. Bártolo, *"A review of additive manufacturing for ceramic production"*, Rapid Prototyping Journal, Vol. 23 Issue: 5, pp.954-963, 2017.

[26] X. Song et al. *“Ceramic fabrication using Mask-Image-Projection-based Stereolithography integrated with tape-casting”*, Journal of Manufacturing Processes, Vol. 20, Part 3, pp 456-464, 2015.

[27] S. Gürgen, W. Li, M.C. Kushan. “*The rheology of shear thickening fluids with various ceramic particle additives”*. Materials & Design, Vol. 104, pp 312-319, 2016.

[28] B. A. Horri et al. *“A new empirical viscosity model for ceramic suspensions”*, Chemical Engineering Science, Vol. 66, Issue 12, pp 2798-2806, 2011.

[29] M Pfaffinger et al. *“Thermal Debinding of Ceramic-Filled Photopolymers”*, Materials Science forum Vol. 825-826, pp 75-81, 2015.

[30] C. Bae, J.W. Halloran, *“Influence of Residual Monomer on Cracking in Ceramics Fabricated by Stereolithography*”, International journal of applied ceramic technology, Vol. 8, Issue: 6, pp 1289-1295, 2011.

[31] A.J.A. Winnburst, M.M.R. Boutz, *“Sintering and Densification; New Techniques: Sintering Forging”*, Key engineering materials Journal, Vol. 153-154 pp 301, 1998

[32] O.C. Standard, C.C. Sorrell, *“Densification of Zirconia – Conventional Methods”*, Key engineering materials Journal, Vol. 153-154 pp 251-300, 1998.

[33] Stawarczyk, B., Özcan, M., Hallmann, L. et al.” The effect of Zirconia sintering temperature on flexural strength, grain size and contrast ratio”, Clinical Oral Investigations, Vol. 17, pp 269-274, 2013.

[34] W. Harrer, M. Schewentenwein, T. Lube, R. Danzer, *“Fractography of zirconia-specimens made using additive manufacturing (LCM) technology”*, Journal of the European Ceramic Society, Vol. 37, Issue: 14, pp 4331-4338, 2016.

[35] C. Hinczewski, S. Corbel, T. Chartier, *“Ceramic Suspensions Suitable for Stereolithography”*, Journal of European Ceramic Society, Vol. 18, Issue 6, pp 583-590, 1998.

[36] M. Trunec, J. Hrazdera, *“Effect of Ceramic Nanopowders on Rheology of Thermoplastic Suspensions”*, Ceramics International, Vol. 31, Issue 6, pp 845-849, 2005.

[37] *“Advanced Ceramics | Zirconia Powders.”* Zirconia Powders | Https://Www.tosoh.com/, Tosoh Powders Website. www.tosoh.com/our-products/advanced-materials/zirconia-powders.

[38] *“Daiichi Powders Specifications.”* Composite Oxide, Daiichi Powders. www.dkkk.co.jp/english/products_e/p03e.html.

Appendices

A. Raw Powder Characteristics

a. 3Y-TZP Tosoh Powders

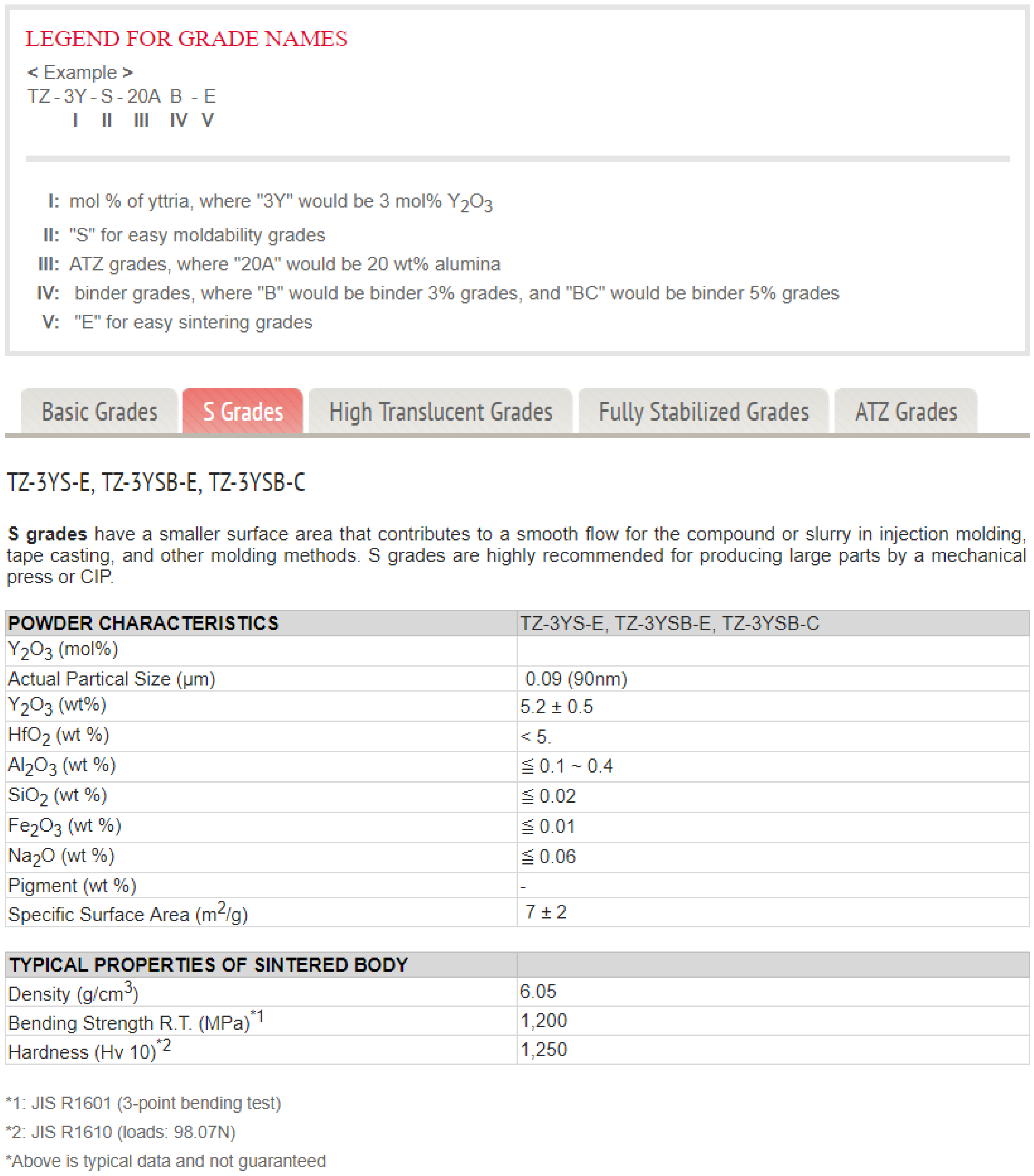

LEGEND FOR GRADE NAMES

< Example >
TZ - 3Y - S - 20A B - E
I II III IV V

I: mol % of yttria, where "3Y" would be 3 mol% Y_2O_3

II: "S" for easy moldability grades

III: ATZ grades, where "20A" would be 20 wt% alumina

IV: binder grades, where "B" would be binder 3% grades, and "BC" would be binder 5% grades

V: "E" for easy sintering grades

TZ-3YS-E, TZ-3YSB-E, TZ-3YSB-C

S grades have a smaller surface area that contributes to a smooth flow for the compound or slurry in injection molding, tape casting, and other molding methods. S grades are highly recommended for producing large parts by a mechanical press or CIP.

POWDER CHARACTERISTICS	TZ-3YS-E, TZ-3YSB-E, TZ-3YSB-C
Y_2O_3 (mol%)	
Actual Partical Size (μm)	0.09 (90nm)
Y_2O_3 (wt%)	5.2 ± 0.5
HfO_2 (wt %)	< 5.
Al_2O_3 (wt %)	≦ 0.1 ~ 0.4
SiO_2 (wt %)	≦ 0.02
Fe_2O_3 (wt %)	≦ 0.01
Na_2O (wt %)	≦ 0.06
Pigment (wt %)	-
Specific Surface Area (m^2/g)	7 ± 2

TYPICAL PROPERTIES OF SINTERED BODY	
Density (g/cm^3)	6.05
Bending Strength R.T. (MPa)[*1]	1,200
Hardness (Hv 10)[*2]	1,250

*1: JIS R1601 (3-point bending test)

*2: JIS R1610 (loads: 98.07N)

*Above is typical data and not guaranteed

B. Image Analysis and Grain Size Measurement – Sintered Components

a. 3Y-TZP – Tosoh Powders

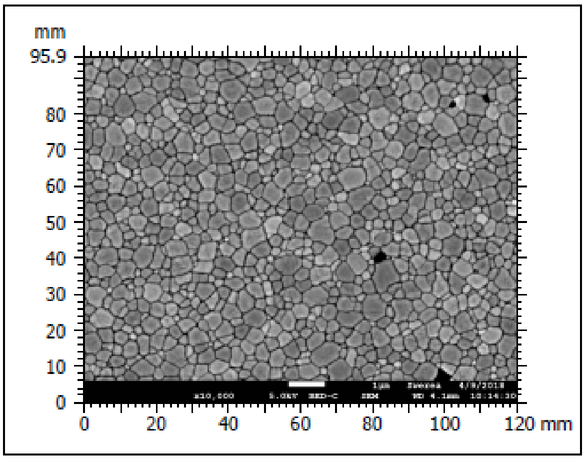

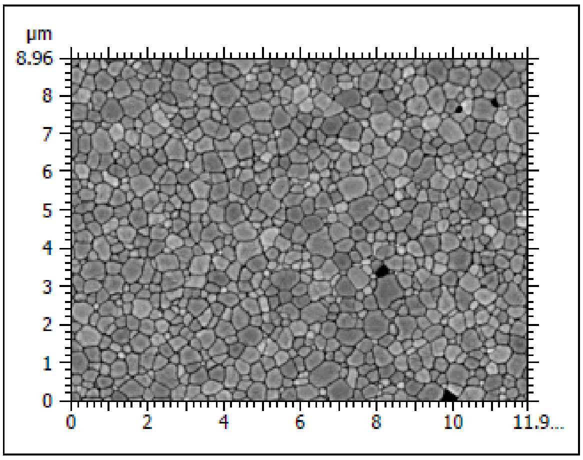

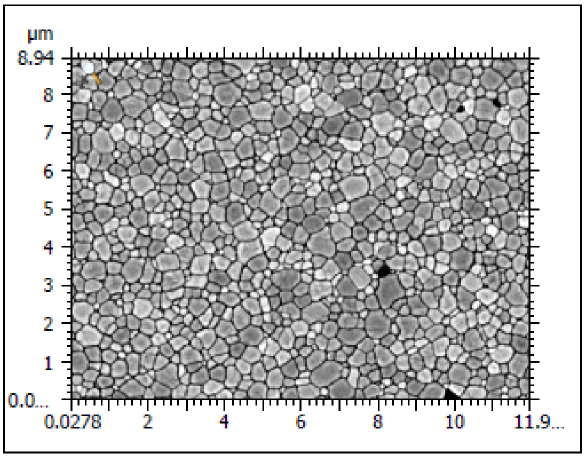

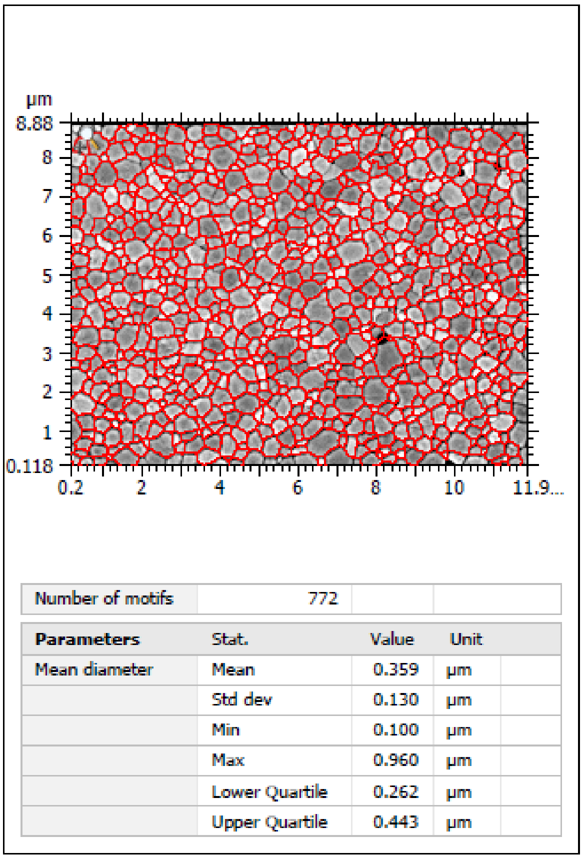

Number of motifs	772		

Parameters	Stat.	Value	Unit
Mean diameter	Mean	0.359	µm
	Std dev	0.130	µm
	Min	0.100	µm
	Max	0.960	µm
	Lower Quartile	0.262	µm
	Upper Quartile	0.443	µm

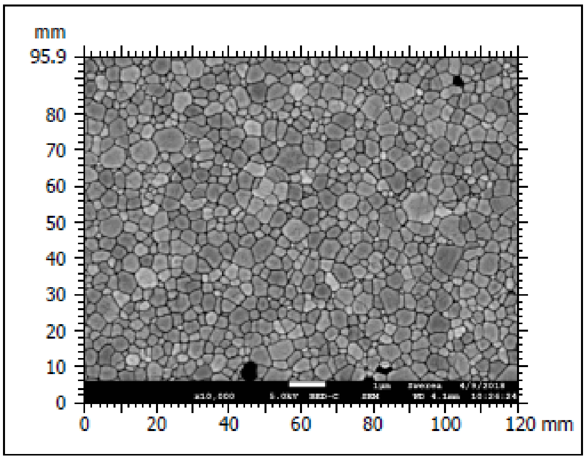

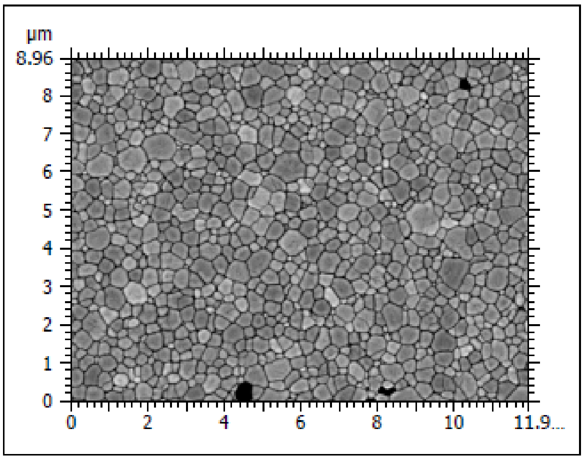

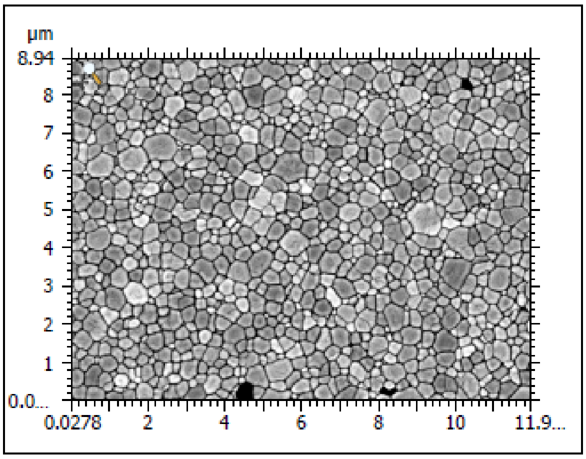

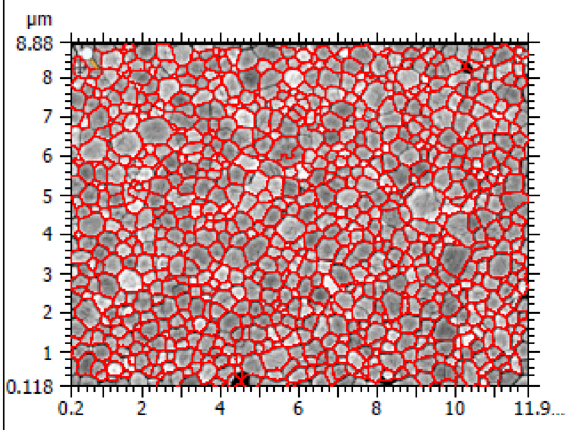

Number of motifs	802		

Parameters	Stat.	Value	Unit
Mean diameter	Mean	0.353	µm
	Std dev	0.125	µm
	Min	0.111	µm
	Max	0.937	µm
	Lower Quartile	0.264	µm
	Upper Quartile	0.429	µm

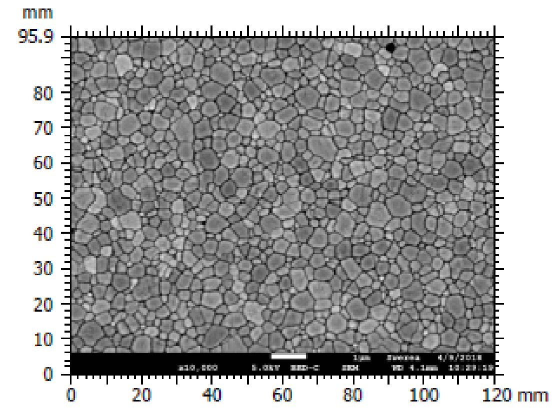

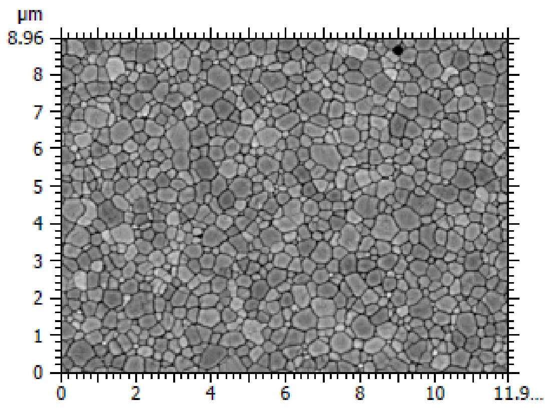

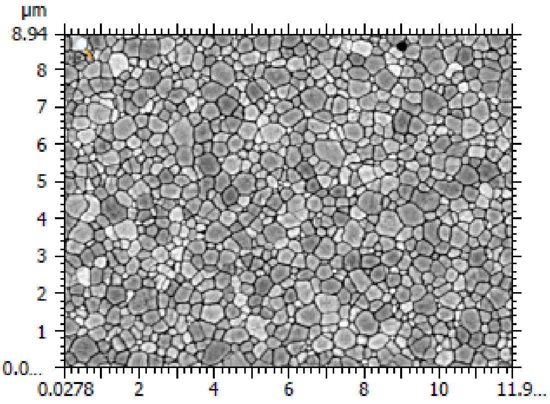

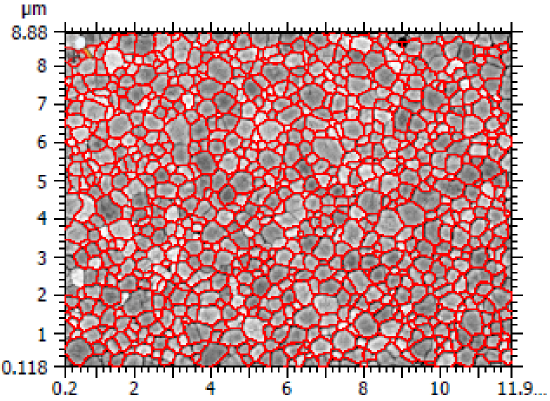

Number of motifs	790		

Parameters	Stat.	Value	Unit
Mean diameter	Mean	0.354	µm
	Std dev	0.129	µm
	Min	0.104	µm
	Max	0.853	µm
	Lower Quartile	0.259	µm
	Upper Quartile	0.426	µm

b. Mg-TZP – Daiichi Powders

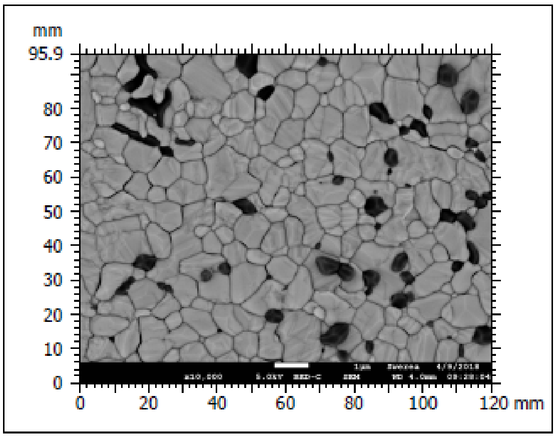

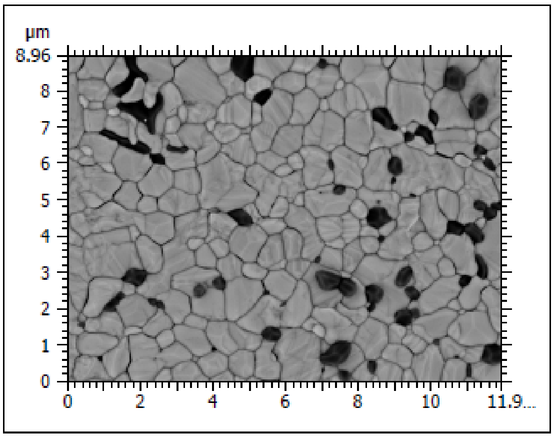

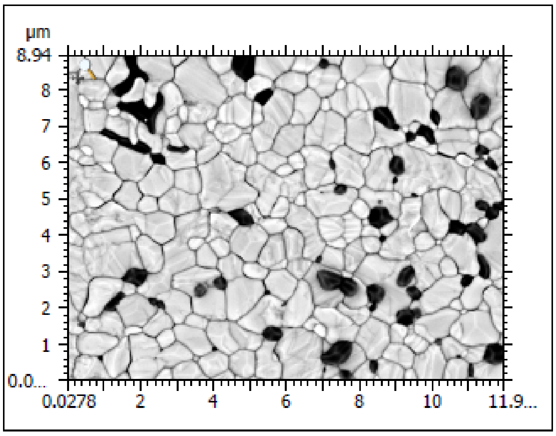

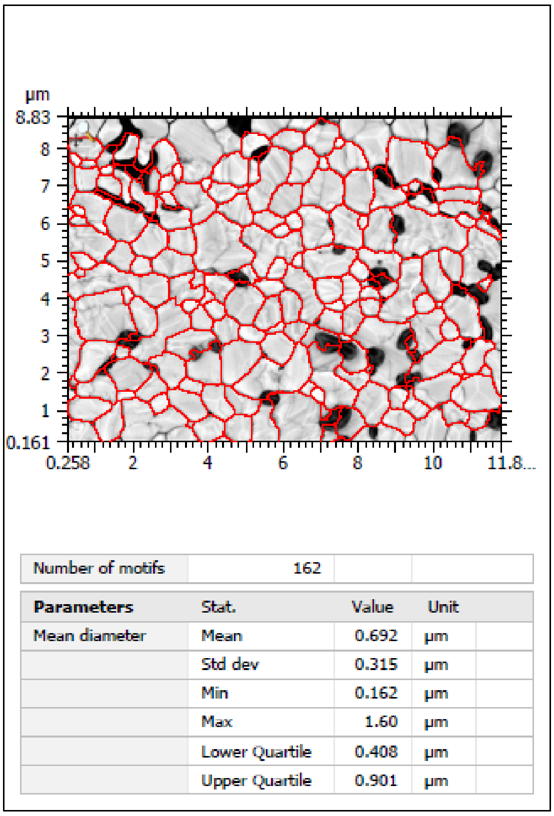

Number of motifs	162		

Parameters	Stat.	Value	Unit
Mean diameter	Mean	0.692	µm
	Std dev	0.315	µm
	Min	0.162	µm
	Max	1.60	µm
	Lower Quartile	0.408	µm
	Upper Quartile	0.901	µm

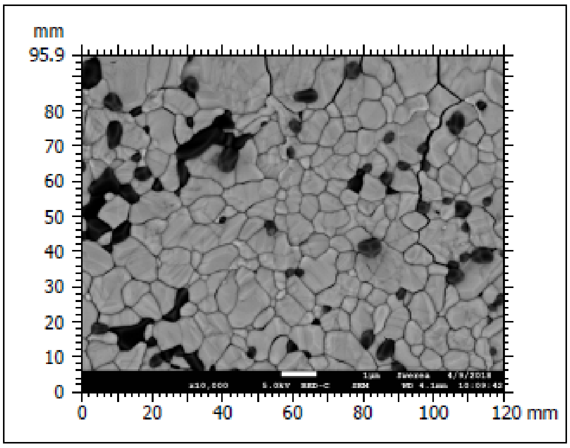

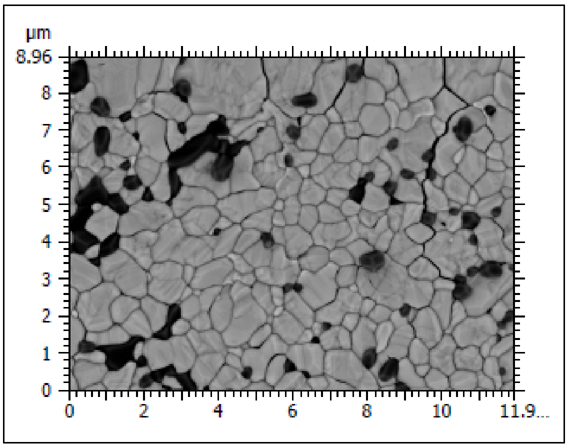

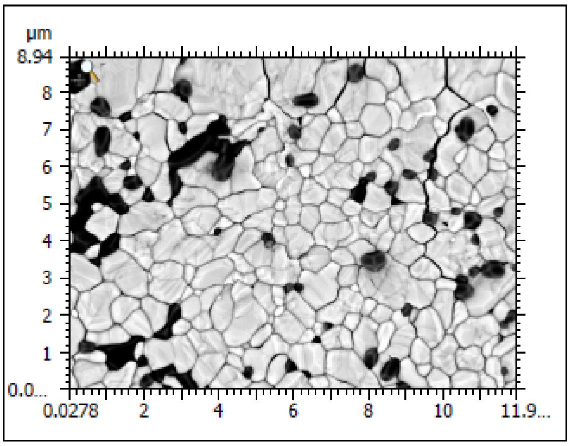

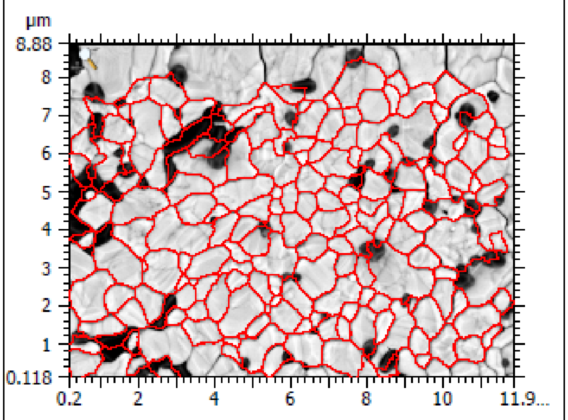

Number of motifs	173		

Parameters	Stat.	Value	Unit
Mean diameter	Mean	0.667	µm
	Std dev	0.262	µm
	Min	0.185	µm
	Max	1.47	µm
	Lower Quartile	0.470	µm
	Upper Quartile	0.817	µm

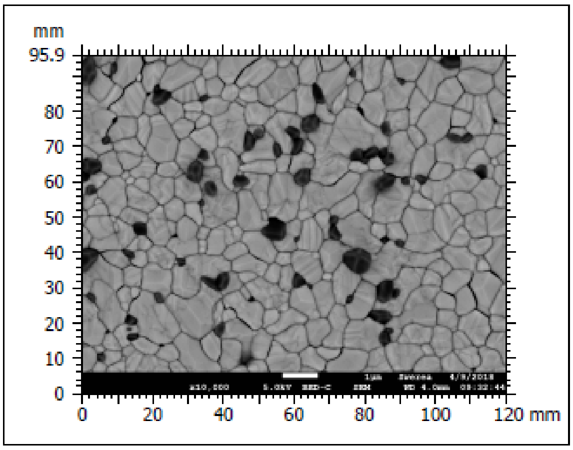

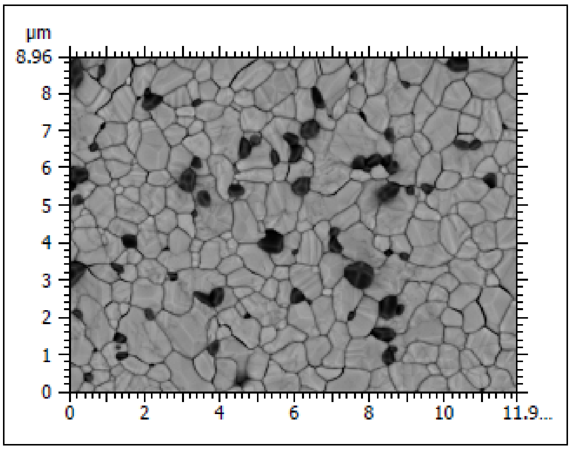

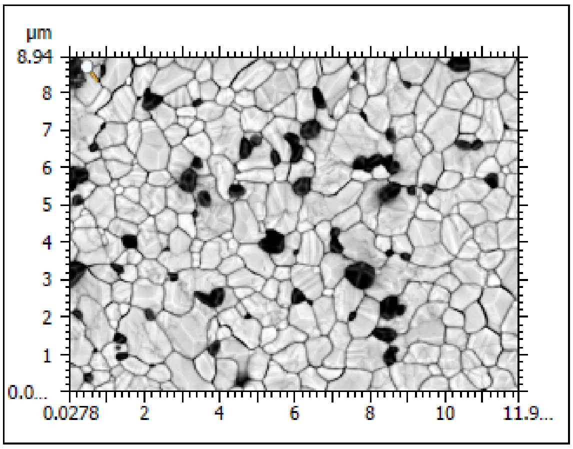

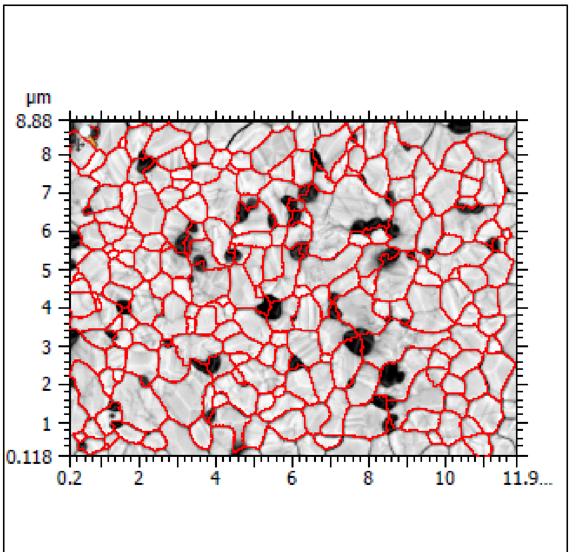

Number of motifs	204		

Parameters	Stat.	Value	Unit
Mean diameter	Mean	0.650	µm
	Std dev	0.274	µm
	Min	0.142	µm
	Max	1.94	µm
	Lower Quartile	0.466	µm
	Upper Quartile	0.828	µm